NTNU

Norwegian University of
Science and Technology

Numerical Analyses of Moment Resisting Timber Connections with Friction Connector and Threaded Rods as Fasteners

Tobias Baartvedt
Henrik Dietrichson Pharo

Civil and Environmental Engineering
Submission date: June 2018
Supervisor: Kjell A Malo, KT

Norwegian University of Science and Technology
Department of Structural Engineering

Department of Structural Engineering
Faculty of Engineering
NTNU- Norwegian University of Science and Technology

ACCESSIBILITY

OPEN

MASTER THESIS 2018

SUBJECT AREA:	DATE:	NO. OF PAGES:
Structural engineering	08.06.2018	93 + 30 Appendix

TITLE:

Numerical Analyses of Moment Resisting Timber Connections with Friction Connector and Threaded Rods as Fasteners

Numeriske analyser av momentstive treforbindelser med friksjonsforbinder og gjengestenger som forbindelsesmidler

BY:

Tobias Baartvedt

Henrik Dietrichson Pharo

SUMMARY:

This Master thesis is a continuation of an ongoing study on rigid beam-to-column connections in timber structures using long threaded rods as fasteners. As part of the research project *Wood frame solutions for free space design in urban buildings*, its objective has been to develop a connection with moment resisting qualities that is easy to assemble on site. The main focus of the thesis has been to achieve as high rotational stiffness as possible, while still keeping the solution practical. This has been done through numerical analyses.

Separate threaded rods in the beam and the column was used. A T-profile was connected to the rods in the beam and two L-profiles were connected to the rods in the column with a small gap between them. The web of the T-profile was placed in the gap between the L-profiles, before two prestressed bolts tied the connection together. Numerical analyses were done to improve the different components of the connection.

For optimizing the rod-to-grain angles in the timber elements, a more detailed modeling technique was carried out. Analyses resulted in the rod-to-grain angle in the beam to be changed from 5° to 10°, as this gave a higher rotational stiffness. A rod-to-grain angle of 75° in the column gave the second highest rotational stiffness with 7850 kNm/rad, and this solution was considered the most practical. The configuration with the highest rotational stiffness had a combination of 55° and 70° rod-to-grain angle in the column and achieved a rotational stiffness of 9188 kNm/rad. However, this solution was considered less practical.

The new design with the L- and T-profile made great improvements with regards to practicality in the assembly phase, compared to solutions in previous theses. The rotational stiffness must be further improved but shows great potential. Detailed analyses of the connection showed that the threaded rods in the column was the weakest component, and further development of the connection should therefore focus on improving this component.

RESPONSIBLE TEACHER: Kjell Arne Malo
SUPERVISOR(S): Kjell Arne Malo, Haris Stamatopoulos
CARRIED OUT AT: Department of Structural Engineering, NTNU

MASTEROPPGAVE 2018

Tobias Baartvedt og Henrik Dietrichson Pharo

Numerical Analyses of Moment Resisting Timber Connections with Friction Connector and Threaded Rods as Fasteners

(Numeriske analyser av momentstive treforbindelser med friksjonsforbinder og gjengestenger som forbindelsesmidler)

Kandidatene skal, gjennom numeriske analyser, videreutvikle en bjelke-søyle forbindelse i limtre som bruker skråstilte lange aksialbærende treskruer (gjengestenger) som forbindelsesmidler. Siden arbeidet er en del av WoodSol prosjektet, skal det fokuseres på å utvikle en forbindelse med momentstive egenskaper som også er praktisk å montere på byggeplass. Hovedmålet med oppgaven er å forbedre rotasjonsstivheten til tidligere løsninger, samt gjøre løsningene mer praktiske.

Oppgaven omfatter en litteraturstudie og analyser av numeriske modeller av hele knutepunktet. Disse analysene skal brukes til å forbedre rotasjonsstivheten til de individuelle komponentene i forbindelsen slik at den totale rotasjonsstivheten til forbindelsen blir så høy som mulig.

Forutsetninger: De numeriske modellene skal modelleres så detaljert som mulig og evalueres ut i fra eksperimentelle forsøk og andre numeriske modeller der dette er tilgjengelig.

Veileder: Kjell Arne Malo
Medveileder: Haris Stamatopoulos

Besvarelsen skal leveres til Institutt for konstruksjonsteknikk innen 11. juni 2018.

Preface

This Master thesis is part of the 5-year degree program Civil and Environmental Engineering. The study is written at the department of Structural Engineering, NTNU, during the spring semester of 2018. The study is a part of the ongoing research project *Wood frame solutions for free space design in urban buildings*, led by Kjell Arne Malo for NTNU.

The study is based on numerical analyses of timber connections. The main focus is to optimize a solution involving axially loaded threaded rods in order to design a moment resisting beam-to-column connection.

We would like to express our gratitude to Kjell Arne Malo and Haris Stamatopoulos for great supervision, input and guidance throughout the entire thesis. Their doors have always been open, and we appreciate all the feedback they have given us. We would also like to give a big thanks to PhD-candidate Aivars Vilguts for all his help and input, especially regarding the FEM-software Abaqus, and wish him the best of luck with the continuation of his thesis. Finally, we would like to thank all our classmates from the Civil and Environmental Engineering class of 2013 for making the years at NTNU so wonderful.

Trondhiem, Thursday 8th June 2018

Tobias Baartvedt

Henrik Dietrichson Pharo

Abstract

This Master thesis is a continuation of an ongoing study for rigid beam-to-column connections in timber structures using long threaded rods as fasteners. As part of the research project *Wood frame solutions for free space design in urban buildings*, its objective has been to develop a connection with moment resisting qualities that is practical and easy to assemble on site. The main focus of the thesis has been to achieve as high rotational stiffness as possible, while still keeping the solution practical. This has been done through numerical analyses.

A configuration with separate threaded rods in the beam and the column that were inserted at an angle of 45° in the column and 5° in the beam, was originally used. A T-profile was connected to the rods in the beam and two L-profiles were connected to the rods in the column with a small gap between them. The idea was for the web of the T-profile to be placed in the gap between the L-profiles, before two prestressed bolts were used to tie the connection together.

Numerical analyses of models created in the FEM-software Abaqus were done to improve the different components of the connection. The L- and T-profiles were optimized using a simplified numerical model, that only partly represented the withdrawal properties of the threaded rods. This was done to save time, as simpler models are more computationally efficient. The optimization process concluded that thicknesses of 30 mm for the L-profiles and 26 mm for the T-profiles should be used. These thicknesses were considered optimal as the increase rate in rotational stiffness was clearly reduced for greater thicknesses.

For optimizing the rod-to-grain angles in the timber elements, seven different configurations using a more detailed modeling technique was carried out. This technique was time consuming both when modeling and when running analyses, but it had shown good correlation with experimental results in previous work and was believed to give accurate results. Analyses resulted in the rod-to-grain angle in the beam to be changed from 5° to 10°, as this gave a higher rotational stiffness. In the column, a rod-to-grain angle of 45° was found to be poor with regards to stiffness. An angle of 75° gave the second highest rotational stiffness with 7850 kNm/rad, this solution was considered the most practical. The configuration with the highest rotational stiffness had a combination of 55° and 70° rod-to-grain angle. In that case the rotational stiffness achieved was 9188 kNm/rad, but the solution was considered less practical, as assembling the L-profiles would be challenging due to the different angles.

The new design made great improvements with regards to practicality in the assembly phase, compared to solutions in previous theses. The rotational stiffness must be further improved but shows great potential. Detailed analyses of the connection showed that the threaded rods in the

column was the weakest component, and further development of the connection should therefore focus on improving this component.

Sammendrag

Denne masteroppgaven er en videreføring av en pågående studie om momentstive bjelke-søyle-forbindelser i trekonstruksjoner med bruk av skråstilte lange aksialbærende treskruer (gjengestenger) som forbindelsesmidler. Siden oppgaven er en del av forskningsprosjektet *Wood frame solutions for free space design in urban buildings*, har målet vært å utvikle et knutepunkt med momentstive egenskaper som er praktisk og enkelt å montere på byggeplass. Fokuset i oppgaven har vært å oppnå en så høy rotasjonsstivhet som mulig, samtidig som løsningen holdes praktisk gjennomførbar. Dette har blitt gjort gjennom numeriske analyser.

En løsning med separate gjengestenger i bjelken og i søylen med innskruingsvinkler på 45° i søylen og 5° i bjelken, ble opprinnelig brukt. Et T-profil ble festet til stengene i bjelken, og to L-profiler ble festet til søylen med et lite mellomrom mellom dem. Ideen var at steget til T-profilet skulle plasseres mellom L-profilene, før to forspente bolter bandt forbindelsen sammen.

Numeriske analyser av modeller laget i FEM-programvaren Abaqus ble gjort for å forbedre de ulike komponentene i forbindelsen. T- og L-profilene ble optimalisert med en forenklet modell som kun delvis representerte uttrekksegenskapene til gjengestengene. Dette ble gjort for å spare tid, da forenklede modeller tar kortere tid å simulere. Optimaliseringsprosessen konkluderte med at tykkelser på 30 mm for L-profilene og 26 mm for T-profilet burde brukes. Disse tykkelsene ble vurdert som optimale siden økningen i rotasjonsstivhet ble tydelig redusert for større tykkelser.

For å optimalisere innskruingsvinkelen til gjengestengene ble syv ulike konfigurasjoner modellert med en mer detaljert modelleringsteknikk. Denne teknikken var tidskrevende både under modellering og simulering av analyser, men har vist god korrelasjon med eksperimentelle resultater i tidligere arbeid og er antatt å gi nøyaktige resultater. Analysene resulterte i at innskruingsvinkelen i bjelken ble endret fra 5° til 10°, da dette ga høyere rotasjonsstivhet. I søylen ble en innskruingsvinkel på 45° vurdert som en dårlig løsning med tanke på rotasjonsstivhet. En vinkel på 75° ga nest høyest stivhet med 7850 kNm/rad, og denne løsningen ble vurdert som den mest praktiske. Konfigurasjonen med høyest rotasjonsstivhet brukte en kombinasjon av 55° og 70° innskruingsvinkel i søylen, og oppnådde 9188 kNm/rad. Denne løsningen ble vurdert som mindre praktisk, da monteringen av L-profilene ville bli vanskelig på grunn av de ulike vinklene.

Den nye løsningen med L- og T-profilet var en stor forbedring med tanke på en praktisk montering sammenlignet med løsninger fra tidligere oppgaver. Rotasjonsstivheten må fortsatt forbedres men viser stort potensiale. Detaljerte analyser av forbindelsen viste at gjengestengene

i søylen var den svakeste komponenten, og videre utvikling av forbindelsen burde derfor fokusere på å forbedre denne komponenten.

Contents

1 Introduction

This thesis is a continuation of previous work that has been done as part of the research project *Wood frame solutions for free space design in urban buildings,* or WoodSol. Knowledge obtained from previous work, along with other relevant literature, has been used to develop a practical solution for a beam-to-column connection in a rigid timber frame, using threaded rods as fasteners, that also has satisfying rotational stiffness.

This chapter describes the WoodSol project and wood as a building material, summarizes previous work and explains the objective and limitations of this thesis.

1.1 WoodSol project

WoodSol is funded by the Norwegian research council. Its main goal is to develop industrialized structural solutions for urban timber buildings up to 10 stories, with large architectural freedom [1]. The project uses prefabricated floorings systems. In these flooring systems, the load bearing beams are integrated, so the entire flooring system will be connected to the columns in one piece. To achieve architectural freedom, load bearing elements cannot be too closely spaced, hence moment resisting frames are to be used. This type of structural system allows for larger spans and more open spaces in a building. Moment resisting frames requires connections between beams and columns to be strong and rigid. All the load bearing elements are made of glued laminated timber, g*lulam*, as this type of wood-based material allows for larger spans.

WoodSol aims to develop solutions that can be used in an industrialized structural system. To achieve that, solutions need to be simple and practical to assemble on site. It is desirable that the structural system requires as little on-site labor as possible.

1.2 Wood as a building material

Wood is a complex anisotropic material, meaning the mechanical properties depend on the loading direction. This anisotropy is caused by the structure of the wood itself. Wood has been used as a building material for thousands of years and is still widely used today. Historically, wood has been used for a variety of things, such as building, bridges, ships and planes, but today it is mainly used for buildings and bridges [2]. In Norway, timber structures have gotten more and more popular over the last years, partly due to today's focus on green sustainable solutions [3]. This is a trend seen also on a global scale. According to statistics from FAO [4], the global production of sawn wood and wood-based panels in 2016 was 884 million cubic meters. This was an increase of 3.8 % from 2015 and 19.5 % from 2012.

1.2.1 Structure of wood

Wood is a fiber composite material made up of 2-4 mm long cells running axially along the length of the tree. These cells are hollow and only a few nanometers wide and are bundled together and stacked on top of each other as the tree grows, see Figure 1.1. This big difference between the cell's length and width is why timber is much stronger in longitudinal direction than in tangential- and radial direction [2].

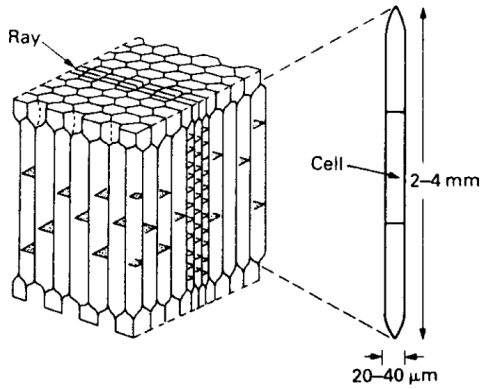

Figure 1.1: Wood cells [2]

Due to rapid growth in spring and slower growth in autumn and winter, the density and size of the newly formed wood cells vary, creating what is known as year rings, or growth rings, in the radial direction [2]. Figure 1.2 shows the different components of the tree stem, along with the coordinate system used to describe timber properties.

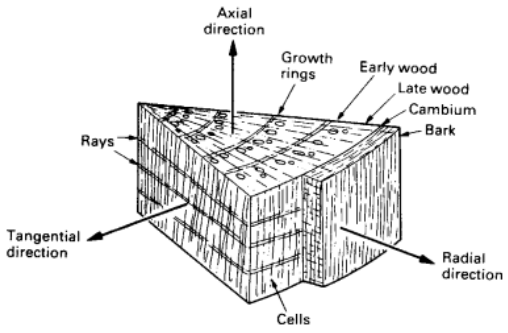

Figure 1.2: Section of a tree stem [2]

New cells are made in the cambium. The outer, most recently formed part of the stem, known as sapwood, is the active part of the tree that performs all the non-structural purposes. Sapwood also contributes to structural performance of the tree. The inner, and older, part of the stem, known as heartwood, has no living cells and preforms only structural purposes. In the production of timber, heartwood is always used, and the small layer of sapwood is often removed at the sawing mill, especially in cases where appearance is of importance, as heartwood often has a darker and more appealing color [5].

1.2.2 Moisture

The moisture content of wood has a big impact on the strength, weight and durability. Wood cells can store water in two ways, chemically bound within the cell wall, called bounded water, and free flowing in the hollow space inside the cell wall, called free water. The state where a cell carries its maximum amount of bound water and practically no free water, is called the fiber saturation point, FSP. The FSP depends on the wood type but is usually between 25-35% [6]. Figure 1.3 illustrates a wood cell in its natural state, at fiber saturation point and at a dry state.

(a) Naturally wet cell (b) FSP (c) dry cell

Figure 1.3: Stages of moisture content [6]

Moisture content below the fiber saturation point will cause shrinkage [7]. By drying the wood, it becomes lighter, most strength parameters increase, and it becomes less prone to fungal attack. It is also necessary to dry the wood before any form of chemical treatment [5]. It is desirable to dry the wood until it has a moisture content that is in equilibrium with the humidity of the environment it will be used in. If the wood is installed in an environment with big

variations in humidity, it can shrink down and swell up repeatedly, causing movement in the timber elements which again can lead to cracking and unwanted stresses from swelling or shrinkage [2].

1.2.3 Durability

Biological decay is the biggest challenge for the durability of wood. It can be caused by fungi, insects or bacteria attacking the wood and decomposing it. Fungal and bacterial attacks can happen when the moisture content is above approximately 20 % [8]. The natural resistance of wood against these attacks varies from species to species. In accordance with NS-EN 350:2016 [9], the durability is categorized into classes ranging from “very durable” to “not durable”. Most wood used for structural purposes is considered moderately durable or slightly durable, which requires either chemical treatment to increase durability, or a design that isolates the timber elements from humid environments [9].

1.2.4 Glulam

There are several types of wood-based materials used in today’s structures. As this thesis is part of the WoodSol project, glued laminated timber, or glulam, has been used. Glulam is a material that consists of four or more timber laminations glued together with the fiber directions parallel to each other. The glue is water resistant and should be strong enough to give no relative slip between the laminations [10]. Normal lamination thickness in Norwegian glulam elements is 45 mm, but for curved elements this thickness is smaller depending on the radius of the curvature. The outermost laminations have higher strength than the rest, as this part of the cross section usually experiences higher stresses due to bending [11].

Production is done by applying high pressure to the laminations while the glue hardens. Glulam technology enables the production of much bigger cross sections than for normal sawn timber, which again allows timber systems to have larger spans and carry higher loads [12]. Figure 1.4 shows a glulam member next to a normal sawn timber board [13].

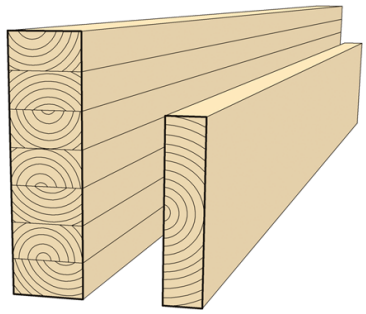

Figure 1.4: Glulam beam [13]

1.2.5 Timber compared to other materials

Material properties

Timber is inferior to other materials, like steel and concrete, when it comes to strength and stiffness. However, the self-weight is much smaller, so it is a lighter material that is easier to work with. This means that when it comes to the material properties per unit weight, as seen in Table 1.1, timber is very competitive against steel and concrete [2].

Table 1.1: Material properties per unit weight [2]

Material	$\frac{E}{\rho}$	$\frac{\sigma_y}{\rho}$	$\frac{K_c}{\rho}$
Woods	20-30	120-170	1-12
Al-alloy	25	179	8-16
Mild steel	26	30	18
Concrete	15	3	0.08

Environmental impact

Today, timber is becoming more and more popular, and part of the reason is its environmental advantages compared to steel and concrete [3]. Trees grow naturally by taking advantage of clean solar energy. By planting at least the same number of trees as are taken down, wood can be sustainably utilized as a structural material. As a tree grows, it works as a carbon sink, absorbing carbon dioxide from the surrounding air and emitting valuable oxygen. The production of timber elements from a tree requires a lot less energy than producing concrete or steel elements [7]. Figure 1.5 (a) shows the energy needed to make a 38x89 stud-based timber frame, and a 100 mm thick concrete wall. The energy efficiency of timber is further illustrated in Figure 1.5 (b), showing that the production of a glulam element requires 5 times less energy than that of a reinforced concrete block, and 6 times less energy than for a steel I-profile [7].

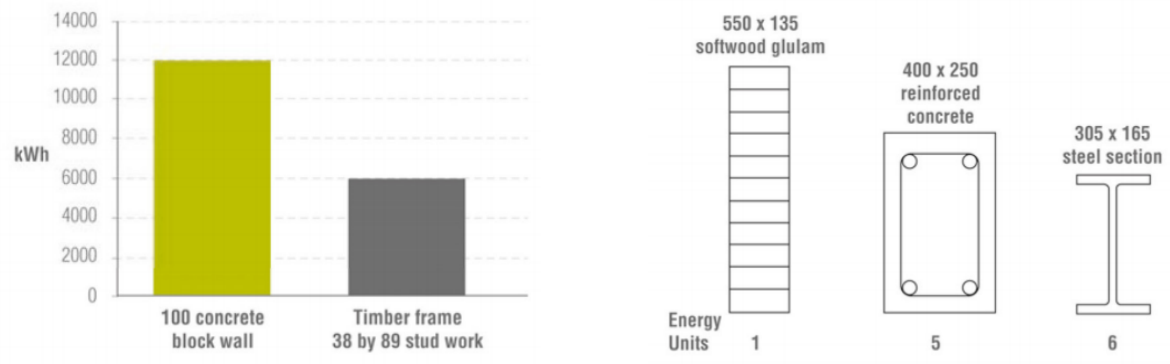

(a) Concrete wall vs. timber frame (b) Glulam section vs. RC and steel sections

Figure 1.5: Energy production cost for different materials [7]

1.3 Previous work

This section gives a summary of the most relevant past research done on the topic of long threaded rods and their usage in rigid beam-to-column connections.

1.3.1 Stamatopoulos & Malo – Withdrawal Capacity and stiffness of threaded rods embedded in timber elements

The withdrawal capacity of axially loaded threaded rods was researched in a study from Stamatopoulos & Malo in 2015 [14]. Here, the main parameters were embedment length and rod-to-grain angle. Theoretical predictions and experimental testing had good correlation, and an approximately linear relation between embedment length and withdrawal capacity was observed, see Figure 1.6. Some other conclusive remarks were that smaller rod-to-grain angles gave a more brittle behavior than larger angles, and that embedment lengths over 600 mm gave a more ductile behavior.

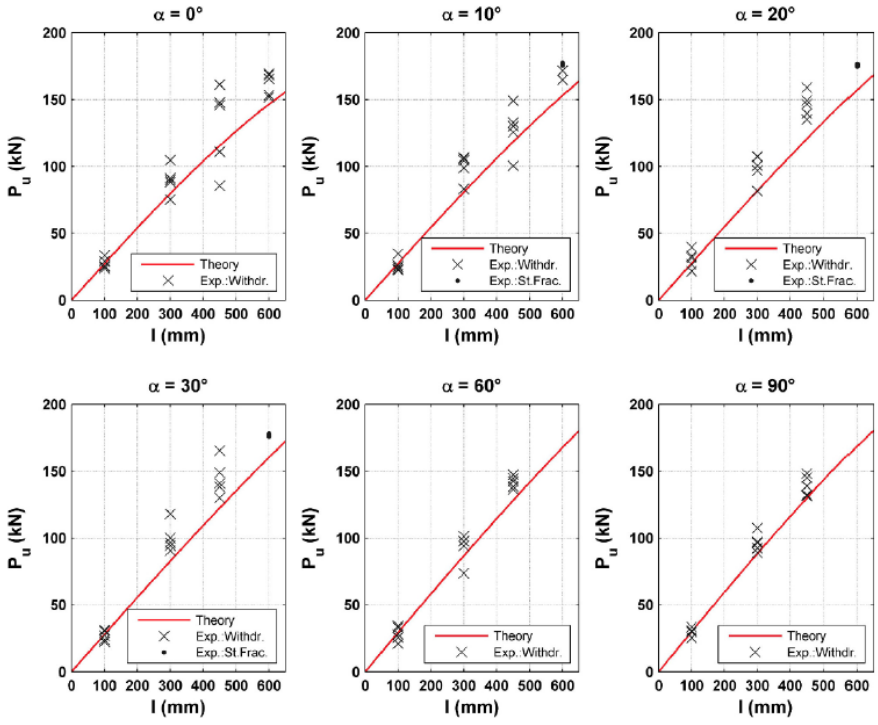

Figure 1.6: Withdrawal capacity of threaded rods [14]

The failure modes varied with the rod-to-grain angle, but as seen in Figure 1.7, withdrawal of the rod along the interface plane between the wood and the outer diameter of the rod occurs several times, often in combination with other failure modes. Figure 1.7 (b), (c), (e), (f), (i), (j) and (l), clearly shows this interface plane which proves to be a critical area for an axially loaded threaded rod.

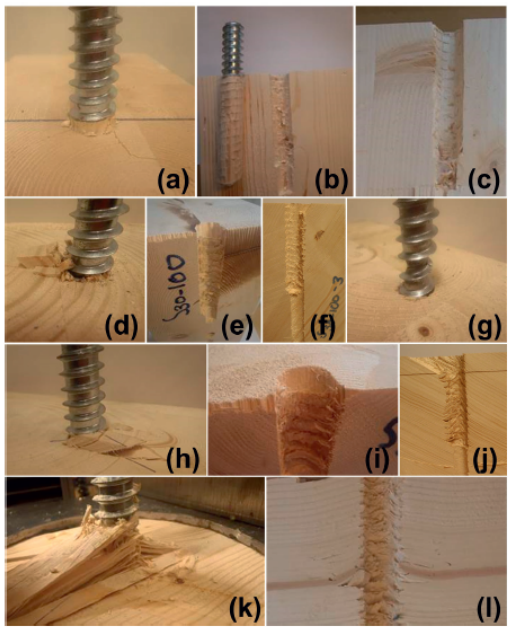

Figure 1.7: Failure modes of specimens with α = 0° (a)-(c), α = 30° (d)-(g), α = 60° (h)-(j), α = 90° (k)-(l) [14]

A different article by Stamatopoulos & Malo from 2016 [16], studied withdrawal stiffness of axially loaded threaded rods embedded in timber elements. Theoretical, numerical and experimental analyses were run. The theoretical and experimental results correlated well. The numerical results showed good correlation with the experimental results for large angles and large embedment lengths, see Figure 1.8. Conclusive remarks here were that long embedment lengths and small rod-to-grain angles gave the highest stiffness values, and that the stiffness increase rate gradually became smaller for large embedment lengths.

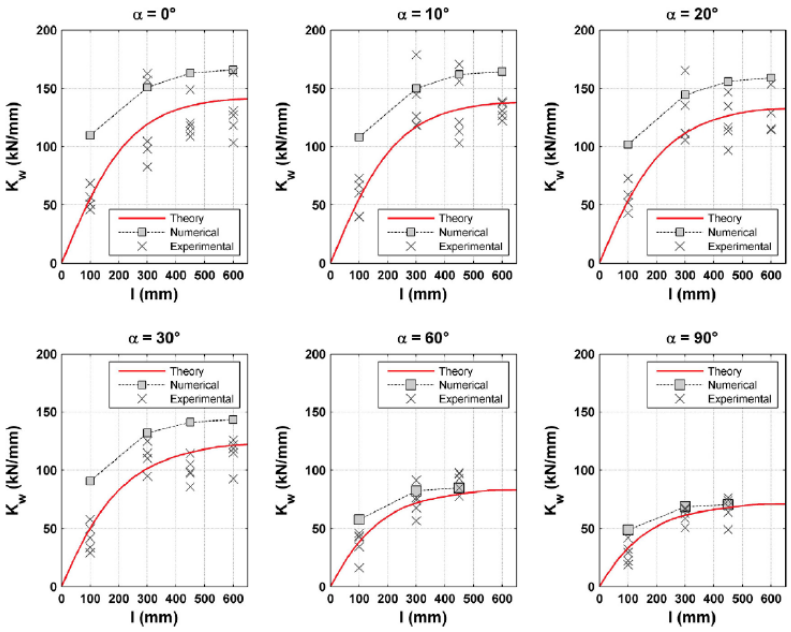

Figure 1.8: Withdrawal stiffness of threaded rods [14]

1.3.2 Lied & Nordal: *"A conceptual study of glulam using threaded rods and connecting circular profile"*

In fall 2016, a conceptual study was made on a glulam beam-to-column connection using long threaded rods as fasteners [16]. The solution had separate rods in the beam and the column and a steel connector was used to connect the rods from the beam to the rods of the column. Three different configurations were analyzed analytically and numerically, before they were tested experimentally in the lab.

Description of research

The steel connector used was developed in a previous thesis by Veium [17] for a beam-to-beam connection and adapted for use in a beam-to-column connection. The connector was a circular steel profile with holes adapted for the rods from the beam and column. Each profile connected one rod from the beam and two from the columns, see Figure 1.9. Theoretical stiffness values were calculated numerically with the FEM-software Abaqus, and with a calculation method developed as part of the thesis, called the component method. The entire connection was also experimentally tested in full scale. Four connections were made and tested, where the first two were identical.

The timber elements were of quality GL30c, and had dimensions 140x450 mm. All the rods had diameter 20 mm. The first two tests were on identical configurations. Two connectors were placed in the upper part of the connection, and one inclined rod was used in the lower part of the connection, threaded through both the column and the beam. The configurations in tests 3 and 4 had two circular profiles in both the upper and lower part of the connection, but the rod-to-grain angle and embedment length varied. The geometry of the three different configurations are shown in figure 1.9.

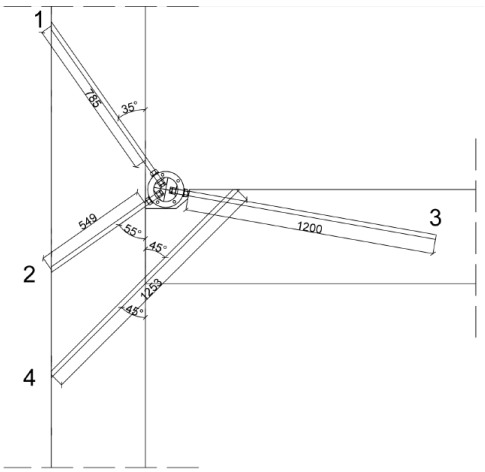

(a) Test 1 and 2

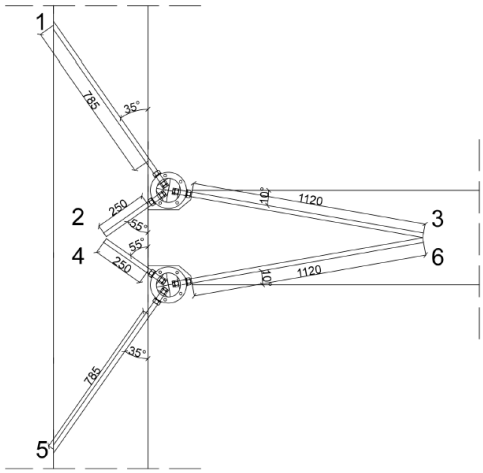

(b) Test 3

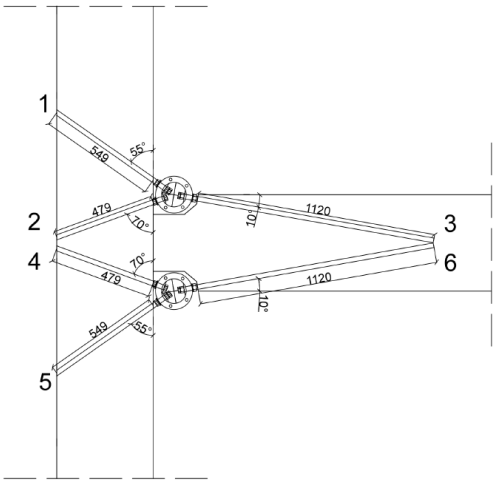

(c) Test 4

Figure 1.9: Geometry of Lied & Nordal configurations [16]

The circular profile had premade holes for the threaded rods. It came in two parts, cut in half along the circumference, see Figure 1.10. This way, it could be applied from each side of the rods and tightened with four bolts.

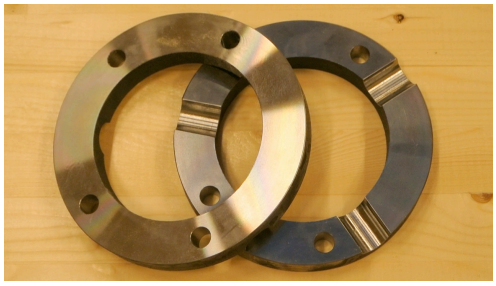

Figure 1.10: Circular profile [16]

Two theoretical evaluations were done, one numerical in Abaqus, and one analytical. In Abaqus, a simplified spring model was made where the rods were represented by spring-elements. Withdrawal stiffness were represented by a spring in longitudinal direction, and transverse stiffness was represented by springs perpendicular to the rod direction. The theoretical and experimental results obtained from the 4 different tests are presented in Table 1.2.

Table 1.2: Strenght and stiffness for Test 1-4 [16]

Test	1	2	3	4
Moment [kNm]				
Theoretical	163.4	163.4	163.4	163.4
Experimental	105.3	104.3	78.8	133.3
Stiffness [kNm/rad]				
Theoretical – component method	2132	2132	11 398	15 225
Theoretical – Abaqus model	2667	2667	2130	-
Experimental	6571	7137	9079	7603

Evaluation

This solution showed some promising results. Test 4 gave the highest strength, whereas test 3 gave the highest rotational stiffness. The configuration used in test 1 and 2 would make the assembly challenging since the bottom rod needs to be threaded through both the beam and the column, which would have to be done on-site. The configurations used in test 3 and 4 however, gives the opportunity to pre-thread the rods in the beams and columns before they arrive on site.

A problem with the circular profile is that it would be hard to tighten the nuts for the rods since access from the side is blocked by other components of the flooring system used in WoodSol. Even with side access, there are a lot of nuts that need to be tightened. Four bolts with nuts must be fastened for each circular profile, and another three nuts are required for the three rods connected to each profile. Another issue would be that columns with flooring systems on both sides, would see rods in the column colliding if this configuration was used. So even though this was a clever idea that potentially could achieve satisfying stiffness, it is not very practical.

1.3.3 Drageset & Hoff: *"Numerical Analyses of Moment Resisting Beam-to-Column Connections in Timber Structures"*

In spring 2017, a new thesis was done as a continuation of the rigid beam-to-column connection tested in Lied & Nordal [16]. This paper used the same principle, with separate rods in the beam and column, but developed a new connector to replace the circular profile [18]

Description of research

Eight rods in the column and four rods in the beam were used. The circular steel profile tested by Lied & Nordal [16] was replaced by a steel plate bent to accommodate the rod inclinations. No experimental testing was done on this connector, only numerical and analytical analyses. Numerical analyses of the circular profile were also carried out and compared to the experimental testing done by Lied & Nordal [16].

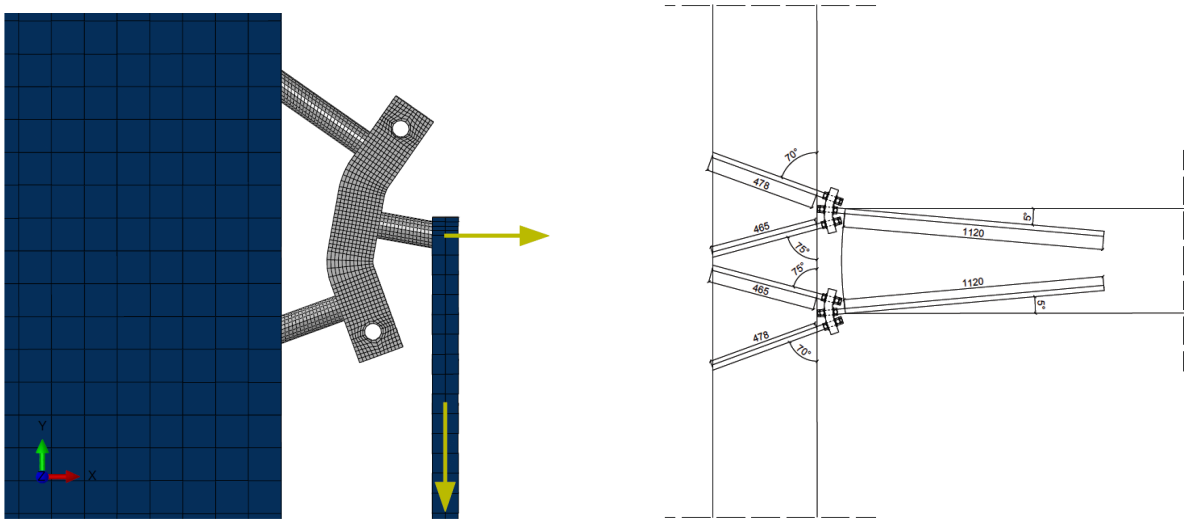

(a) Connector displayed in numerical model (b) Sketch of configuration

Figure 1.11: Connection configuration, Drageset & Hoff [18]

Two different types of plates were developed with regards to assembly. One was based on the same principle as the ring, cut in half down the middle. The other had open holes for the column rods so that it would be placed on the beam rod first, and then pushed in place once aligned. Both types are shown in Figure 1.12. By replacing the ring with a plate, the horizontal distance between the beam-rod connection point and the column-rod connection points was reduced. As a result, the eccentricity was reduced from about 100 mm, to only a few mm. This contributed to a higher rotational stiffness than what was achieved with the circular profile.

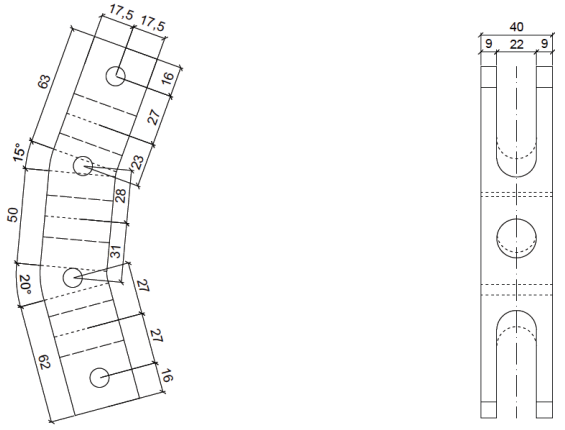

(a) Alternative 1 (b) Alternative 2

Figure 1.12: Plate alternatives for assembly [18]

Nine configurations with varying rod-to-grain angles and dimension were analyzed numerically with Abaqus. Three of them with the circular profile used by Lied & Nordal [16], and the remaining six with the new plate profile. This was a complete analysis with beam, column, rods and connectors as separate parts. Based on earlier simplified calculations in Abaqus, a plate thickness of 35 mm was decided. Table 1.3 shows the rotational stiffness of the different

configurations. The *Model* column explains the rod-to-grain angles used for the analyses. The configuration in Figure 1.11 (b) is referred to as 75-70-05.

Table 1.3: Rotational stiffness for the 9 configurations, Drageset & Hoff [18]

Connector	Model	Numerical	Analytical	Experimental
Circular	55-35-10	10 545	12 052	9079
	70-55-10	13 813	14 263	7603 (9189)[1]
	75-70-05	16 842	17 402	N/A
Plate	70-70-05	15 416	16 288	N/A
	70-70-10	12 470	12 001	N/A
	75-70-05	20 796	16 570	N/A
	75-70-10	14 649	12 188	N/A
	70-70-10 (h = 500)	18 686	15 475	N/A
	65-70-05	18 733	16 156	N/A

[1] Digital Image Correlation measurements.

The configuration with angles 75-70-05 gave the highest rotational stiffness with 20 796 kNm/rad. By comparing the numerical and experimental results obtained for the circular profile, it was assumed that if tested experimentally, the solution with the plate profile could achieve an overall rotational stiffness of around 11 404-13 783 kNm/rad.

The thesis mentions the free end of the rods as a parameter that likely had a large impact on the rotational stiffness. The free end is the part of the rod that was exposed, not inside the beam or column. Since that part was exposed, it was much more prone to bending than the part surrounded by solid timber, meaning it had a negative effect on the overall stiffness. It would also be negative in fire conditions, as the steel would be unprotected. This free end was longer for the plate than the circular profile. However, the overall stiffness was still higher, possibly due to the reduced eccentricity.

Evaluation

This plate profile had higher rotational stiffness than the circular profile, and the assumed experimental stiffness showed promising results. The solution is not so promising when it comes to the assembly phase. The first plate alternative has the same number of bolts and nuts that need tightening as the circular profile. The second plate alternative would only require the nuts on the rods to be tightened and reduces the required labor. However, both solutions would have trouble getting access to all the nuts that require fastening, due to the flooring systems. Colliding rods for columns with floors on both sides would be an issue for this solution as well.

1.3.4 Baartvedt & Pharo: *"Numerical analysis of a steel connector, for use in moment resisting beam-to-column connections in timber structures"*

As an introduction to this master thesis, a project study was done in fall 2017 [19]. The study wanted to further develop the ideas from Lied & Nordal [16] and Drageset & Hoff [18], by finding a solution that was more practical in the assembly phase, while still having good rigid qualities. A new rod configuration was used, and a new connector was developed, both believed to have large improvements when it comes to the assembly. Only numerical testing in Abaqus was carried out.

Description of connection

Ten inclined rods were used in the column, all with 45° rod-to-grain angle, five on each side of the vertical centerline of the column. The rods on each side of the centerline pointed in opposite directions. Two L-profiles were connected to the rods in the column with a gap between them. In the beam, four rods were used with a 5° rod-to-grain angle. A T-profile was attached to the rods at the end of the beam, and its web was inserted in the gap between the L-profiles on the column. The sides of the profiles that were not connected to the beam or column had holes in them that would align once the beam was in place, where two bolts were inserted to tie it all together. A more detailed description will be given in Chapter 2.

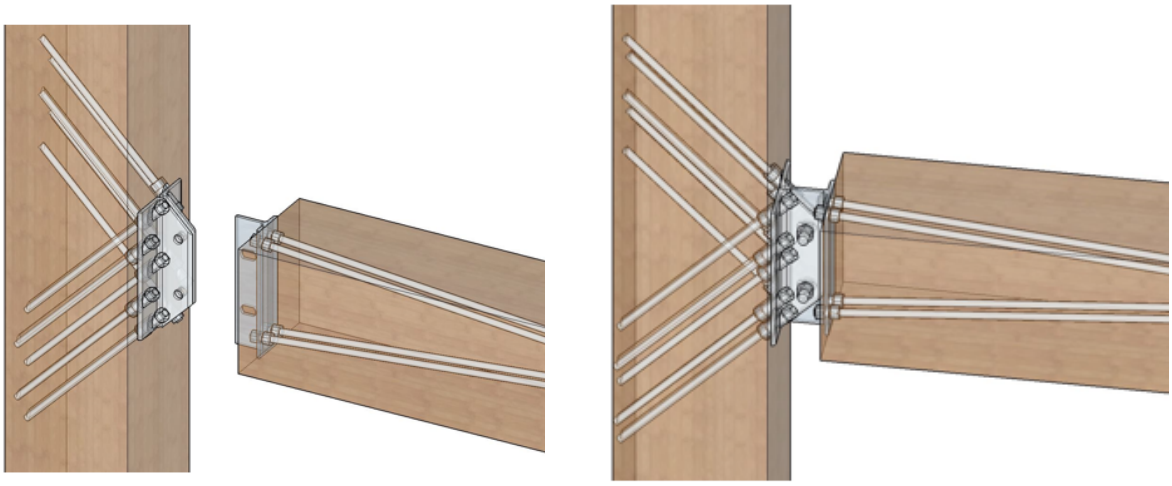

(a) Connection before fastening (b) Connection once fastened

Figure 1.13: Connection configuration, Baartvedt & Pharo [19]

Description of research

First, a simple model containing all the components of the connection was made in Abaqus. This model treated the T- and L-profiles as one rigid component and defined the column and beam as rigid bodies. The profiles were tied to the beam and column over the entire contact surface, meaning the effect of rods was neglected. T-profiles with thicknesses 13 mm and 26 mm were tested for this configuration.

The initial model was further developed by introducing friction between the T- and L-profiles instead of tying them together, and by applying forces to represent the two bolts in the connection. The timber and beam elements were still defined as rigid bodies, so the effect of the rods was still neglected from the analyses. Lastly, a model was made that included the effect of the rods. They were tied to the beam and column, and the profiles were tied to the tips of the rods, rather than the beam and column. The friction and the force representing the bolts were still included, and the timber elements remained rigid bodies. For the last two models, two T-profile thicknesses and two distances between the forces representing the bolts were tested.

All models had a load situation where a point load of 100 kN was applied to the beam 1 m away from the connection. The results from the analyses are presented in Table 1.4. A partial stiffness of 10 000 kNm/rad was assumed for the timber elements. By treating the connection as a series of two springs, one representing the timber elements and one representing the steel profiles, or connector, the overall rotational stiffness, $K_{\theta_{tot}}$, could be assumed by using equation 1.1.

$$\boldsymbol{K_{\theta_{tot}}} = \frac{10000 * K_{connector}}{10000 + K_{connector}} \tag{1.1}$$

Table 1.4: Rotational stiffness from Test 1-7, Baartvedt & Pharo [19]

Numerical model	**Configuration**	**Thickness T-profile [mm]**	**Distance between bolts [mm]**	**Vertical displacement [mm]**	$\boldsymbol{K_{\theta_{connector}}}$ $[\frac{kNm}{rad}]$	$\boldsymbol{K_{\theta_{tot}}}$ $[\frac{kNm}{rad}]$
1	No	13	200	-0.4105	243 605	9605
2	friction	26	200	-0.3706	269 833	9643
3	Friction and	13	200	-2.306	43 365	8126
4	pressure	13	340	-0.680	146 994	9363
5	load	26	340	-0.582	171 880	9450
6	Rods	13	200	-5.601	17 854	6410
7	included	26	340	-3.017	33 146	7682

Evaluation

This new solution was much more practical than the previous solutions. All the rods and the profiles can be attached to the timber elements before they are brought on site. Once on sight, only two bolts need to be fastened per connection. These two bolts are accessible from above and below, and so the flooring system would not block the access. Because the rods in the column have a 45° inclination and go in opposite directions, a column with connections on both sides will not have rods colliding.
The rotational stiffness was also promising. Simplifications such as having the rods tied to the column, and timber elements being rigid bodies made the stiffness values larger than what they would be in real life. However, the connection has several aspects that can be improved, such as thickness of L-profile, the locations of the rods in the column and rod-to-grain angles.

1.3.5 Summary

The previous work described in this section, shows promising results. The work done by Stamatopoulos & Malo [14,15], gives valuable information on withdrawal properties of threaded rods, as well as critical failure modes for axially loaded threaded rods. Solutions developed by Lied & Nordal [16] and Drageset & Hoff [18], gives positive results regarding strength and stiffness. The idea of having separate rods in beams and columns tied together with some type of connector, seems to be a good solution. However, both solutions lack practicality in the assembly phase. In the project study by Baartvedt & Pharo [19], vast improvements were made with regards to assembly, while the rotational stiffness still looked promising.

This previous research gives reason to believe that desired rigid qualities can be achieved using long threaded rods as fasteners. It also indicates that these qualities can be achieved with a practical solution that could be used in an industrialized structural system.

1.4 Scope of thesis

The objective in this master thesis has been to further develop the solution created in the project study by Baartvedt & Pharo [19]. The main focus has been to improve the rotational stiffness of the connection without making the solution less practical in the assembly phase. This has been done through numerical analyses of detailed models in the FEM-software Abaqus. The different components of the connection have been evaluated and improved based on the results from these numerical analyses.

Creating detailed and accurate models in Abaqus is very time consuming. The software is not suited for parametric modelling. Often when one part or parameter is changed, several other components need to be changed as well. Many of these detailed analyses take a long time to run. A remote power station with larger computational capacity than a normal lap top, has been used to run the analyses. There have been several technical issues with this power station, and some analyses had to be started over because of these technical issues. In addition, the staffing capacity in the lab has been low throughout the period of this thesis. As a result of these limitations, no experimental testing has been done, and the primary focus has been limited to improving the rotational stiffness through numerical analyses and maintaining the practicality of the solution.

2 Conceptual layout

This chapter gives a detailed explanation of the solution for a rigid timber beam-to-column connection using threaded rods as fasteners, that this thesis aims to develop. As mentioned in subsection 1.3.4, the solution was created during a project study that was done as a preparation to this thesis.

2.1 Moment resisting frames

The WoodSol project is based on the usage of moment resisting frames [1]. This is a structural system where the connections are rigid and can transfer bending moment, as well as axial- and shear forces, unlike pinned connections that only transfers axial- and shear forces through the connection. Using rigid frames allows for large architectural freedom and larger spans, since there are no cross bracings or shear walls present [20].

It is practically impossible to achieve a completely rigid connection in a timber structure as there will always be some rotation [21]. Limiting this rotation is important to achieve the desired rigidity. According to an article from Malo & Stamatopoulus [20], the required rotational stiffness for a rigid connection in a medium-rise timber building with 30 m total height, is between 10 000 – 11 000 kNm/rad. This is to fulfill the serviceability requirement of horizontal displacement, $\delta_H \leq \frac{H}{300}$, which the study assumed to be appropriate. However, higher values should be aimed for in order to have a safety margin to account for inaccuracies and errors in the production- and assembly phase. Inserting threaded rods precisely is challenging, and inaccuracies can have large effects on the structural performance.

2.2 Connections in timber structures

In timber structures, it is common to use metal plates or profiles together with nails, screws, dowels or bolts when designing a connection. Timber is a brittle material, which means that if it fails it will give brittle failure, failure without any prior visible deformation. Due to the lack of noticeable warnings in brittle failures, they are very dangerous and should be avoided. The metal components used in connections are ductile, meaning they can deform plastically before they fail. This gives a visible warning before failure, and it is therefore usually the connections that are designed to be the softest point in a timber structure [21]. The connections need to perform well enough to transfer the required loads, but at the same time be ductile enough so that a potential failure can be discovered before it actually fails.

2.3 Threaded rods

A threaded rod is a type of fastener used in timber connections. Unlike the common screw, its thread is made by forging a wire rod around the core, giving a smaller shank diameter than the maximum outer-thread diameter [22]. Predrilled holes with the same size as the shank diameter, are always made before inserting the rod. Threaded rods have high withdrawal capacity and stiffness and can transfer shear stresses throughout its length. This allows the rods to prevent cracks from growing in areas loaded perpendicular to the grain, as the rods take the shear stress instead of the cracked timber. Because of these qualities, threaded rods are commonly used in moment resisting timber connections [22].

Figure 2.1: Threaded rods [22]

2.4 Connection with LT-connector

As mentioned in section 1.4, the objective in this thesis is to further develop the solution from Baartvedt & Pharo [19], as this was considered a practical solution that at the same time showed promising rotational stiffness. This solution consists of three main components:

1. *Timber elements*, the beam and column
2. *Fasteners*, the threaded rods inserted in the timber elements
3. *Connector*, the L-profiles and T-profile joined together by two prestressed bolts, transferring forces from the fasteners in the beam to the fasteners in the column. This will in this thesis be referred to as the *LT-connector*.

The combination of all three components is what makes the *connection*. These annotations will be used in the rest of the thesis, so the difference between fastener, connector and connection should be noted.

In this section, all the components in the connection are described in detail. Several aspects of this connection were changed throughout the duration of this thesis. These changes will be described in detail in later chapters, but this section describes the configuration as it was at the beginning of this thesis.

2.4.1 Timber elements

Beam

Part of the WoodSol project is to use flooring systems that can be premade in factories. This means that the beams are already attached to the rest of the flooring system when they arrive on site. One flooring system is planned to be around 2.4 m x 10 m, and to be about 700 mm high. Various components of the flooring systems, such as isolation, fire protection etc., require a certain thickness, so the load carrying beams are restricted to a height of 460 mm and a width of 405 mm. The load bearing beams are made of glulam.

Column

WoodSol aims to build structures up to 10 stories, where each story will have a height of 3.5 m. The columns will be 450x405 mm and are also made of glulam.

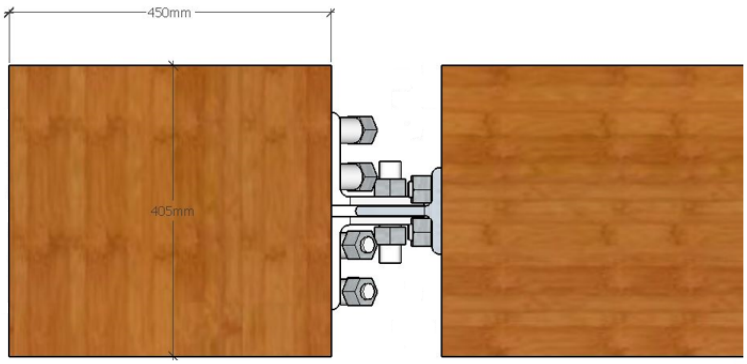

Figure 2.2: Connection with LT-connector seen from above

2.4.2 Fasteners

The fasteners used are long threaded rods with an outer diameter of 22 mm. In the beam, the rods had a rod-to-grain angle of 5°, and a total of four rods were used. The embedment length of the rods in the beam were approximately 1004 mm when tested numerically, as the beam used in the analyses were 1 m long. Spacing between rods is described in subsection 2.4.3.

Figure 2.3: Threaded rods in beam

In the column, the rods had a rod-to-grain angle of 45°, and a total of ten rods were used. The rods were placed in two groups of five on each side of the column's vertical centerline. The groups of five point in opposite directions, as seen in Figure 2.4 (a). By pointing in opposite directions, columns with double connections avoid having colliding rods, since the rods from the two sides will intertwine, see Figure 2.4 (b).

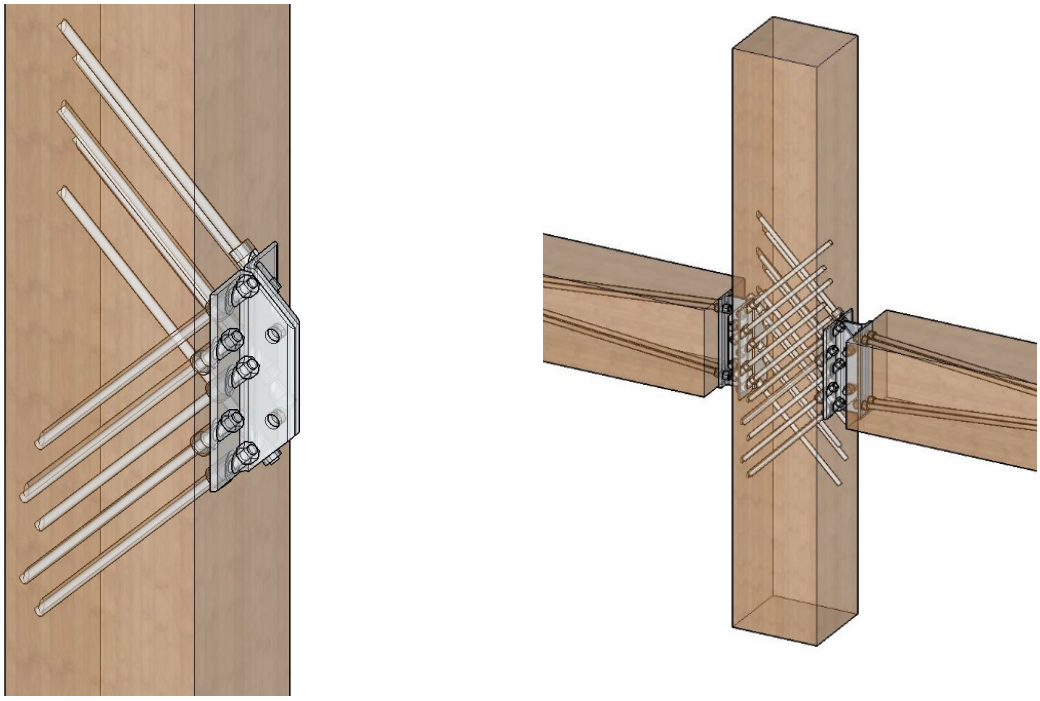

(a) Column with single connection (b) Column with double connection

Figure 2.4: Threaded rods in column

The free end of the rods, which was considered important to reduce by Drageset & Hoff [18], is practically zero in this solution, as both the L- and T-profiles are in contact with the timber elements. With rods inserted at an angle, it will be necessary with an extra component to create a flat bearing surface for the nuts. One solution could be to use beveled washers like those in Figure 2.5.

(a) Circular beveled washer (b) Square beveled washer

Figure 2.5: Beveled washers [32]

2.4.3 Connector

The connector consists of two L-profiles with thickness 12 mm and one T-profile with thickness 26 mm, that are tied together using two prestressed bolts. Each L-profile is attached to the column with five rods, and the T-profile is connected to the beam with four rods. The two prestressed bolts are of type M30. In the column, the group of 5 rods connected to one L-profile is oriented in two parallel lines of two and three. This increases the distances between the rods and can keep the local stresses around the nut heads from overlapping. The geometry of the L- and T-profile is shown in Figure 2.6.

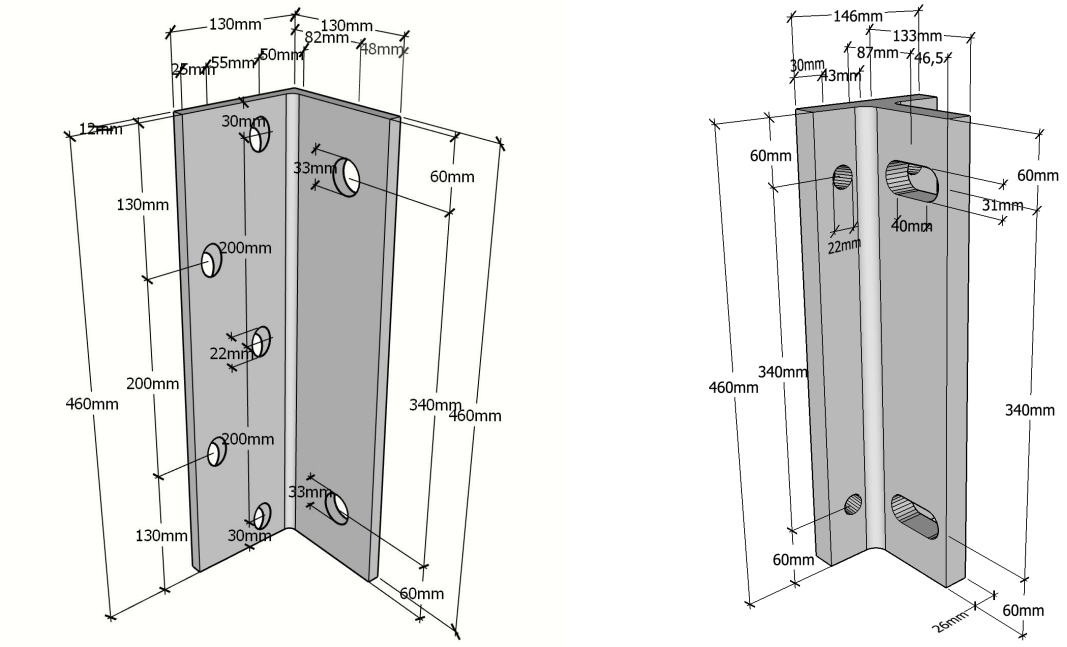

(a) L-profile (b) T-profile

Figure 2.6: Geometry of connector

The purpose of the connector is to tie the fasteners from the beam and column together. This is done by inserting the web of the T-profile between the two L-profiles before tying them together with the two prestressed bolts, see Figure 2.7. The forces from these bolts creates frictional forces in the interaction surfaces between the L-profiles and the T-profile that will contribute to the overall stiffness of the connection.

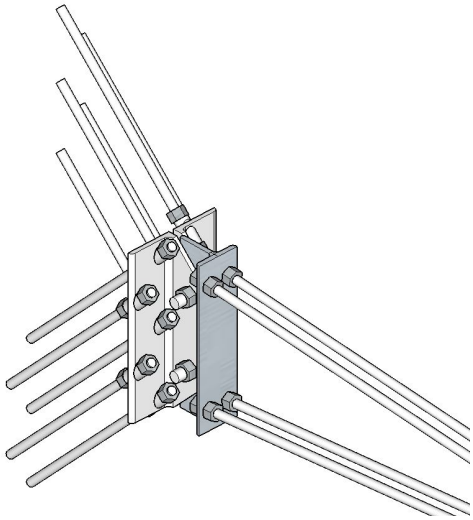

Figure 2.7: Connector with fasteners

2.4.4 Connection

An illustration of the full connection is given in Figure 2.8. One of the biggest positive aspects of this connection is its practicality in the assembly phase. Both inserting the fasteners and attaching the L- and T-profiles can be done before the components arrive on site. Once on site it is just the prestressed bolts that need to be tightened. This means that a full 24 m^2 flooring system can be assembled by fastening a total of 8 bolts, 2 per connection. The challenge is to give the connection satisfying strength and stiffness. The most important factors to achieve high rotational stiffness for this connection are believed to be:

- Thicknesses of profiles
- Rod-to-grain angles
- Spacing between fasteners
- Friction parameters between profiles

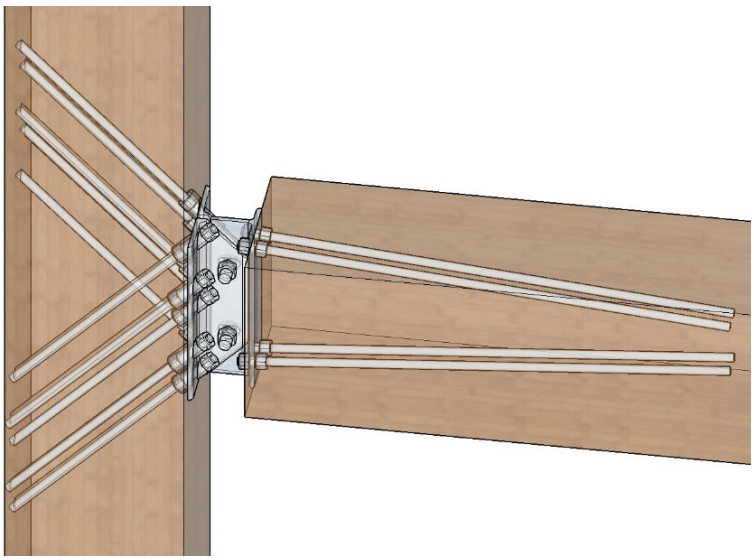

Figure 2.8: Full connection

3 Connection

This chapter describes the work done to further improve the solution described in chapter 2. The steel connector and the configuration of the fasteners in the beam and column have been further optimized.

First, relevant choices made regarding the general numerical modeling in the FEM- software Abaqus, and the theory behind them, will be explained. A modeling technique with a simplified representation of the threaded rods will then be used to optimize the connector and the locations of the fasteners, and a final proposal for the connector will be presented. Finally, models using a detailed representation of the threaded rods are used to test different rod-to-grain angles and a few other parameters.

3.1 Numerical modelling in Abaqus

Abaqus is a general-purpose finite element analysis program that enables the user to solve complex structural problems with the use of numerical solutions. In Abaqus, standard simulations have been used to run the analyses, which solves the numerical problem defined implicitly. The numerical problems solved in this thesis were linear static problems, and linear static analyses were thus applied in Abaqus.

In this section, theory related to numerical modelling, and how the numerical models were defined in Abaqus in general, will be presented. Only theory that was necessary for the choices made in the numerical models will be reviewed.

3.1.1 Element type

Choosing the right type of elements when modelling in Abaqus is important, as this can have a big effect on both simulation time and the accuracy of the results. When further developing the beam-to-column connection, using 3D solid elements in the models was essential [18]. All components in the connection were therefore modeled as solid elements and assigned the robust three-dimensional continuum element type C3D8.

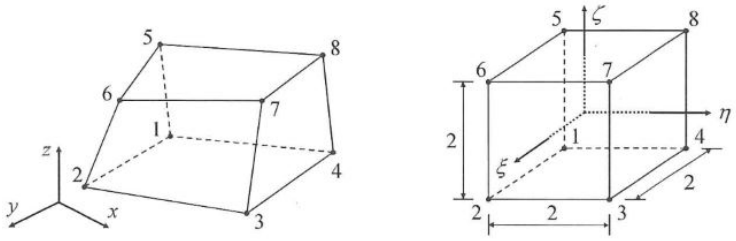

Figure 3.1: 8-node brick element, also referred to as the trilinear hexahedron element [24]

C3D8 is an eight-node linear brick element, fully integrated with 2x2x2 integration points, and representation of displacement in each direction x, y and z [23]. C3D8 is a plane stress/plane strain element which requires displacement continuity between the elements of the model [24].

The main concern regarding the C3D8 element is that it exhibits shear locking when asked to display the beam-bending mode due to spurious shear strain. This results in overly stiff behavior in bending, due to energy going into shearing the element rather than bending it [24].

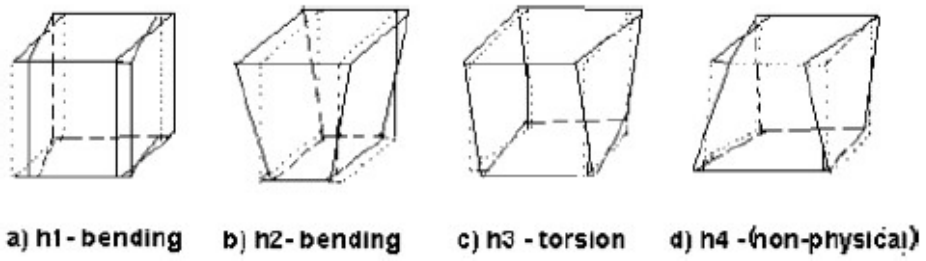

Figure 3.2: Spurious mode patterns [18]

To avoid this problem the reduced integration element C3D8R can be used. Due to reduced integration, the locking phenomena in the C3D8 element do not show, since it just has one integration point at the centroid which softens the behavior of the element. The reason for this is that some polynomial terms are zero at the Gauss points of a low-order rule and thus make no contribution to the element stiffness [25]. Reduced integration elements also reduces the computational time, which may be important for large numerical problems [23].

However, these elements exhibit other shortcomings such as hourglassing. This can be a concern in stress and displacements analyses, as hourglassing easily can propagate through the mesh and give unreliable results [23]. It occurs when the elements deform in such a manner that the strain calculated at the integration points is equal to zero, meaning the deformation is a zero-energy mode, which implies deformation but no strain in the integration points [24]. This is noticeable when hourglass-looking shapes can be seen in the deformed shapes of the elements in Abaqus. Built-in hourglass controls that limits the problems are available in Abaqus, but they

should be used with reasonably fine meshes and the artificial energy used to control hourglassing must be verified less than 1% relative to the internal energy [23,25].

Even though reduced integration elements have some advantages compared to the full integration elements, the chosen element in this thesis has been the C3D8 element, that is full integration. The beam-to-column connection that was modeled in this thesis involved several contact interactions between different parts. Full integration elements are better suited for numerical problems that involves contact between parts and provides more accurate results. Reliable results achieved from the simulations were essential in order to correctly evaluate the connection and achieve results comparable to what can be expected in experimental testing. Full integration elements were therefore preferred rather than reducing the computational time by using reduced integration elements.

3.1.2 Contact interactions

Numerical models involving contact between several parts, lead to different interactions that need to be considered. This results in complex numerical problems. In the connection, there were mainly two contact interactions that had to be implemented in the numerical models. These were the interaction between the connected steel profiles in the LT-connector, and the interaction between the threaded rods and timber elements. The two contact interactions are shown in Figure 3.3.

Abaqus defines three different approaches for modelling contact [23]:

- *General contact*
- *Contact pairs*
- *Contact elements*

The first two are surface based and recommended to use if possible [23]. For all simulations carried out in this thesis, the general contact approach was used, as this offers capabilities to model surface-to-surface contact which was the primary formulation used [23].

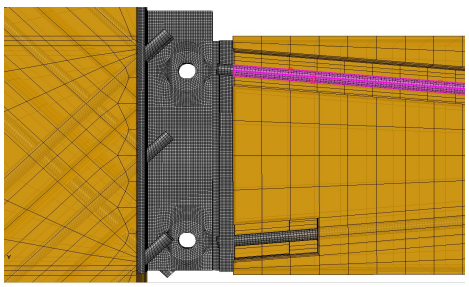

(a) Rod-wood interaction, pink surface

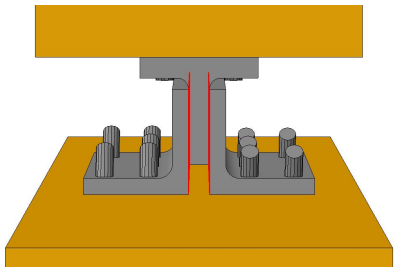

(b) Interaction between steel parts in LT-connector, red surface

Figure 3.3: Contact interactions in connection

3.1.2.1 Friction

As described in section 2.4, the steel profiles in the connector will be connected using prestressed bolts, which will be exposed to shear forces in the connection. The surfaces between the connecting parts and their frictional resistance will have an influence on the design force of the prestressed bolts. The clamping pressure which occurs between the connected parts, due to pre-tensioning of the bolts, enables load to be transferred by frictional resistance [26]. Hence, the connection between the steel profiles can be described as a friction connection. How the load is transferred between the connected surfaces can be seen in Figure 3.4.

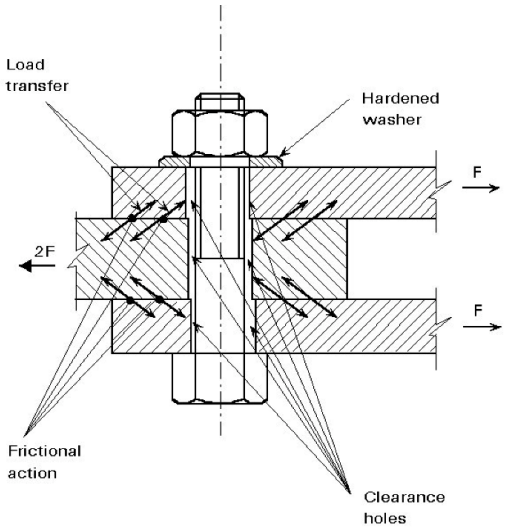

Figure 3.4: Load transfer in friction connection with prestressed bolts [26]

In order to implement the frictional behavior of the connecting parts in the numerical models, the mechanical contact properties must be defined. The relevant mechanical contact properties in this thesis were:

- *Normal behavior*
- *Tangential behavior*

Normal behavior

Normal behavior defines the contact pressure-overclosure relationship between the connecting surfaces [23]. When defining normal behavior, the default and most common contact pressure-overclosure relationship is *hard* contact. Here, pressure can only be transmitted once the surfaces are in contact. If no contact is established between the connecting surfaces, no pressure is allowed to be transmitted [23], see Figure 3.5.

In the numerical models, the hard contact relationship was chosen as this minimizes the penetration of the slave surface into the master surface at the constraint locations and does not allow the transfer of tensile stresses across the interface [23].

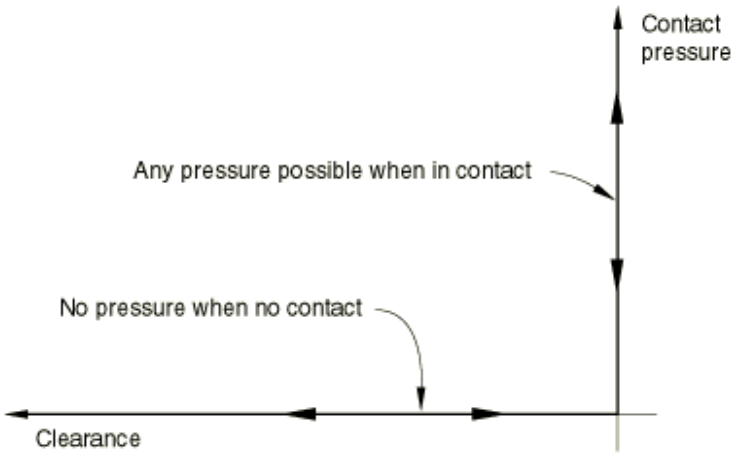

Figure 3.5: Hard contact pressure-overclosure relationship

Hard contact offers three different constraint enforcement methods:

- *Penalty*
- *Augmented Lagrange*
- *Direct*

as well as a *default* constraint enforcement method that depends on the interaction characteristics used [23].

Baartvedt & Pharo analyzed and compared different constraint enforcement methods in their study [19], focusing on the differences between the methods penalty, augmented Lagrange and default. Results from running simulations on a simplified numerical model of the connection, showed little to no variation between the methods used. The default method however, was facing some convergence issues when running simulations, while augmented Lagrange and the penalty method nearly gave the same results. The penalty method reduces the number of iterations which gives a lower computational time, especially for larger numerical problems [23]. Since results seemed to be independent of the method used, and that penalty was more computationally efficient, this was the preferred method used for simulations carried out in this thesis.

Tangential behavior

The tangential behavior defines how friction between connecting surfaces is applied in Abaqus. There were mainly two interesting schemes for defining the friction formulation in the numerical models, being the *penalty* and *Lagrange multipliers* scheme.

By default, penalty scheme is used by Abaqus as the primary method to impose friction constraints. This scheme allows some relative motion of the connecting surfaces, when they should be sticking, where the shear stress is set proportional to the relative motion of the surfaces, see Figure 3.6 [23]. The amount of relative motion depends on slip tolerance and contact surface length. This is in difference to the Lagrange multipliers approach, which strictly enforces the sticking regions and does not allow any relative motion of the surfaces until a critical shear stress is attained [23]. The Lagrange multipliers scheme can therefore produce more accurate results than the penalty scheme, but at a higher computational cost due to an increased number of iterations needed for a converged solution [23].

Baartvedt & Pharo compared the two methods in their project study [19], by running simulations on a simplified numerical model of the connection, where only the friction formulation was the changing parameter. The stiffness results extracted from the simulations showed no difference between the two friction constraints. However, since this was a fairly simplified numerical model, and larger numerical problems are to be simulated in this thesis, the penalty approach was chosen. This was considered the best option as the penalty approach reduces the computational time and minimalizes overconstraints that may occur using Lagrange multipliers scheme, which can prevent convergence for large numerical problems [23].

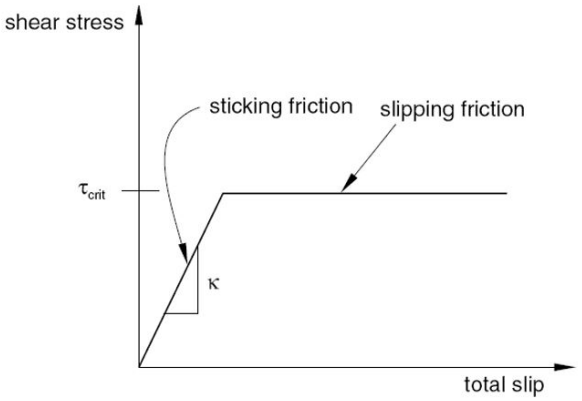

Figure 3.6: Frictional behavior with the penalty enforcement method [23]

The friction coefficient value can be a function of several parameters. For the numerical models in this thesis, the friction coefficient was taken as a constant value equal to $\mu = 0.45$. This is the same value used in previous simulations done by Baartvedt & Pharo [19]. However, the control of the friction coefficient between the connected parts is very important, as it influences the slip factor of the mating surfaces of the plate which is decisive for the shear resistance in a friction connection [26]. A study regarding the friction coefficient value was planned but was not carried out in this thesis due to a lack of time.

Master and slave surfaces

When two surfaces are in contact, they are not allowed to include any of the same nodes, and hence it must be decided which surface will be the slave and which will be the master [23]. To select the appropriate master and slave surfaces can be crucial for any interaction. Usually, if the surfaces are of comparable size, the master surface should be the surface of the stiffer body or should have coarser mesh than the slave surface [23]. In other cases, it is best to choose the larger surface as the master surface.

The choice of master and slave surfaces can have a significant effect on performance of the simulation, but the effect on the results with a surface-to-surface contact formulation is less noticeable [23]. This was indicated in the project study by Baartvedt & Pharo [19]. With a simplified numerical model of the connection, two simulations were conducted, changing only the master and slave surfaces between the connected steel profiles in the LT-connector. Comparison between the two simulations gave no difference in results, nor in the performance of the simulations. However, as the comparison were done on relatively simple numerical models, it was believed that the choice of master and slave surface could have a larger effect on the numerical models simulated in this thesis, as they were more detailed. The guidelines on how to select master and slave surface was thus chosen as recommended in the Abaqus user's manual [23].

For the friction interaction between the steel profiles in the LT-connector, the slave surface has been appointed to the T-profile while the larger L-profiles was chosen as master surface, see Figure 3.7. This was applied for all numerical models simulated in this thesis.

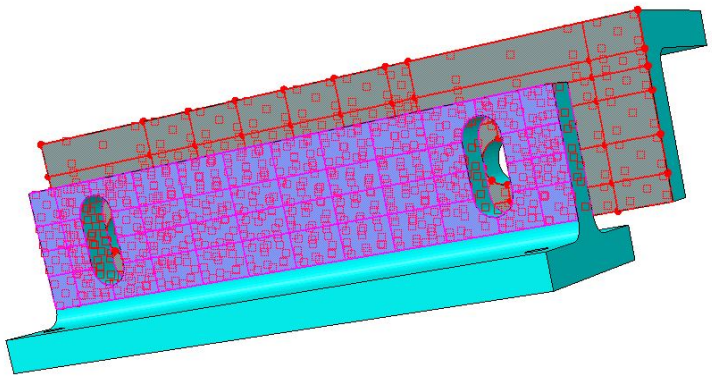

Figure 3.7: Slave and master surface displayed in pink and red respectively.

Small versus finite sliding

Abaqus provides two sliding formulations for defining relative surface motions of two bodies with respect to each other, namely *small* and *finite* sliding. Both formulations allow the connecting surfaces to undergo large motions and rotation [23,27]. However, with small sliding formulation only a relatively small amount of sliding of one surface along the other is allowed, but arbitrary rotation of the connecting bodies is permitted [27]. In finite sliding there is separation and sliding between the two surfaces, and arbitrary rotation is allowed [27]. The advantages with small sliding contact is that it requires less computational time than finite sliding contact, as it is an approximation of the general contact master-slave algorithm [23,27].

Which formulation that will be suitable is often difficult to predict, as it depends on the relative amplitudes of the displacements involved. Baartvedt & Pharo performed simulations comparing the two formulations in their project study [19]. The results obtained gave no variation of results, leaving small sliding as the favorable formulation in this thesis due to the lower computational time.

3.1.2.2 Cohesive zones

The rod-wood interaction between the threaded rods and the timber elements was solved using cohesive zones in Abaqus. Cohesive zones are for most parts implemented in fracture analyses and used to simulate crack growth. However, the use of cohesive zones to simulate the withdrawal of threaded rods has been proven to be applicable [18].

Cohesive zone models

Cohesive zone models are based on the theory of linear elastic fracture mechanics and can be useful in many different varieties of fracture issues in homogeneous solids. They do not represent any physical material but describes the cohesive force which occur when material elements are being pulled apart [23]. The method behind cohesive zone modelling are based on concepts proposed independently by Barenblatt [28] and Dugdale [29], who used cohesive zones to represent a crack propagation path.

Traction-separation law

In Abaqus, cohesive zone models can be implemented by using either cohesive zone elements or cohesive surfaces. The latter is the method used in this thesis. The cohesive surfaces are defined as a surface interaction property, which means that it uses material properties as interaction properties [23]. A linear elastic traction-separation law is used to describe the material separation and are defined in each fracture mode by an initial elastic stiffness. The relationship between traction (force) and separation (displacement) is displayed in Figure 3.7 by the bi-linear traction-separation response curve.

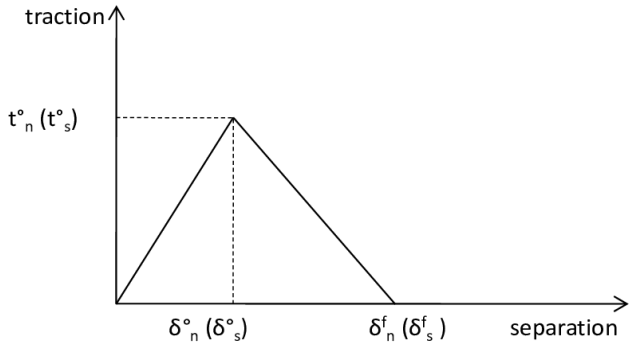

Figure 3.8: Bi-linear traction-separation response curve [23]

Abaqus utilizes this relationship to simulate the elastic behavior up to the cohesive strength, δ_n^o and subsequent softening, to model the degradation of material properties up to failure, δ_n^f. In order to describe the material behavior from linear elastic to failure, both damage initiation and damage evolution needs to be specified. However, in this thesis only the linear elastic behavior was of interest.

The traction-separation model in Abaqus assumes a linear elastic behavior, where the elastic behavior is written in terms of a constitutive matrix **K,** containing the stiffness parameters [23]. The elastic behavior is written as:

$$\mathbf{t} = \begin{Bmatrix} t_n \\ t_s \\ t_t \end{Bmatrix} = \begin{bmatrix} K_{nn} & K_{ns} & K_{nt} \\ K_{ns} & K_{ss} & K_{st} \\ K_{nt} & K_{st} & K_{tt} \end{bmatrix} \begin{Bmatrix} \delta_n \\ \delta_s \\ \delta_t \end{Bmatrix} = \mathbf{K\delta} \tag{3.1}$$

In this thesis, no coupling between stiffness coefficients was specified, therefore all the terms outside the diagonal of the **K** matrix were assumed zero. The elastic behavior can then be written as:

$$\mathbf{t} = \begin{Bmatrix} t_n \\ t_s \\ t_t \end{Bmatrix} = \begin{bmatrix} K_{nn} & 0 & 0 \\ 0 & K_{ss} & 0 \\ 0 & 0 & K_{tt} \end{bmatrix} \begin{Bmatrix} \delta_n \\ \delta_s \\ \delta_t \end{Bmatrix} = \mathbf{K\delta} \tag{3.2}$$

where K_{nn}, K_{ss} and K_{tt} are the cohesive zone stiffness properties in normal, first shear and second shear direction.

Cohesive withdrawal properties

The elastic stiffness properties were simplified to $K_{tt} = K_{ss}$. Based on an ongoing study by Stamatopoulos, Vilguts & Malo [30], $K_{tt} = K_{ss} = 18.5$ kNm/rad was used as cohesive input values in all numerical models in this thesis. As it is assumed that K_{nn} has a minor influence when the rods are subjected to a vertical force, $K_{nn} = 10^8$ kNm/rad was used as input value in all models [18,30].

Cohesive zones utilized in Abaqus

Two different approaches for simulating the withdrawal of the threaded rods using cohesive zones were utilized in Abaqus. These will be referred to as the *cylindrical rod model* and *threaded rod model* and are displayed in Figure 3.9.

The cylindrical rod model used a single cylindrical part to represent a rod. The rod-wood interaction was then idealized as a cylindrical interaction between steel and wood, defined with cohesive surfaces. This approach reduced the number of elements and was therefore more computationally efficient.

The threaded rod model used a more detailed modelling technique which included the thread of the rods. This modeling technique was developed by Postdoctoral Fellow Haris Stamatopoulos [30], and is thoroughly explained in section 4.3. However, the cohesive withdrawal properties in both approaches were equal and as given above.

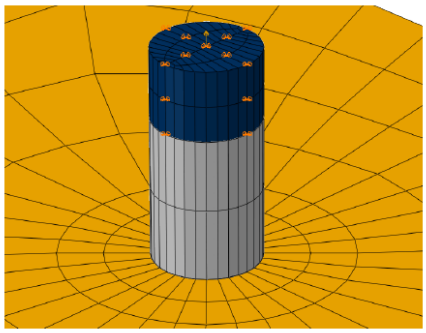

(a) Cylindrical rod model [18]

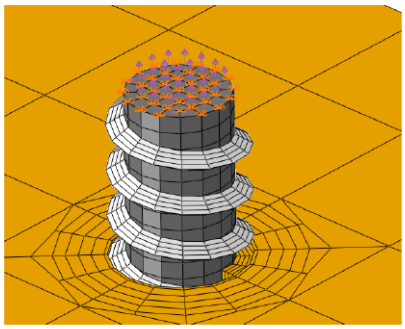

(b) Threaded rod model [30]

Figure 3.9: Withdrawal approaches used in Abaqus

3.1.3 Boundary conditions and load

Boundary conditions and loads were applied to the geometric regions of the parts rather than the mesh itself. This made it easy to vary the mesh without re-specifying the loads and boundary conditions. An overview of how the boundary conditions and loads were applied in the numerical models is shown in Figure 3.10 (a).

Boundary conditions were applied to single lines on the top and bottom surfaces of the column, preventing any displacements in x-, y- and z-direction. The top and bottom of the column in the model represents the middle points between two stories in a real frame. By applying boundary conditions to a single line only, the column is allowed to rotate at these points, which would be the case in a real frame. The beam was prevented from lateral movement in the loading area.

A load was applied at a distance L from the column face on top of the beam surface, where the distance dependent on the numerical model simulated. To prevent convergence issues during simulations, the loading applied was defined as a boundary condition with a predetermined displacement in the negative vertical direction with total value of u = 20 mm, rather than a point load. Therefore, to determine the moment acting in the connection, the reaction forces in the column had to be extracted from the models.

To reproduce the effect of the prestressed bolts connecting the steel profiles in the LT-connector, pressure forces were applied to predefined surfaces surrounding the bolt holes on each side of the connector, see Figure 3.10 (b). The predefined surfaces had radius r = 40 mm, to simulate the washers size, and the pressure force used was a total force of 600 000 N per bolt. The forces representing the bolts were applied in a step before the vertical displacement was enforced, so the connection had the full effect of the friction connection when loaded.

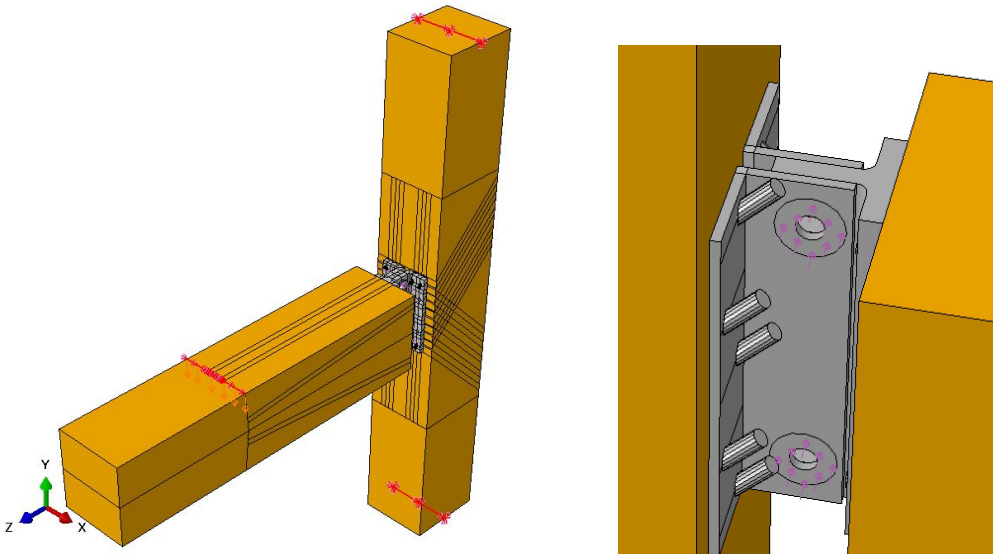

(a) Overview of BC and loads (b) Pressure load applied on predefined surfaces

Figure 3.10: Boundary conditions and loads applied to the model geometry in Abaqus

In Figure 3.10 (a) the boundary conditions are marked in red, while the load is marked in orange. The model displayed in the figure does not necessarily represent the different configurations simulated in this thesis, but the intent of the figure is to display how the boundary conditions and loads were applied to the models.

3.1.4 Material properties

For the numerical simulations, only the elastic material properties were defined, as plastic behavior was not of interest in this thesis. The anisotropic behavior of timber can be approximated as orthotropic material in Abaqus. A numerical study carried out by Stamatopoulos & Malo [15] showed that there was little difference between modelling wood as fully orthotropic and transversely isotropic. Hence, the material was defined as transversely isotropic, giving equal properties in the radial and tangential direction. The elastic material properties used in the numerical simulations for timber and steel, are displayed in Table 3.1. It was chosen to use the same material properties as Drageset & Hoff [18].

Table 3.1: Material properties

Material	Material property	Symbol	Value	Input for simulation
Wood	Mean density [$\frac{kg}{m^3}$]	ρ_M	470	470
	Moduli of Elasticity [MPa]	$E_{0,mean} = E_L$	13000	1300
		$E_R = E_T$	410	410
	Shear Moduli [MPa]	$G_{0,mean} = G_{LR} = G_{LT}$	760	760
		G_{RT}	65	30
	Poissons ratios	ν_{LR}	0.501	0.6
		ν_{LT}	0.695	
		ν_{TR}	0.315	0.6
		ν_{RT}	0.835	
Steel	Mean density [$\frac{kg}{m^3}$]	ρ_M	7850	7850
	Moduli of Elasticity [MPa]	$E_{0,mean} = E_L$	210000	210000
	Poissons ratios	ν	0.3	0.3

3.1.5 Calculation of rotational stiffness

The rotational stiffness of the connection was estimated by measuring the horizontal displacement in a total of eight places. Four measuring points were located on the beam, one in each corner. To take into account the lateral movement of the column, four measuring points were also located here. These were located at the edges of the column facing the connector in equal heights as the measuring points on the beam. The measuring points can be seen in Figure 3.11, marked as red dots.

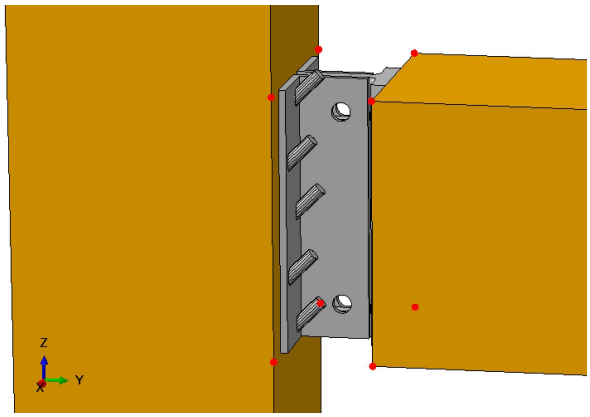

Figure 3.11: Locations for measuring points for horizontal displacement in beam and column

As seen in the figure above, two measuring points were located in the same height on the upper and lower part of both the beam and column. This was done to take into account unsymmetrical horizontal displacement on each side of the vertical symmetry line of the column, due to the opposite directions of the inclined rods on each side.

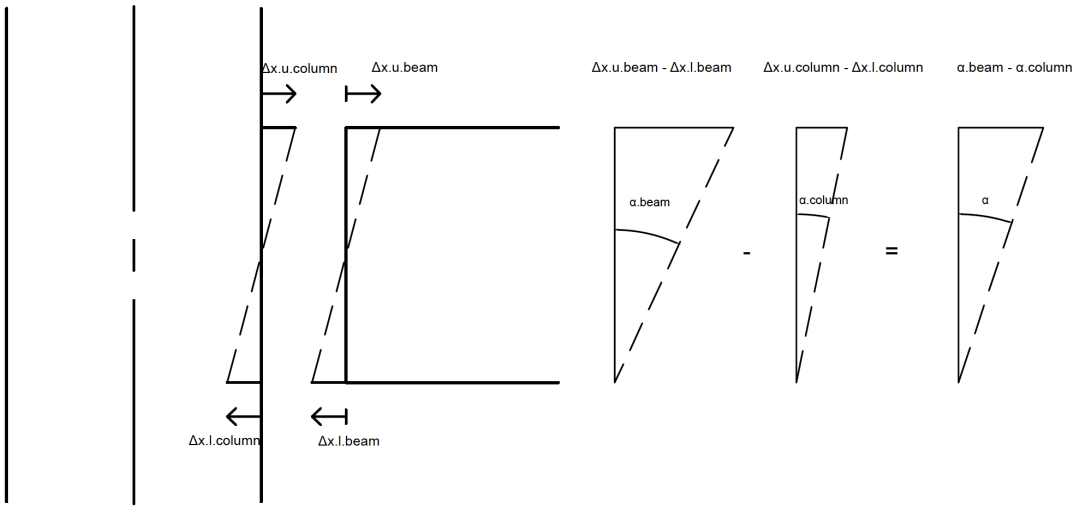

Figure 3.12: Illustration of displacements and rotation in column and beam

The upper and lower horizontal displacements in both the beam and column were calculated by taking the average displacements between the two measuring points in same height. Labels in the equations below are explained in Figure 3.12.

$$\nabla_{x.u.beam} = \frac{\nabla_{x.u.beam.1} + \nabla_{x.u.beam.2}}{2} \tag{3.3}$$

$$\nabla_{x.l.beam} = \frac{\nabla_{x.l.beam.1} + \nabla_{x.l.beam.2}}{2} \tag{3.4}$$

$$\nabla_{x.u.column} = \frac{\nabla_{x.u.column.1} + \nabla_{x.u.column.2}}{2} \tag{3.5}$$

$$\nabla_{x.l.column} = \frac{\nabla_{x.l.column.1} + \nabla_{x.l.column.2}}{2} \tag{3.6}$$

The rotation for each part was then calculated as:

$$\alpha_{beam} = \frac{\nabla_{x.u.beam} - \nabla_{x.l.beam}}{z} \tag{3.7}$$

$$\alpha_{column} = \frac{\nabla_{x.u.column} - \nabla_{x.l.column}}{z} \tag{3.8}$$

where z is the distance between the pair of forces in the beam. The value was assumed to be the same as the full height of the beam, giving:

$$z = 460mm \tag{3.9}$$

The rotation was then calculated by subtracting the rotation of the column from the beam:

$$\alpha = \alpha_{beam} - \alpha_{column} \tag{3.10}$$

Then, knowing the rotation, the estimated rotational stiffness could be calculated as:

$$K_{rot} = \frac{M_{Ed}}{\alpha} \tag{3.11}$$

where M_{Ed} was the moment acting due to the applied load situation:

$$M_{Ed} = L * F \tag{3.12}$$

Since the load was applied as displacement, the force, F, was extracted from the simulations by taking the sum of the reaction forces in the column in the longitudinal direction. L was set as the distance from the applied load to the column face.

3.2 Optimization of connector and rod placement

In this section, the steel profiles that constitutes the LT-connector, and the location of the rods in the column, will be optimized through simulations of numerical models, and a final proposal for the connector will be presented. During the process of optimizing the connection, several parameters were changed simultaneously, and not necessarily in a consistent order. However, to better understand the changes made and the effects of them, each parameter change will be discussed separately.

The improvements of the connection were limited to the connector and the fasteners, as the timber elements were predetermined. As the rotational stiffness has been the main focus of this thesis, this has been the most important parameter to consider when evaluating the changes made to the connection.

3.2.1 Defining numerical models

Using Abaqus made it easy to compare changes done to the connection as the rotational stiffness was easy to extract. This made it possible to evaluate the connection in each step and proceed with the best solution.

The connection in previous studies has been modeled with simplifications such as defining timber elements as rigid bodies and without including the withdrawal of the threaded rods [19]. In this thesis, every aspect of the connection has been included in the numerical models. This was important in order to correctly determine the expected behavior and stiffness of the connection in real life. The dimension used in the models for the beam, column and rods are displayed in Table 3.2, and the material properties given in Table 3.1 were used as input values for the different materials.

Table 3.2: Element dimension used in numerical models

Element	Cross-section [mm^2]	Length [mm]
Beam	405 x 460	1000
Column	405 x 450	2000
Threaded rod	π x 11^2	N/A

All parts in the models are made of the solid eight-node linear brick element C3D8 and are meshed using a structured meshing technique to avoid excessive distortion of elements due to complicated geometry. The mesh parameters used for the parts are listed in Table 3.3 in form of global seeds. The connector and the fasteners are assigned a much higher mesh density than the timber elements, as only improvement of the connector and fasteners were of interest.

Assigning a coarser mesh to the timber elements reduced the computational time which was preferred for the simulations.

Table 3.3: Global seeds assigned elements

Element	**Global seed [mm]**
L-profiles	3
T-profile	3
Steel rods	5
Timber	50

The Cartesian coordinate system of the models is given by the y-axis in the longitudinal direction of the beam and the z-axis in the longitudinal direction of the column, see Figure 3.13. Load and boundary conditions were applied as described in subsection 3.1.3, and L = 1.2 m was used as distance to the load applied on the beam surface. This was the same distance used by Baartvedt & Pharo in their simulations [19].

Friction surfaces was appointed as described in sub-subsection 3.1.2.1, and pressure force was applied to simulate the prestressed bolts connecting the steel profiles. To simulate the withdrawal of the rods, cohesive zones were utilized, using the parameters and configurations described in sub-subsection 3.1.2.2. The cohesive zones were defined for the cylindrical interaction surfaces between steel and wood with the cylindrical rod model, see Figure 3.9 (a).

The rotational stiffness was calculated as described in section 3.5, with the measuring points for extraction of the horizontal displacements located as shown in Figure 3.11. An overview of the model is displayed in Figure 3.13.

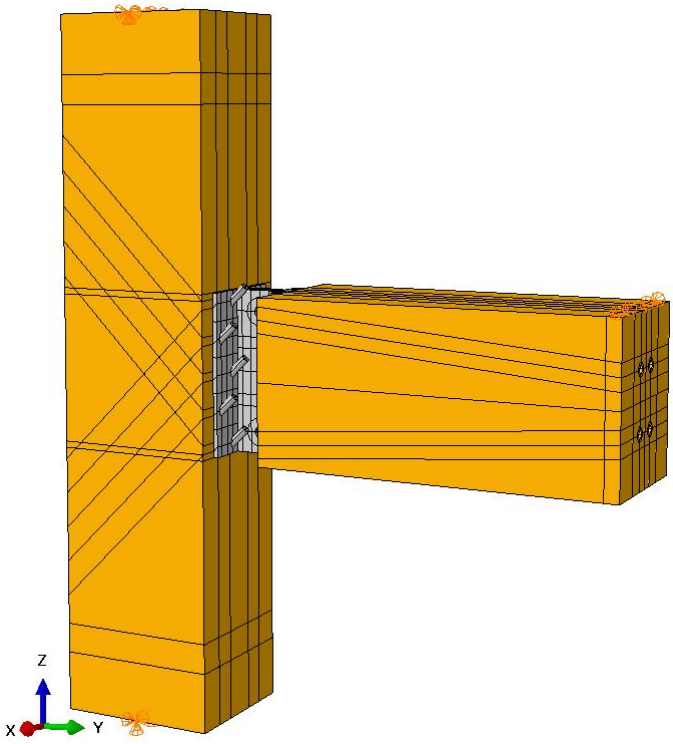

Figure 3.13: Overview of numerical model used for optimization

3.2.2 Rod placement in column

The importance of rod-to-grain angle and embedment length when considering the stiffness of threaded rods in timber elements are well documented and evaluated in previous work, as described in section 1.3, and will not be evaluated in this subsection. For the connection investigated in this thesis, there were bigger uncertainties on where to place the rods in the timber elements and how different locations of the rods would affect the rotational stiffness of the connection.

Figure 3.14 (a) displays how the rods connecting the two L-profiles to the column originally were placed and labels the individual rods for further reference. As mentioned in section 2.4, ten inclined rods were threaded in the column, all with 45° rod-to-grain angle, five on each side of the vertical centerline of the column. The rods on each side of the centerline point in opposite directions. The five rods connected to each L-profile were oriented in two parallel lines of two and three. This increased the distances between the rods and kept the local stresses around the nut heads from overlapping. These advantages were important to maintain.

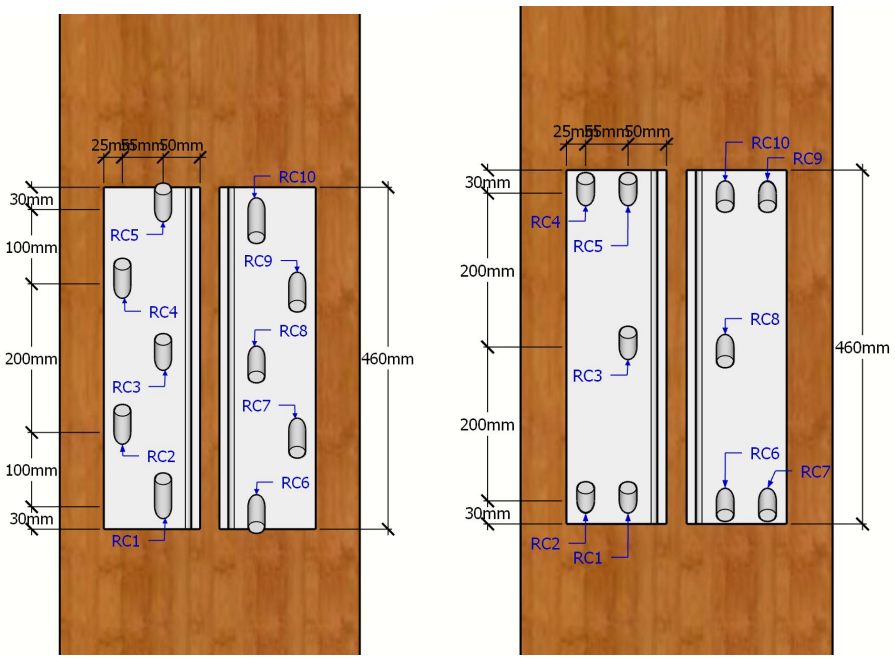

(a) Original rod placements (b) New rod placements

Figure 3.14: Rod placements in column

Optimizing rod placement

The rod placements in the column were evaluated by extracting the stress distributions for the rods from a simulation with the original location of the rods, described as configuration 1 in Table 3.4. The stress distributions are displayed in Figure 3.15, and shows that the upper rods RC5 and RC10, and the lower rods RC1 and RC6, were exposed to high stresses and

displacements compared to the remaining rods located closer to the middle of the connection. This was predicted, as the lower stressed rods were centered closer to the horizontal neutral axis.

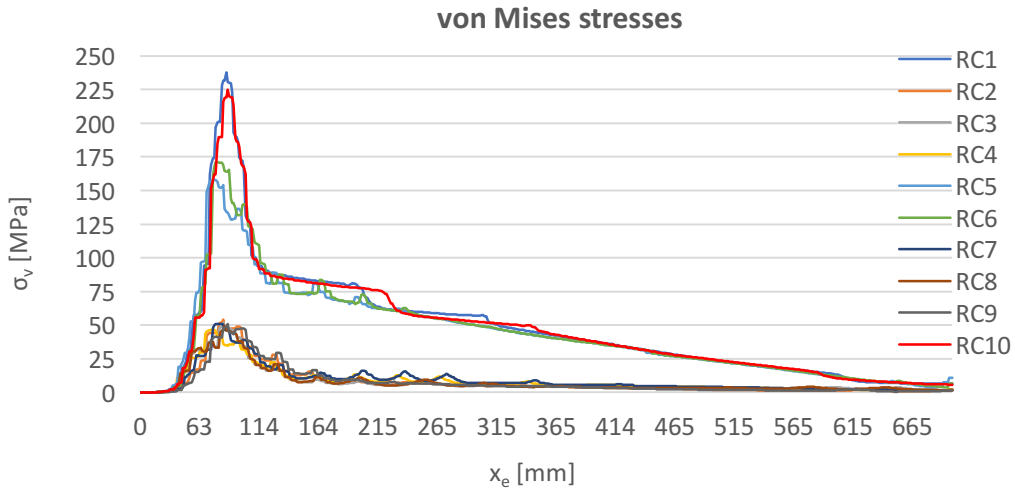

Figure 3.15: Von mises stress distribution in rods for old rod placements. Acting moment in connection: 25.46 kNm

While it was of interest to keep rod RC3 and RC8 at their original places due to their contribution to shear forces, rods RC2, RC7 where moved up, and rods RC4 and RC9 where moved down so they were in parallel horizontal lines with rods RC1 and RC6, and RC5 and RC10 respectively. This would increase the distance from the neutral axis for the moved rods, which was assumed to increase the rotational stiffness for the connection, and result in a more even distribution of stresses between the rods. The new locations of the rods are displayed in Figure 3.14 (b).

A configuration containing the new rod placements in the column was simulated for comparison, listed as configuration 2 in Table 3.4. Since the L-profiles were very thin, only 12 mm thick, it was assumed that the new rod placement would not have a significant effect on the rotational stiffness, as the L-profiles would be too weak to take advantage of the new rod placement. It was therefore decided to model the same two configurations with thickness 20 mm for the L-profiles, listed as configuration 3 and 4 in Table 3.4. The T-profile was modeled with the same dimension as the final proposal from Baartvedt & Pharo [19]. The results are presented in Table 3.4.

Results

Table 3.4: Comparison between different positioning of the rods in the column

Configuration	Rod placements	Thickness L-profiles [mm]	Thickness T-profile [mm]	$K_{\theta_{tot}}$ [kNm/rad]	Change in $K_{\theta_{tot}}$ from previous configuration [%]
1	Old	12	26	8180	-
2	New	12	26	8338	+ 1.93
3	Old	20	26	9484	-
4	New	20	26	10 262	+ 8.20

The new placement of the rods greatly improved the rotational stiffness when L-profiles were modeled with thickness 20 mm, making the connection 8.2 % stiffer. As predicted, the effect of the new rod placements when using L-profiles with thickness 12 mm was very small. This also proved that increasing the thickness was necessary to further stiffen the connection. This follows in subsection 3.2.3.

The stress distributions for the rods from the new rod placement, seen in Figure 3.16, did not improve as much as expected. This was mainly because the force acting in the connection was reaching the rods in the vertical line closest to the center of the column first, and as a result they will be more exposed. Small improvements were noticed for the rods that were moved, and since the rotational stiffness was the most important parameter, the new placement of the rods was kept.

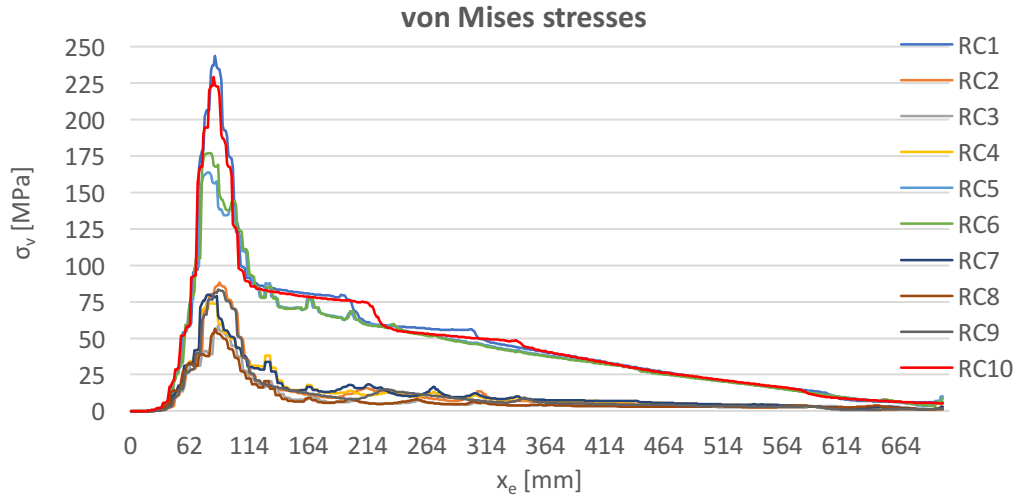

Figure 3.16: Von mises stress distribution in rods with new rod placements. Acting moment in connection: 25.96 kNm

The stiffness value of configuration 4 in Table 3.4 was still not good enough when considering that the numerical models in previous studies have revealed themselves as too stiff compared to what can be expected in experimental testing [18]. As the required rotational stiffness is between 10 000 – 11 000 kNm/rad in a medium-rise building with 30 m total height [20], further improvements of the connection were necessary. Since the timber elements were predetermined, these improvements were implemented in the steel connector.

3.2.3 L-profiles

The L-profiles were assumed to be the critical parts of the LT-connector, mainly because they were designed with a relative small thickness, compared to the T-profile. Changes to both L-profiles were therefore assumed necessary in order to improve the rotational stiffness. This was also briefly indicated by the results in Table 3.4. To observe how the profiles in the connector deformed relative to each other, and to compare their stress distributions, the deformation pattern from configuration 2 in Table 3.4 was examined and are displayed in Figure 3.17. As only the connector is of interest, the timber elements and rods are left out of the figure.

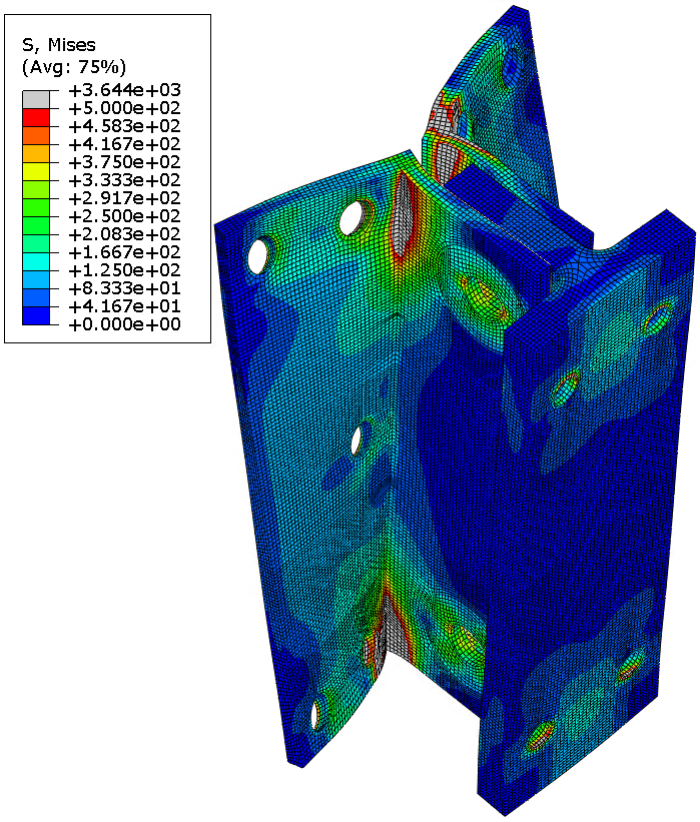

Figure 3.17: Deformation pattern of connector, magnified by a factor of 30. Grey areas indicate stress levels greater than 500 MPa. Acting moment: 77.88 kNm

As seen in Figure 3.17, excessive bending in the top and bottom of both L-profiles occurred, as well as a more concentrated stress distribution compared to the stiffer T-profile. This clearly indicates that the L-profiles were the weakest parts in the connector and were a limiting factor to the overall rotational stiffness of the connection. Hence, improvements to the L-profiles were essential.

Several ideas were discussed on how to strengthen and improve the L-profiles. The ideas believed to give the largest improvements are discussed in this subsection.

3.2.3.1 Increased thickness

Baartvedt & Pharo concluded in their project study that increasing the thickness of the L-profiles was necessary in order to increase the overall stiffness of the connection [19]. This was based on results from where the thickness of the T-profile was changed from 13 mm to 26 mm, which gave an increase in rotational stiffness of approximately 17 % for the connector [19]. Similar results were expected when increasing the thickness of the L-profiles.

Increasing the thickness of the L-profile would only be beneficial to a certain extent. It was believed that after a certain thickness, other parts of the connection would be significantly weaker than the L-profiles, for example withdrawal of rods, making any further increase in thickness inefficient. It was therefore decided to increase the thickness of the L-profiles in multiple steps, to examine how the increase rate of rotational stiffness changed with the increased thickness.

Changing the thickness of the profiles in Abaqus was a time-consuming process, as both profiles and the column had to be adjusted and partly modeled from scratch each time. Increasing the thickness of the profiles also led to some design issues, mainly for the inclined holes going through the profiles. Since the location of the holes were determined based on the rod placements in the column when profiles had thickness 12 mm, see Figure 3.14 (b), it was necessary to relocate the holes as the thickness increased. Since the holes were inclined with an angle of 45°, the edge distance for the lower and upper holes were not sufficient when the profiles were modeled with greater thicknesses.

In Figure 3.18 (a) the original L-profile with thickness 12 mm is displayed with dimensions and rod placements as proposed when the profiles were first designed [19]. Here, the holes going through the profile have sufficient edge distance. L-profiles with 20 mm thickness is displayed in Figure 3.18 (b) and (c) with the same location for the inclined holes as in Figure 3.18 (a). In these cases, the two lower and upper holes passes either below or above the edge on the backside of the profiles, depending on the direction for the inclined rods.

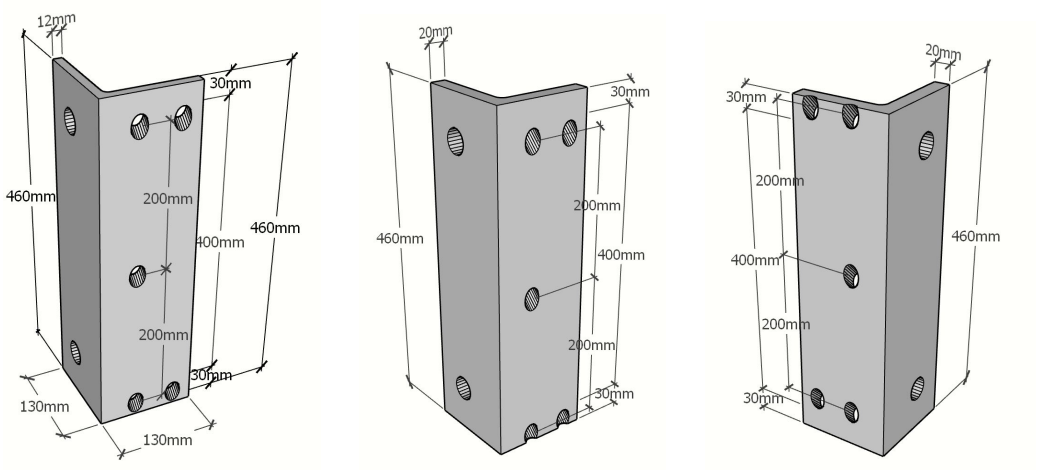

(a) 12 mm profile (b) 20 mm profile (c) 20 mm profile

Figure 3.18: Location of inclined holes for rods in L-profiles with various thickness

While this was assumed to have a minor effect on the rotational stiffness, it would not be a sufficient solution if the profiles were to be designed for experimental testing. To maintain a sufficient edge distance on the backside of the profiles as the thickness changed, the lower and upper holes had to be relocated, giving new edge distances.

The final layout for the inclined holes is shown in Figure 3.19. Here, a new edge distance to the lower edge was set to 60 mm, instead of the original 30 mm. This would secure sufficient edge distances for when the profiles would be made even thicker than in Figure 3.18 (b). The height of the profiles was also changed from 460 mm to 520 mm, an extension of 60 mm. This was done in order to maintain the vertical distances between the holes as both the lower and upper holes had to be relocated. The upper holes were placed 80 mm from the top edge instead of 60 mm to prevent too large eccentricity between the upper rods in the column and in the beam. Therefore, the vertical distance between the holes was set to 190 mm for the innermost line, and 380 mm for the outermost line. The width of the profiles was kept unchanged, as well as the holes for the preloaded bolts connecting the L-profiles and T-profile together.

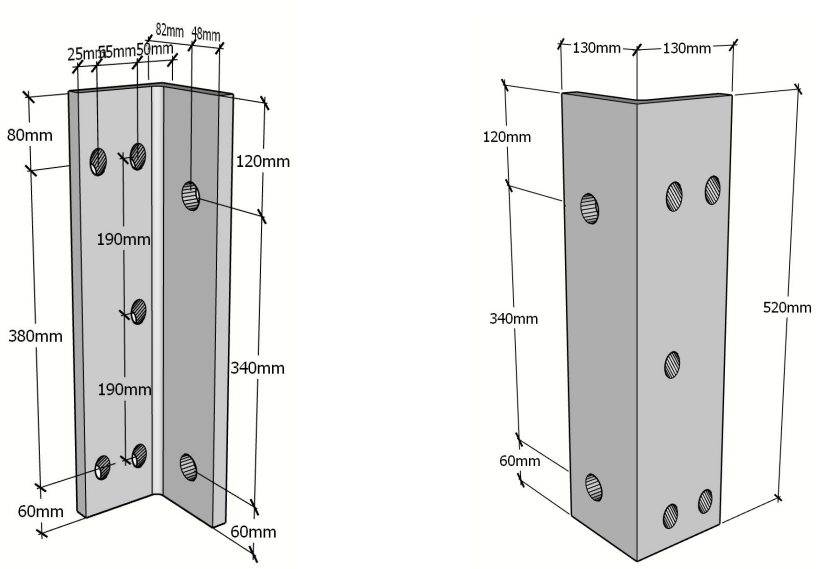

(a) Front-view (b) Back-view

Figure 3.19: Final layout for inclined holes in L-profile

In all simulation comparing different thickness, the profiles were modeled with a height equal to 520 mm. The effects and results of the extended height are thoroughly described in sub-subsection 3.2.3.2.

To examine the influence of increasing the thickness for the profiles, five models with varying thickness in the range from 12 - 40 mm were made and tested. The dimensions of the other parts in the connection remained unchanged, resulting in only the thickness of the L-profiles as the changing parameter. The five configurations simulated, with dimension used and their results, are presented in Table 3.5.

Results

Table 3.5: Comparison between L-profiles with various thickness

Configuration	**Thickness L-profiles [mm]**	**Height L-profiles [mm]**	**Thickness T-Profile [mm]**	$K_{\theta_{tot}}$ **[kNm/rad]**	**Change in** $K_{\theta_{tot}}$ **from previous configuration [%]**
1	12	520	26	8660	-
2	20	520	26	10 539	+ 21,71
3	26	520	26	11 808	+ 12,04
4	30	520	26	12 735	+ 7,85
5	40	520	26	13 796	+ 8,33

Increasing the thickness resulted in a significant improvement of the overall stiffness. Changing the thickness from 12 mm to 40 mm caused the connection to be nearly 60 % stiffer, where profiles with thickness 40 mm possessed the highest rotational stiffness. However, the rate of change in rotational stiffness decreased as thickness increased, as seen in Figure 3.20.

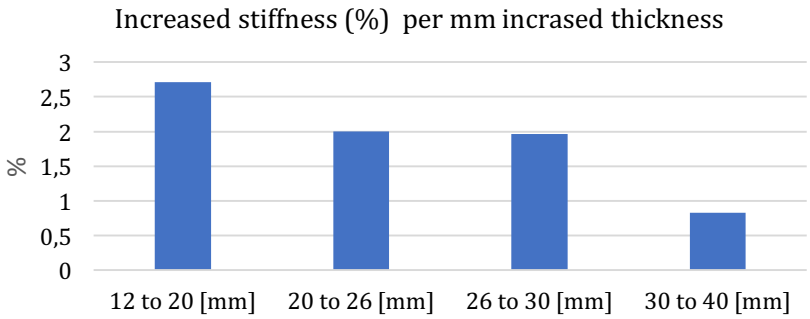

Figure 3.20: Increase in stiffness (%) per mm increased thickness

The increase rate of rotational stiffness was significantly reduced when the profiles were thicker than 30 mm. Between 20 - 30 mm the stiffness increased by approximately 2 % per mm increased thickness, while from 30 - 40 mm this was reduced to only 0.8 %. This was believed to be related to the withdrawal capacity of the rods. For thicknesses up to 30 mm the rods were virtually unaffected by the changes. This resulted in a thickness of 30 mm being chosen as the upper limit for the L-profiles without changing the dimensions or configuration of the rods.

Additionally, the magnitude of steel volume used to produce the profiles were desirable to maintain as low as possible. The cost of steel is relatively low, but for the assembly phase it was desirable to keep the profiles as light as possible while they still maintained sufficient capacity. Considering the relatively low increase in stiffness from 30 - 40 mm compared to the massive increase in steel volume, it was more to gain from investigating other parameters to be changed rather than continue to increase the thickness of the profiles.

3.2.3.2 Extended height

As mentioned is the previous sub-subsection, the edge distance for the holes in the profiles became an issue when increasing the thickness. To maintain the vertical distance between the holes and at the same time secure sufficient edge distances, the height of the profiles had to be increased. The height of the T-profile could not be increased due to restrictions from other parts of the flooring systems mentioned in subsection 2.4.1. The L-profiles could not be extended downwards due to the ceiling of the floor below, so the extension had to be made upwards.

Although the extended height was necessary for practical reasons, it was also assumed to have an impact on the rotational stiffness of the connection.

As only the extended height was necessary for the part facing the column, a solution was proposed where some of the top area on the part of the profiles facing the T-profile was reduced. This would reduce the amount of steel and were assumed to have minor effects on the rotational stiffness of the connection. This was done by cutting the L-profiles at an angle, so that the end face would have the same height as the T-profile of 460 mm. The solution with reduced height is shown in Figure 3.21.

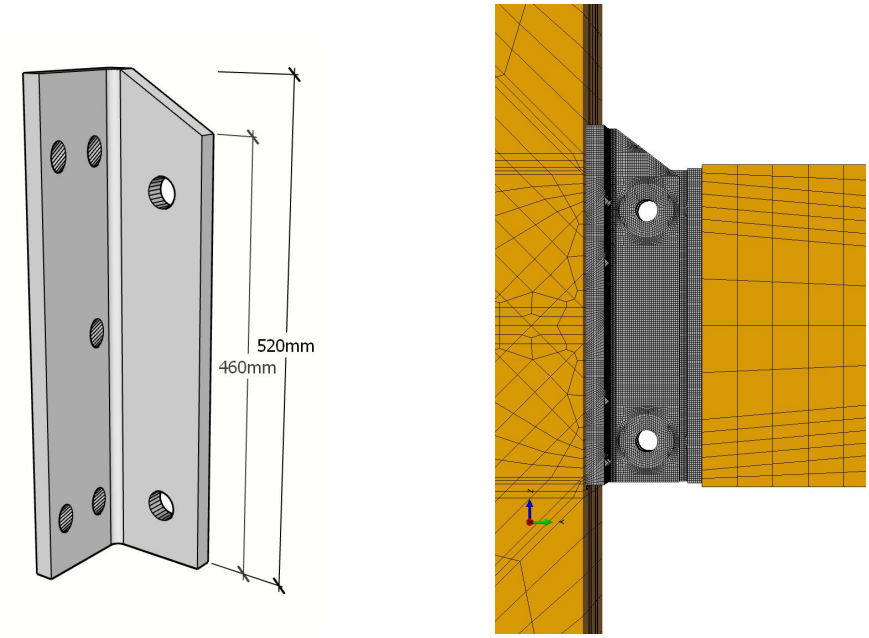

(a) With dimensions (b) Displayed in Abaqus

Figure 3.21: L-profile with angled cut

Six simulations were carried out, and stiffness values were extracted to compare the differences between the solutions. Configuration 1 and 2 in Table 3.6 compares the height difference between the profiles, using the original 12 mm thick L-profiles, while configuration 3 and 4 compares the difference when using 20 mm thick L-profiles. This provides a better basis for evaluating the differences.

Configuration 5 and 6 observes the effect of having the angled cut in the L-profile by comparing configurations with and without the cut. Both configurations used L-profiles with thickness 30 mm as this was considered optimal based on results from 3.2.3.1. The configuration with the angled cut is denoted 520/460 in Table 3.6.

Results

Table 3.6: Comparison between L-profiles with various height

Configuration	Height L-profiles [mm]	Thickness L-profiles [mm]	Thickness T-profile [mm]	$K_{\theta_{tot}}$ [kNm/rad]	Change in $K_{\theta_{tot}}$ from previous configuration [%]
1	460	12	26	8338	-
2	520	12	26	8660	+ 3.86
3	460	20	26	10 262	-
4	520	20	26	10 539	+ 2.70
5	520	30	26	12 735	+ 20.84
6	520/460	30	26	12 719	- 0.13

Results showed that profiles with a height of 520 mm caused the connection to be 2.70 % or 3.86 % stiffer, depending on the thickness used for the profiles. A slightly higher increase in stiffness was obtained when thinner profiles were used for the comparison, but the improvements from extending the height were generally small compared to what was achieved when changing the thickness of the profiles. The increased height was still necessary to have sufficient edge distance for the holes in the profiles as thickness increased.

Making the angled cut in the L-profiles only caused a reduction in stiffness of 0.13 % and was therefore a more favorable solution since this reduced the amount of steel used for the profiles. This was primarily an advantage when the profiles were to be designed for real testing, as the reduced height did not affect the stiffness extracted from the simulations in Abaqus.

3.2.3.3 Continuous profile

As shown in Figure 3.17, excessive bending in the upper and lower parts of the L-profiles were observed. This was desirable to avoid, and hence the thicknesses of the profiles were increased, as thoroughly described in sub-subsection 3.2.3.1. In this process, another solution on how to avoid the excessive bending of the profiles was proposed, where the two L-profiles would be replaced by a continuous profile with two orthogonal plates attached.

To save time when modelling, a new part referred to as the *stiffener*, was modeled and placed between the L-profiles. The stiffener was given the same thickness as the profiles, and tied constraints were used to connect the stiffener to the profiles. By doing this, only the stiffener had to be modeled in Abaqus, which was a relatively quick procedure, rather than making the full continuous profile as a new part. Another advantage with the stiffener was that it made it easy to alternate between two separate L-profiles and a continuous profile depending on the desired configuration. In Figure 3.22 (a), the stiffener can be seen between the two L-profiles.

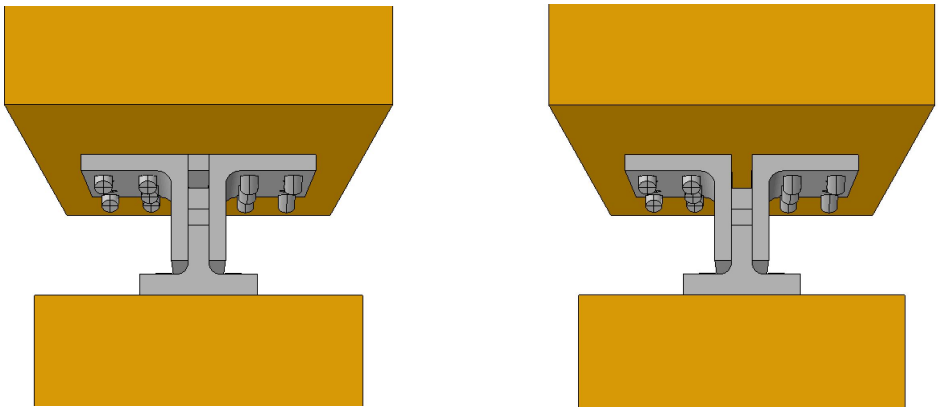

(a) Stiffener between L-profiles (b) Without stiffener

Figure 3.22: Steel connector with and without stiffener

Four models were made and simulated to observe the effect of implementing the continuous steel profile instead of the two separate L-profiles in the connector. As this was a solution that arose while modifying the thickness of the L-profiles, thicknesses of 20 mm and 26 mm was used for the comparison. While the solution with the continuous profile could give great improvements to the stiffness for thinner profiles, this would not necessarily be the case when the profiles were modeled with greater thickness. Therefore, two different profile thicknesses were used to have a better basis when evaluating the effect of the stiffener. The results are presented in Table 3.7.

Results

Table 3.7: Comparison between L-profiles with and without stiffener

Configuration	**Stiffener**	**Height L-profiles [mm]**	**Thickness L-profiles [mm]**	**$K_{\theta_{tot}}$ [kNm/rad]**	**Change in $K_{\theta_{tot}}$ from previous configuration [%]**
1	No	520	20	10 539	-
2	Yes	520	20	11 762	+ 11.65
3	No	520	26	11 808	-
4	Yes	520	26	12 760	+ 8.06

As seen from the results, the configurations which included the stiffener gave an improvement of the rotational stiffness in the range of 8 – 12 %, depending on the thickness. A greater improvement was shown for 20 mm thick profiles than for 26 mm thick profiles. The improvements were however favorable for both cases as a significant increase in rotational stiffness of the connection was observed for both. In addition, the bending that previously was observed in the top and bottom corners of the profile was reduced. In Figure 3.23, where deformation pattern for both solutions are displayed, it can be seen that the stiffener prevents

some bending in the upper and lower part of the profiles as well as providing a smoother and reduced stress distribution in the profile.

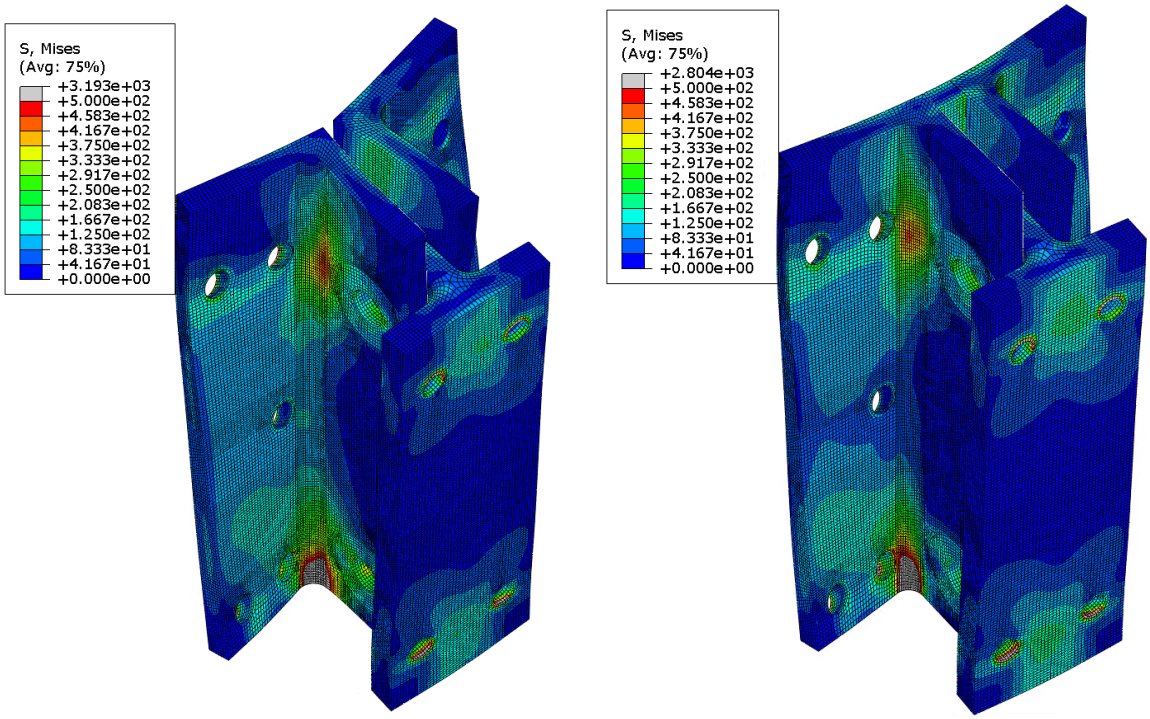

(a) 20 mm profile without stiffener
Acting moment: 93.4 kNm

(b) 20 mm profile with stiffener
Acting moment: 102.84 kNm

Figure 3.23: Deformation pattern connector with and without stiffener, magnified by a factor of 30. Grey are indicates stress level greater than 500 MPa

As described in section 2.4, the idea behind the two L-profiles is the practical assembly phase where each profile easily can be placed on to the inclined rods in the column. Since the inclination of the rods in the column goes in opposite directions on each side of the vertical symmetry line of the column, the separation of the two profiles are essential for the ability to place them on. By adding the stiffener, which would turn the two L-profiles into a continuous steel profile, there would be complications with how to place the profile on to the inclined rods in the column since they go in different directions.

Some solutions on how to solve this was discussed, where one solution was to make large oval holes big enough on one side of the plate so that it was possible to slide the plate onto the inclined rods. However, with the proposed inclination of 45°, a huge part of the plate on one side had to be extracted because of the size the oval holes would need to have. This would reduce the capacity of the connector, especially on the side with reduced area. So, regardless of the benefits with a continuous plate, the solution was not suitable for this type of connection, and hence no further simulations included the stiffener. Before this issue was brought up, two other ideas with a continuous steel profile were discussed, modeled and tested. These were both

discarded for the same reasons, but description of these numerical models with results can be found in Appendix D.

The promising results achieved with the stiffener included, could be of use if the easy assembly phase was maintained. This led to a new proposed solution that involved changing the T-profile. Since the T-profile was a separate part of the connector, the web length between the two L-profiles could be extended all the way to the column face. It was hoped that the extended web of the T-profile could achieve some of the same favorable qualities as with the stiffener included. This is further discussed in subsection 3.2.4.

3.2.3.4 Reduced thickness of area in contact with T-profile

Due to concerns regarding the total thickness of the connecting sides of the L-profiles and T-profile, it was suggested to reduce the thickness of the L-profiles in this area, as it was uncertain how much this part contributed to the rotational stiffness. If this thickness was possible to reduce with minimal loss in stiffness, it would be a favorable solution as it would reduce the thickness in the interaction area between the profiles and also the amount of steel used. In Figure 3.24, two L-profiles are displayed, showing the differences between an L-profile with constant thickness and an L-profile with reduced thickness of the area connected to the T-profile.

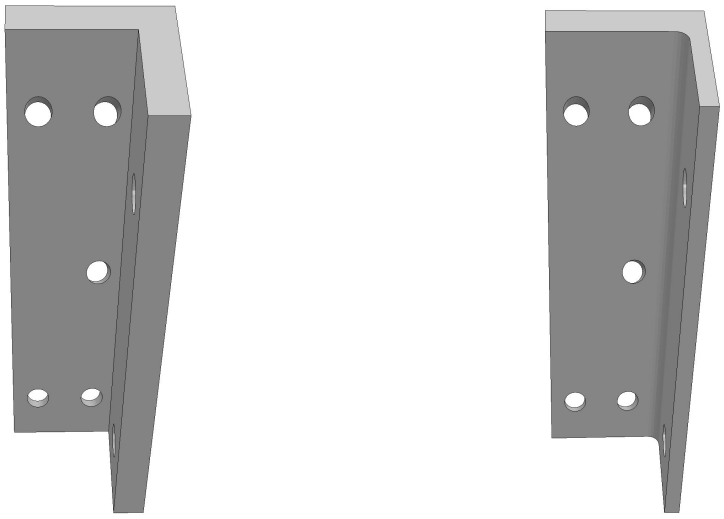

(a) Constant thickness

(b) Reduced thickness of the area connected to the T-profile

Figure 3.24: L-profile with reduced thickness of area in contact with T-profile

To determine the potential loss in rotational stiffness by reducing the thickness, four models were made and simulated. The thickness was reduced by 5 mm for each model, starting with the initially 30 mm thick L-profile, as this was found as the optimal thickness in sub-subsection 3.2.3.1. Stiffness results extracted from the simulations with various thicknesses are displayed

in Table 3.8. In the table, the thickness presented before the backslash denotes the thickness of the profile in contact with the column.

Results

Table 3.8: Comparison between various thickness of area in contact with T-profile

Configuration	**Thickness L-profiles [mm]**	**Height L-profiles [mm]**	**Thickness L-profiles [mm]**	$K_{\theta_{tot}}$ **[kNm/rad]**	**Change in** $K_{\theta_{tot}}$ **from previous configuration [%]**
1	30/30	520	26	12 735	-
2	30/25	520	26	12 171	- 4.43
3	30/20	520	26	11 714	- 3.75
4	30/15	520	26	10 981	- 6.26

The loss in stiffness varied from approximately 4 – 6 % each time the thickness was reduced. Comparing the results in Table 3.8 with results in Table 3.5, shows that L-profiles with thickness 30/20 mm and constant thickness of 26 mm, have similar stiffnesses.

The reduction in stiffness was not of significant magnitude. However, reducing the thickness was not favorable and the area of the L-profiles in contact with the T-profile was affecting the rotational stiffness more than predicted. It was therefore chosen to proceed with one constant thickness for the entire L-profile.

3.2.4 T-profile

Baartvedt & Pharo [19] performed a more detailed study of the T-profile than what was done for the L-profiles. The improvements to the rotational stiffness of the connector was achieved by increasing the thickness of the profile and the distance between the prestressed bolts, as described in subsection 1.3.4. Because of this, the improvements done in this thesis has been related more towards the L-profile, as described in subsection 3.2.3.

However, when optimizing the L-profiles, new ideas on how to improve the T-profile arose, which was desirable to investigate. This was primarily related to extending the length of the web between the two L-profiles, increasing the contact area between the steel parts.

3.2.4.1 Extended web length

The idea arose from the introduction of the stiffener which was placed between the two L-profiles, turning the L-profiles into a continues plate, as explained in sub-subsection 3.2.3.3. While this solution gave great improvement to the overall stiffness and stress distribution, the solution was discarded due to complications in the assembly phase.

The new solution proposed was to extend the length of the web of the T-profile all the way to the column face. This would increase the contact area between the T-profile and the L-profiles, and hopefully exhibit some of the same promising qualities as the stiffener did. The web was therefore extended with 37 mm, which is displayed in Figure 3.25 (b). The original T-profile with the shorter web is displayed in Figure 3.25 (a).

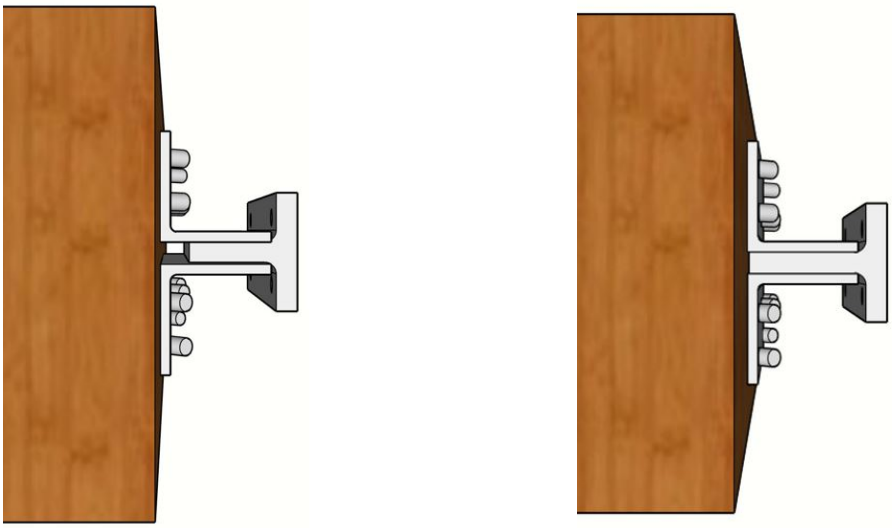

(a) T-profile with short web (b) T-profile with extended web

Figure 3.25: T-profile with various web length

Four models were made and simulated to investigate the effect of the extended web. This was performed with two different L-profile thicknesses, to observe if the effect was similar for different thicknesses. The dimensions used for the L-profiles are displayed in Table 3.9 along with the results.

Results

Table 3.9: Comparison between T-profile with various length

Configuration	Extended web	Thickness L-profiles [mm]	Thickness T-profiles [mm]	$K_{\theta_{tot}}$ [kNm/rad]	Change in $K_{\theta_{tot}}$ from previous configuration [%]
1	No	26	26	11 808	-
2	Yes	26	26	12 114	+ 2.59
3	No	30	30	12 735	-
4	Yes	30	30	12 999	+ 2.07

The new T-profile with the extended web caused the connection to be approximately 2 – 2.6 % stiffer, varying little when thicker L-profiles were used. The extended web also made the contact area between the T-profile and L-profiles bigger, resulting in bigger friction surfaces.

In Figure 3.26 the deformation patter and von Mises stresses of the connector is displayed with the short and long web. As seen in the figure, the extended web prevents some bending in the upper and lower parts of the L-profiles, and a slightly reduced stress field is observed in the profiles.

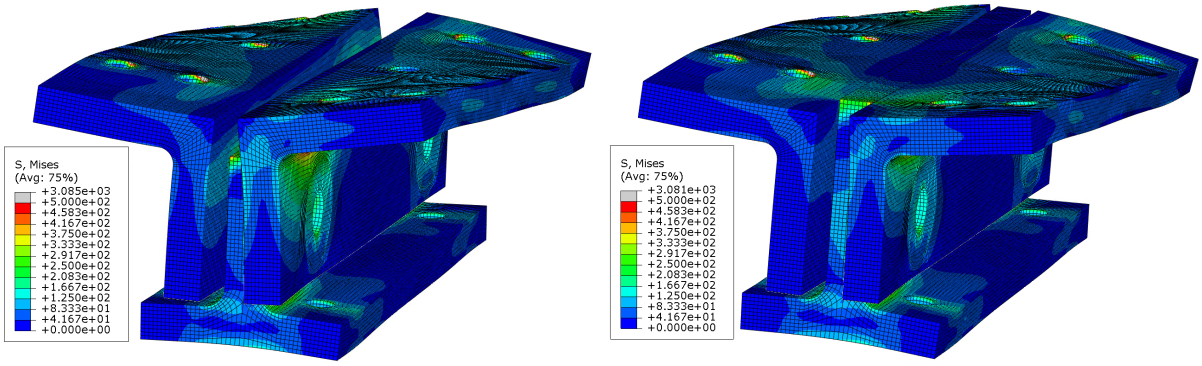

(a) T-Profile with short web
Acting moment: 101.44 kNm

(b) T-profile with long web
Acting moment: 104.07 kNm

Figure 3.26: Deformation pattern connector with and without extended web T-profile, magnified by a factor of 30. Grey area indicates stress level greater than 500 MPa

3.2.5 Final proposal for steel connector

From the optimization described in this section, a final proposal for the connector and placement of the fasteners was established. In this proposal, the connector consisted of the profiles possessing the highest strength and stiffness according to the results listed in previous subsections, while still maintaining its functionality in the assembly phase. In Figure 3.27, the connection is displayed with the final proposal for the steel connector and location of the rods. One of the L-profiles is displayed next to the connection, to get a clearer view of the T-profile and how the rods are placed in the column, and the beam is left out as it remained the same.

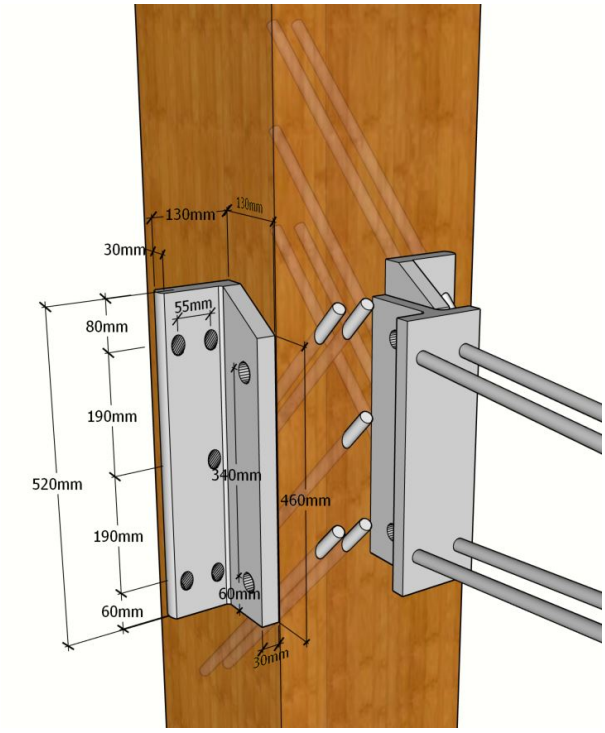

(a) L-profile with dimension in connection

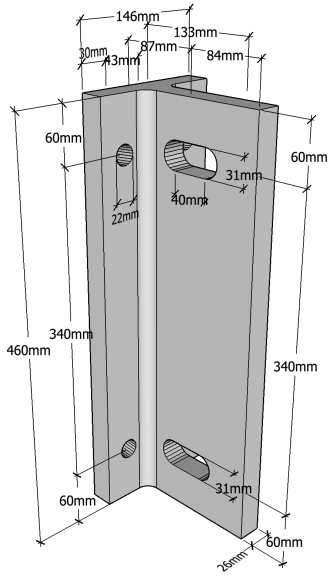

(b) T-profile with dimensions

Figure 3.27: Final proposal of connection

The L-profiles were, based on the results, given a final thickness of 30 mm and height equal to 520 mm, in order to maintain both sufficient vertical distance between the rods and sufficient edge distance. The T-profile solution with the angled cut was suggested, as this solution only led to an insignificant reduction of 0.13 % in the rotational stiffness of the connection. Reducing the thickness in the area connected to the T-profile turned out to affect the stiffness more negatively than what was desirable and was not chosen in the final proposal.

Rearranging the locations of the rods improved the total rotational stiffness considerably when the L-profiles increased in thickness, and the solution displayed in Figure 3.27 was therefore chosen as the optimal placements for the rods. The final proposal for the T-profile included the extended web, while the thickness remained 26 mm as proposed by Baartvedt & Pharo [19].

This final proposal was simulated and compared to the first model that was simulated in this thesis to see the total increase in rotational stiffness achieved from the optimization in this section. The original configuration used for comparison is configuration 1 in Table 3.4 which is the one described in section 2.4. The results are presented in Table 3.10, and as the table shows, an increase in rotational stiffness of almost 60 % was achieved by this optimization process.

Table 3.10: Comparison between original and final configuration

Configuration	$K_{\theta_{tot}}$ **[kNm/rad]**	**Change in** $K_{\theta_{tot}}$ **from configuration above [%]**
Original	8180	-
Final proposal	12 991	+ 58.82

3.3 Threaded rod model

The results obtained in subsection 3.2.5 were above the desired stiffness values of 10 000 – 11 000 kNm/rad. However, the simplified cylindrical rod model used to represent the threaded rods was believed to give stiffer results than what would be expected in a full-scale experiment. In order to get more accurate results from the numerical analyses, it was neccesary to use a better representation of the interactions between the rods and the timber elements.

To achieve this, the threaded rod model mentioned in sub-subsection 3.1.2.2 was made in Abaqus. This model was based on a method developed by Postdoctoral fellow Haris Stamatopoulos [30]. Numerical analyses using this method have previously been done for the circular profile solution tested by Lied & Nordal [16], where results showed good correlation with the experimental results in the elastic area, as seen in Figure 3.28. It was therefore believed that this modelling method would give good and accurate results also for the solution with the LT-connector.

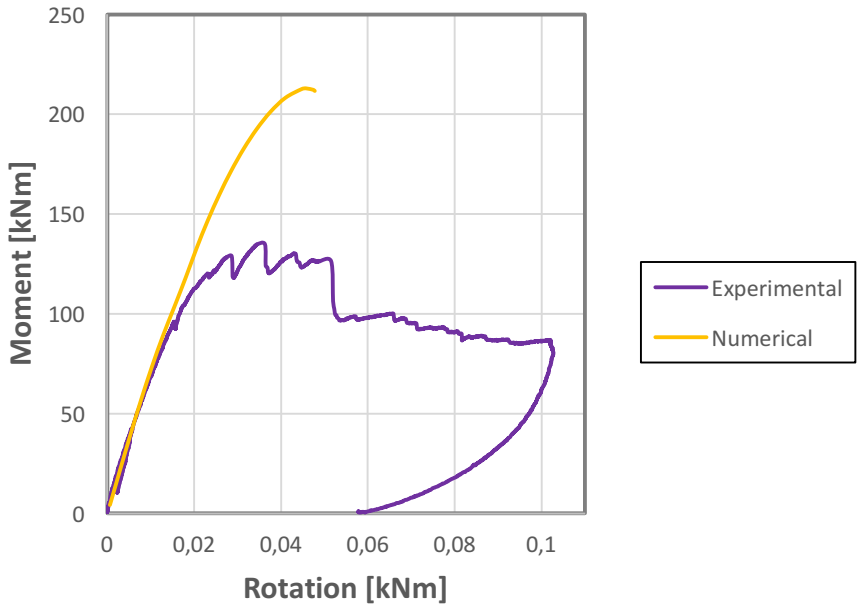

Figure 3.28: Comparison of experimental results from test 4 by Lied & Nordal [16] and numerical results of the same configuration, using threaded rod model [30]

3.3.1 Description of parts

This subsection describes how the different parts of the connection were modeled and assembled in Abaqus with the threaded rod model. In the previously described cylindrical rod model, a rod was represented by one cylindrical part, and connected to a circular hole in the beam or column. In the threaded rod model, the rods were represented by two parts, referred to as *core* and *thread*, and the holes in the timber elements were represented by two other parts, referred to as *female* and *square*.

Core and thread

Modelling the threaded rods in two separate parts allowed for a better representation of the actual geometry of a threaded rod, shown in Figure 3.29.

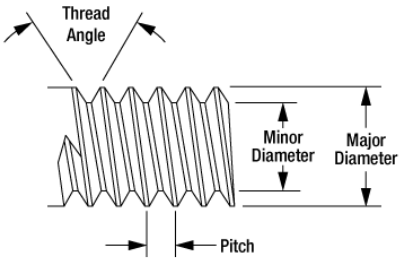

Figure 3.29: Parameters of a threaded rod [31]

The first part, Figure 3.30 (a), represents the core, or minor diameter, and the second part, Figure 3.30 (b), represents the thread. The thread part was made by revolving the triangle marked in red in Figure 3.30 (b) 360 degrees, with a pitch of 8 mm. The red triangle was 2.95 mm wide while the core had a diameter of 16.1 mm, giving the full rod a major diameter of 22 mm. The thread angle was 46°.

(a) Core part (b) thread part

Figure 3.30: Parts representing a threaded rod

In the parts module in Abaqus, each part was made as a single small segment of a full rod length. To make a full rod, the linear pattern tool in the assembly module was used. This tool allows one part to be repeated as many times as needed, in any direction and with any given spacing between repetitions. By using this tool, the length of one rod could easily be modified

by changing the amount of repetitions. This method was practical for modeling the connection this thesis aims to improve, since the rods in the beam and the column had different lengths. Figure 3.31 shows a pattern of 12 cores and 6 threads, making a 48 mm long threaded rod. The original core and thread parts are marked in red.

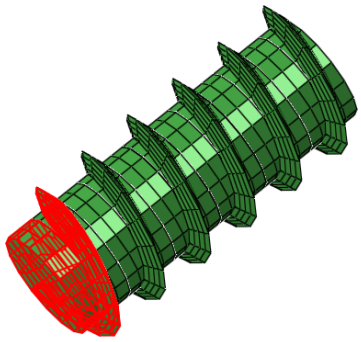

Figure 3.31: Segment of threaded rod

The outer surface of the core and the inner surface of the thread were tied together using tie contstraints, making the two pars act as one solid rod. In Figure 3.32, the surfaces used for the tie constraint are shown, the pink is the outer surface on the core and the red is the inner surface of the thread. Both parts were given material properties of steel as defined in Table 3.1.

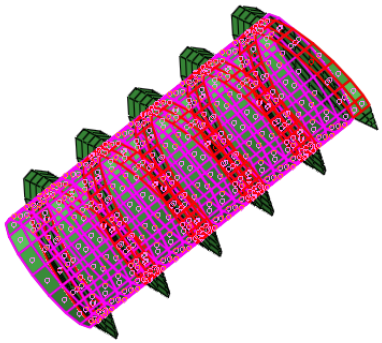

Figure 3.32: Surfaces for tied constraints on threaded rod

Female

As mentioned in subsection 1.3.1, the interface plane between the wood and the outer diameter of the rod can be a critical area. In the threaded rod model, this area was modeled as a separate part, named female. Figure 3.33 shows one of the failure modes from Figure 1.7 [14] which gives a good image of this interface plane.

Figure 3.33: Interface plane between wood and rod [14]

The female part was made as a hollow cylinder with a spiral cut on the inside that fits the thread. The part was made the same way as the thread, by revolving a geometry, marked with red in Figure 3.34 (a), 360 degrees with a pitch of 8 mm. Figure 3.34 (b) shows a linear pattern of two female parts. Here, the spiral cut that fits the thread is marked in red. The large green squared elements on the inside of the cylinder is where the core part makes contact.

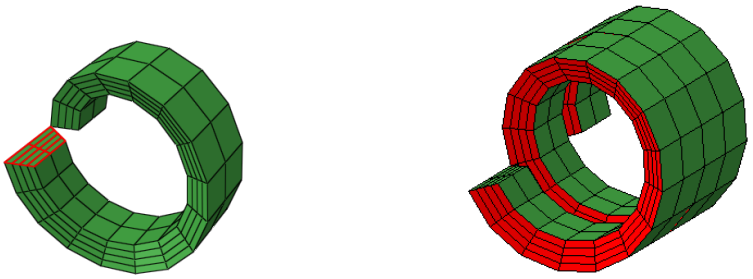

(a) Single female part (b) Surface connected to thread

Figure 3.34: Female part

Timber properties were assigned to the female part as defined in Table 3.1. The contact surfaces between core and female, and between thread and female, were given an interaction property with tangential- and normal behavior, see sub-subsection 3.1.2.1. The tangential behavior was given the friction formulation penalty with a friction coefficient equal to 0.2. The normal behavior was given pressure-overclosure hard contact and default constraint enforcement method was used.

Figure 3.35 shows a liner pattern of cores, threads and female parts put together. The cores and threads are grey, while the females are yellow.

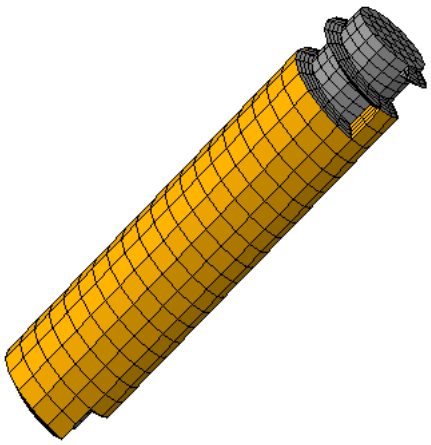

Figure 3.35: Segment of threaded rod in female part

Square

To get accurate results, it was necessary to have a fine mesh in the threaded rods and around the holes in the beam and column. However, the rest of the beam and column was less critical, as it is not a direct part of the connection, and a coarser mesh could be used to save computational time. In the threaded rod model, this was done by making the part shown in Figure 3.36. The part was a square with a cylindrical hole, that had a finer mesh on the inside, and a coarser mesh on the outside. This allowed the female part with the fine mesh to be connected to the inside, and the outside of the square to be connected to the beam or column with a coarser mesh.

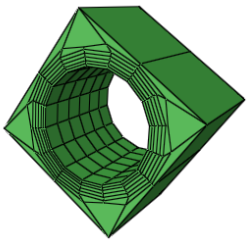

Figure 3.36: Square part

The square part was made by merging two half cylinders, one full cylinder, and four corners. Figure 3.37 shows the half cylinder. It was simply made by solid extrusion and given the same mesh density as the outside of the female part.

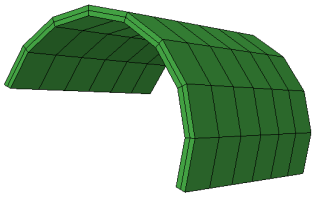

Figure 3.37: Half cylinder for square part

The full cylinder, Figure 3.38 (a), was made by revolving a long, thin rectangle made from one solid line on one side, and six short lines on the other side, Figure 3.38 (b). When the rectangle was revolved, the outside was given a coarser mesh than the inside.

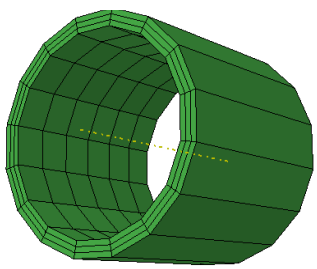

(a) Full cylinder

(b) Section used to make the full cylinder

Figure 3.38: Full cylinder for square part

The corner part, Figure 3.39, was also simply made by solid extrusion, and given a mesh that matches the outside of the full cylinder. As seen in the figure, the straight edge on the outside of the corner is one large element.

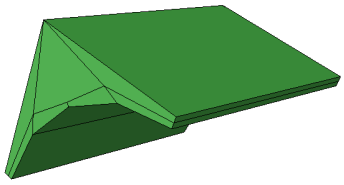

Figure 3.39: Corner for square part

In the assembly module, two half cylinders were placed inside the full cylinder which then was covered by four square-corners. Finally, both geometry and mesh were merged, and the square part in Figure 3.36 was created. The outside of the square had dimensions 30x30 mm, and the diameter of the inside was the same as the major diameter of the threaded rods, 22 mm.

Now, the core, thread, female and square parts could be assembled in the assembly module and patterned to the desired rod length. Figure 3.40 shows a segment of the four parts assembled together. Cores are dark grey, threads are light grey, females are yellow, and squares are red.

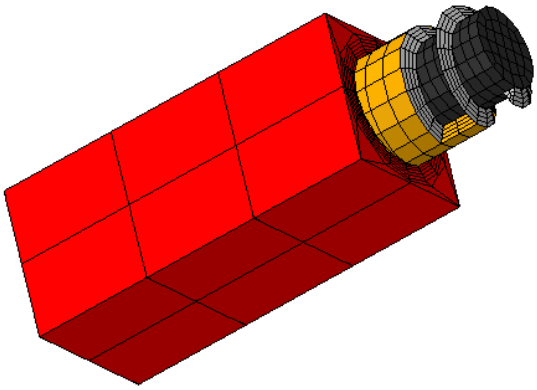

Figure 3.40: Segment of the four parts of the threaded rod model

The contact surface between the inside of the square and the outside of the female part, see Figure 3.41, was assigned the interaction property cohesive behavior with a stiffness of 18.5 kNm/rad, as described in sub-subsection 3.1.2.2.

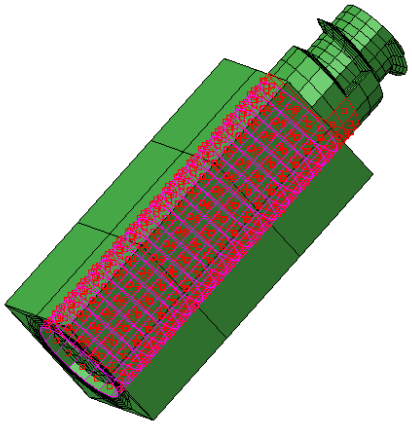

Figure 3.41: Surfaces for cohesive behavior

Beam and column

The beam and column were modified and given square holes that would fit the square parts. Tie constraints were used between the beam/column and the squares, making them act as one solid component.

In the assembly module, the four-parted rods were patterned and rotated to the desired length and angle for the column and the beam. Figure 3.42 shows the beam with the four parts in place, and Figure 3.43 shows the same for the column.

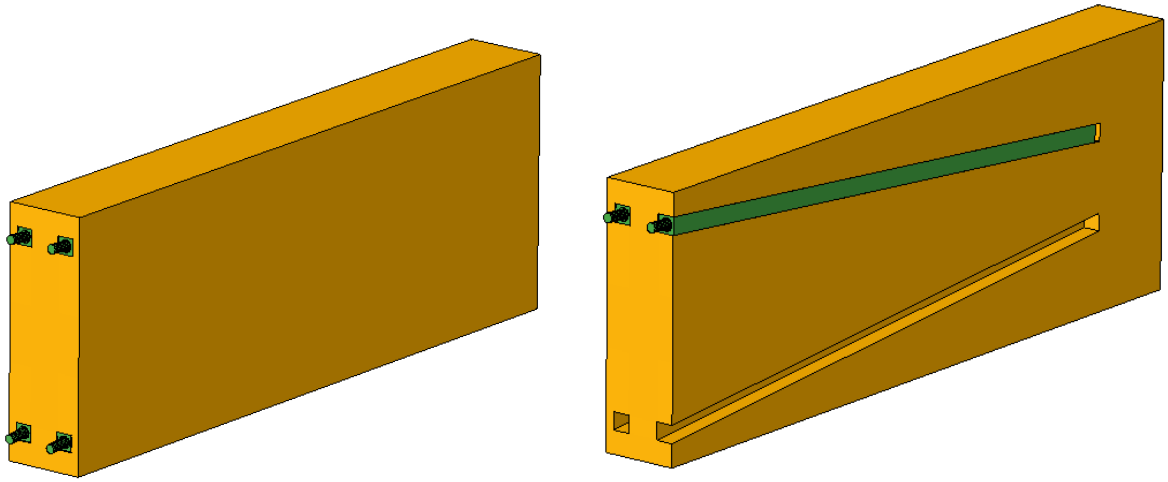

Figure 3.42 Beam with rods

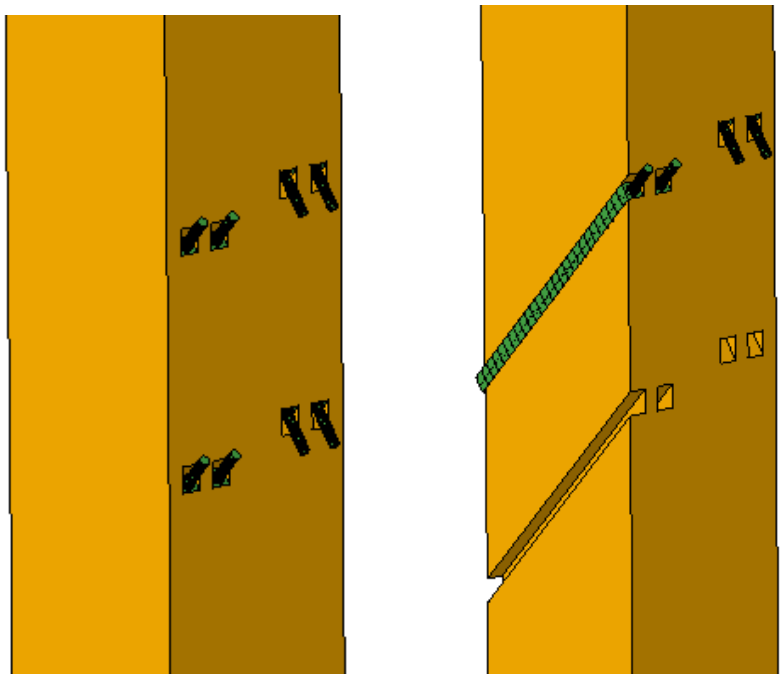

Figure 3.43: Column with rods

3.3.2 Description of analyses

Seven different configurations were made and tested using the threaded rod model. Configuration 1 was almost identical to one of the tests run by Lied & Nordal [16], only with the circular profiles being replaced by the LT-connector. This was done to compare the stiffness of the actual connectors, and not the whole connection. Configuration 2, 3, 4 and 5 looked at four parameters, regarding rod-to-grain angles and rod spacing, that were different in configuration 1 and the final proposal in subsection 3.2.5. The final two configurations were made based on what was believed to give the best combination of practicality and total rotational stiffness according to the findings in this thesis. Detailed geometry of the configurations is provided in Appendix A.1, and a figure of a full numerical configuration with the threaded rod model is given in Figure E.6.

Some convergence issues occurred when running analyses with the threaded rod models. Description of the issues, and solutions, are given in Appendix A.2.

Connector comparison

It was first decided to compare the rotational stiffness of the circular profile connector from Lied & Nordal [16] with the LT-connector. Lied & Nordal did four tests with different configurations in their thesis, and the configuration used for this comparison was referred to by them as Test 4 [16]. The configuration is shown in Figure 3.44.

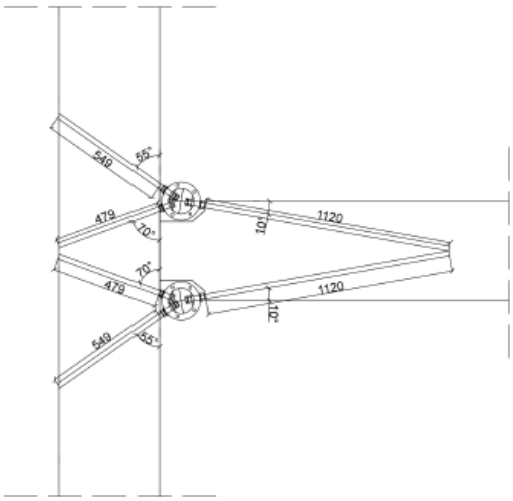

Figure 3.44: Configuration for Test 4 from Lied & Nordal [16]

As mentioned, a numerical analysis of the configuration in Figure 3.44 had been done with the threaded rod model in an ongoing study [30]. This will be referred to as configuration 0. In configuration 0, several parameters were different from the proposal described in subsection 3.2.5. To solely compare the connectors, the models had to be as similar as possible. Therefore, the following changes had to be made in configuration 1:

- Rod-to-grain angles were changed to 10° in the beam, and 55° and 70° in the column.
- The vertical spacing between rods in the beam was changed from to 410 mm
- The two middle rods in the column were removed, so only 8 rods were used.
- The width of the beam was changed from to 146 mm
- The length of the beam was changed from to 2 m, and the displacement was applied to the beam at a distance L = 1960 mm

In addition, the angled cut of the L-profiles described in sub-subsection 3.2.3.2 was neglected to simplify the modeling process, as this showed practically no effect on the rotational stiffness. All other parameters of the connection were the same as for the configuration described in subsection 3.2.5, and the remaining details of the numerical modelling were defined as in subsection 3.2.1.

A few differences between configurations 0 and configuration 1 were necessary due to the design of the L- and T-profiles. The beam was cut where the rods exit as this is necessary to attach the T-profile, unlike for the circular profile where the beam is extended between the rings, see Figure 3.45.

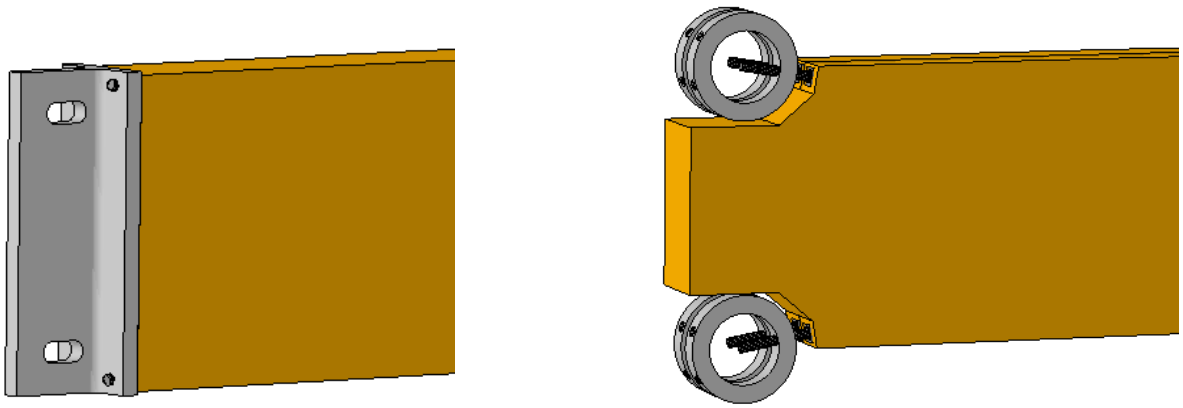

(a) New configuration (b) Lied & Nordal configuration

Figure 3.45: Differences between beams

Also, the design of the L-profile requires the rods to be in two different vertical planes, rather than in the same plane as they were for the circular profile, see Figure 3.46. In addition, it was decided to have the rods in the same vertical plane go in the same direction.

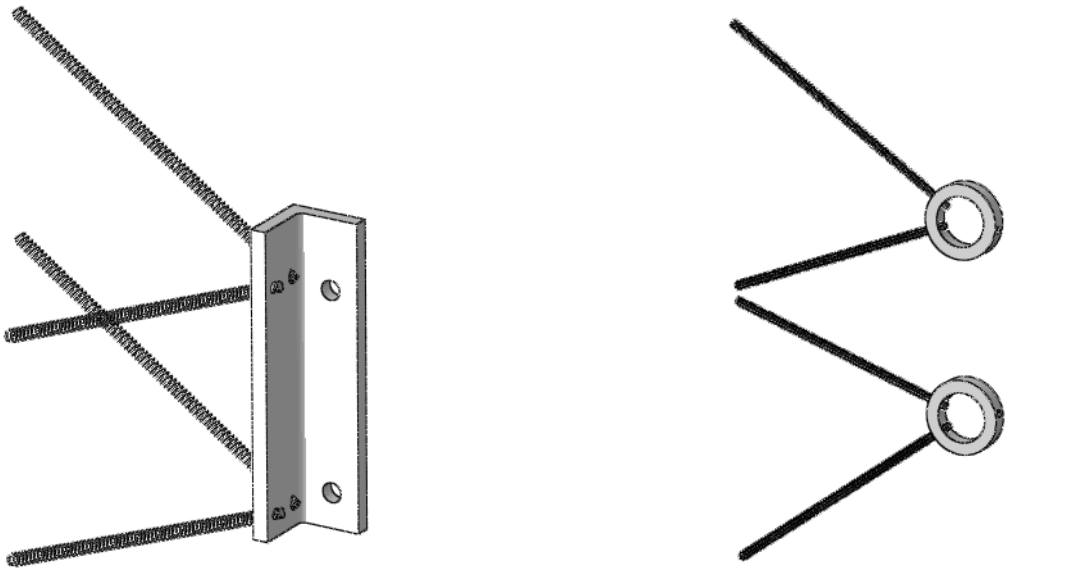

(a) New connector (b) Lied & Nordal connector

Figure 3.46: Differences in rod placements

Rod-to-grain angles and rod spacing

Since there were so many differences between configuration 1 and the final proposal presented in subsection 3.2.5, it was desirable to know what impact each of the changes had on the rotational stiffness. Therefore, four more tests were done changing one parameter at the time. The beam dimensions and distance to the enforced vertical displacement was not changed back, as it was believed not to have a big impact on the rotational stiffness. The two middle rods in the column were not put back as they were located on the neutral axis and would therefore not contribute to the rotational stiffness. Table 3.11 shows the configurations for the four tests. Configuration 5 is the most similar to the proposal from subsection 3.2.5.

Table 3.11: Configuration 2-5

Configuration	Rod-to-grain angle beam [deg]	Rod-to-grain angle column [deg]	Maximum spacing between rods in beam [mm]
2	10	45*	410
3	10	45	410
4	05	45	410
5	05	45	340

* Rods on one L-profile go in opposite directions

Final models

Based on all the different analyses that have been described so far in this thesis, two final models were made with configurations believed to give the best combination of practicality and rotational stiffness. Table 3.12 shows the configurations, and as seen in the table, the only difference between the two configurations is the rod-to-grain angle in the column. The values of 70° and 75° were chosen based on findings from Lied & Nordal [16], and Drageset & Hoff [18].

Table 3.12: Configuration 6 and 7

Configuration	Rod-to-grain angle beam [deg]	Rod-to-grain angle column [deg]	Maximum spacing between rods in beam [mm]
6	10	70	410
7	10	75	410

4 Results

This chapter presents the most relevant results obtained from the seven configurations that were done with the threaded rod model. Rotational stiffness, withdrawal stress distributions along the rods and von Mises stress distributions are included. Table 4.1 gives a summary of the seven configurations described in subsection 3.3.2.

Tabell 4.1: Description of configurations using threaded rod model

Configuration	Rod-to-grain angle beam [deg]	Rod-to-grain angle column [deg]	Maximum spacing between rods in beam [mm]
0*	10	55, 70	410
1	10	55, 70	410
2	10	45**	410
3	10	45	410
4	05	45	410
5	05	45	340
6	10	70	410
7	10	75	410

* Circular profile

** Rods on one L-profile go in opposite directions

4.1 Rotational stiffness

This section presents the rotational stiffness results from the configurations in subsection 3.3.2. The rotational stiffness is calculated as described in subsection 3.1.5.

4.1.1 Connector comparison

As described in subsection 3.3.2, configuration 1 was made to compare the LT-connector with the circular profile connector. Table 4.2 presents the results and the percental difference in rotational stiffness. Both the experimental results and the numerical results, named configuration 0, for the circular profile is included. As seen in the table, the LT-connector was 23.5 % stiffer than the circular profile connector, based on the numerical analyses.

Table 4.2: Rotational stiffness for configuration 0 and 1

Configuration	$K_{\theta_{tot}}$ [kNm/rad]	Change in stiffness from previous configuration [%]
Experimental*	7603	-
0**	7442	- 2.1
1	9188	+ 23.5

* [16]
** [30]

4.1.2 Rod-to-grain angle and spacing

The next four configurations were made to see the effect of each parameter that was different in the cylindrical model and the threaded rod model. Table 4.3 presents the results for these four configurations, together with configuration 1 for comparison.

Table 4.3: Rotational stiffness for configuration 1-5

Configuration	$K_{\theta_{tot}}$ [kNm/rad]	Change in stiffness from previous configuration [%]
1	9188	-
2	6427	- 30.1
3	6063	- 5.7
4	5607	- 7.5
5	4497	- 19.8

Two parameters proved to have a big impact on the rotational stiffness. Changing from a 55° and 70° rod-to-grain angle configuration in the column to a 45° configuration, reduced the rotational stiffness by 30 %. The other critical parameter was spacing between rods in the beam. 340 mm spacing was almost 20 % less stiff than a spacing of 410 mm.

The two other parameters had less of an impact but were still worth noticing. Having rods on one L-profile go in the same direction as opposed to opposite directions reduced the stiffness by almost 6 % for a 45° rod-to-grain angle. Changing the rod-to-grain angle in the beam from 10° to 5° resulted in 7.5 % lower stiffness.

4.1.3 Final models

The two final models both had beam rods with 410 mm spacing and 10° rod-to-grain angle. In addition, all four rods connected to one L-profile went in the same direction. Therefore, the most appropriate configuration to compare them to was configuration 3. Table 4.4 shows that

changing the rod-to-grain angle in the column from 45° to 70° or 75° increased the rotational stiffness by 25.7 % or 28.7 % respectively.

Table 4.4: Rotational stiffness for configuration 3, 6 and 7

Configuration	$K_{\theta_{tot}}$ [kNm/rad]	Change in stiffness from previous configuration [%]
3	6063	-
6	7619	+ 25.7
7	7850	+ 3.0

4.1.4 Partial stiffnesses

It was interesting to know how the different components of the connection contributed to the overall rotational stiffness. This way it became clear where improvements should be made. Partial stiffnesses were therefore calculated for the column fasteners, the connector and the beam fasteners. The calculation method was similar to the one explained in subsection 3.1.5, but the rotation of each of the three components were calculated separately, rather than for the full connection. This was done for configuration 1-7, and the results are presented in Table 4.5.

Table 4.5: Partial stiffnesses for configuration 1-7

Configuration	Rotational stiffness [kNm/rad]			
	Column	Connector	Beam	Overall
1	23 154	34 049	25 619	9188
2	11 055	35 392	24 607	6427
3	9901	37 557	24 763	6063
4	9857	36 959	18 799	5607
5	9868	42 167	9940	4497
6	15 016	36 412	25 281	7619
7	15 608	36 453	25 272	7850

As seen in the table, the connector was consistently the stiffest component of the connection, and its partial stiffness was fairly constant only with a small increase in configuration 5. The beam fasteners were the second stiffest component for all configurations. Its partial stiffness dropped when the spacing between rods decreased, configuration 5, and when the rod-to-grain angle was changed, configuration 4. This was expected as the overall stiffness was lower for these configurations, and the only changes made were in the beam. For all seven configurations, the fasteners in the column was the weakest component of the connection. In configuration 1, the beam fasteners and column fasteners had quite similar stiffnesses, but for all the other configurations there was a significant difference in the partial stiffnesses of the column fasteners and the two other components.

4.2 Withdrawal stress distribution

Shear stress in the interaction surface between the timber elements and the outer diameter of the rods, can be referred to as withdrawal stress. In the threaded rod model, this interaction surface was between the female part and square part. This was an interesting parameter to observe as it tells how exposed the rods were to withdrawal, which has an impact on the rotational stiffness.

Withdrawal stress distributions were created for the interaction surfaces around one beam rod, one downward-going column rod and one upward-going column rod, for configuration 1-7 with the threaded rod model. All the surfaces were located in the tension zone. Each interaction surface had 16 circumferential paths along its length. Figure 4.1 has five of these paths marked in red.

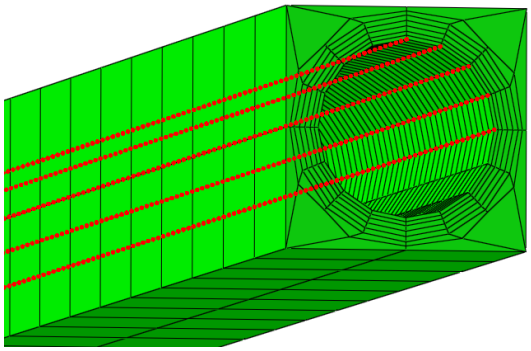

Figure 4.1: Circumferential paths along rod-timber interaction surface

All 16 paths gave separate withdrawal stress distributions and a mean distribution was calculated for each surface. All the distributions are presented in Appendix B, along with a more detailed description of which surfaces the distributions were obtained from. The distributions were all gathered from the same load increment step, where acting bending moments were in the range 21-33 kNm.

Typical withdrawal stress distributions for the three different surfaces are presented in Figure 4.2. They are all from configuration 3, where the acting bending moment was 25 kNm. The x-axis represents embedment length, X_e and the y-axis represents withdrawal stress, $\tau(X_e)$.

The seven different configurations showed fairly similar distributions. The value of $\tau(0)$ should be zero as it is at a free end, so there are some entry level inaccuracies in the plots provided, especially for the column surfaces, but the mean distributions appear to be reasonable. Withdrawal stresses seemed to approach zero around 400 mm embedment length around both column rods and the beam rod.

The distributions for the 16 circumferential paths on one surface are very similar for the surface around the beam rod, but more scattered for the surfaces around the two column rods. This was the case for all seven configurations. In general, the surfaces around the beam rod and upwards-going column rod experienced the highest stresses, and around the downward-going column rod stress levels were lower.

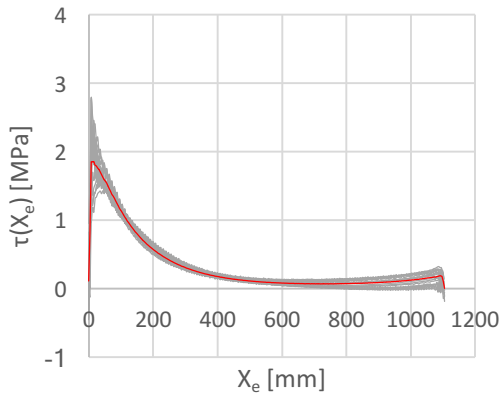

(a) Surface around beam rod

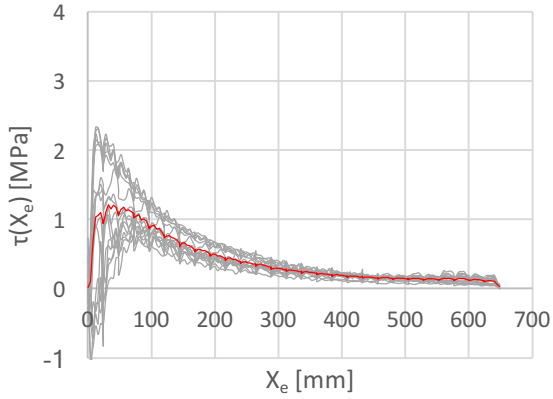

(b) Surface around downward-going column rod

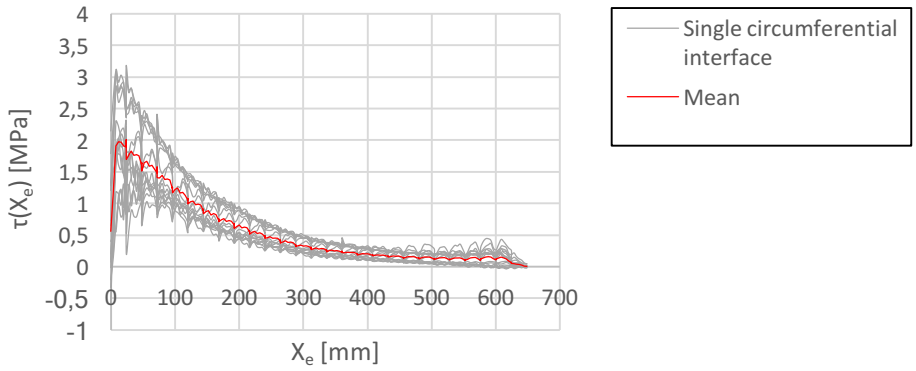

(c) Surface around upward-going column rod

Figure 4.2: Withdrawal stress distributions configuration 3

4.3 Von Mises stress distribution

Strength was not the main focus in this thesis. However, by observing the deformation patterns and distribution of von Mises stresses, it became clear what components of the connection that experienced the highest stresses, which is related to the rotational stiffness. Distributions for configuration 1-7 are provided in appendix C.

It was not a big difference in the von Mises stress distributions for the different configurations. An important observation was that the connector experienced very low stresses and deformations compared to the rods. Figure 4.3 shows the distribution and deformation pattern of the fasteners and connector from configuration 3. Here, the deformation scale factor is 30, and yet the connector is fairly undeformed compared to the rods. The difference in stresses in the connector and the fasteners is also very clear.

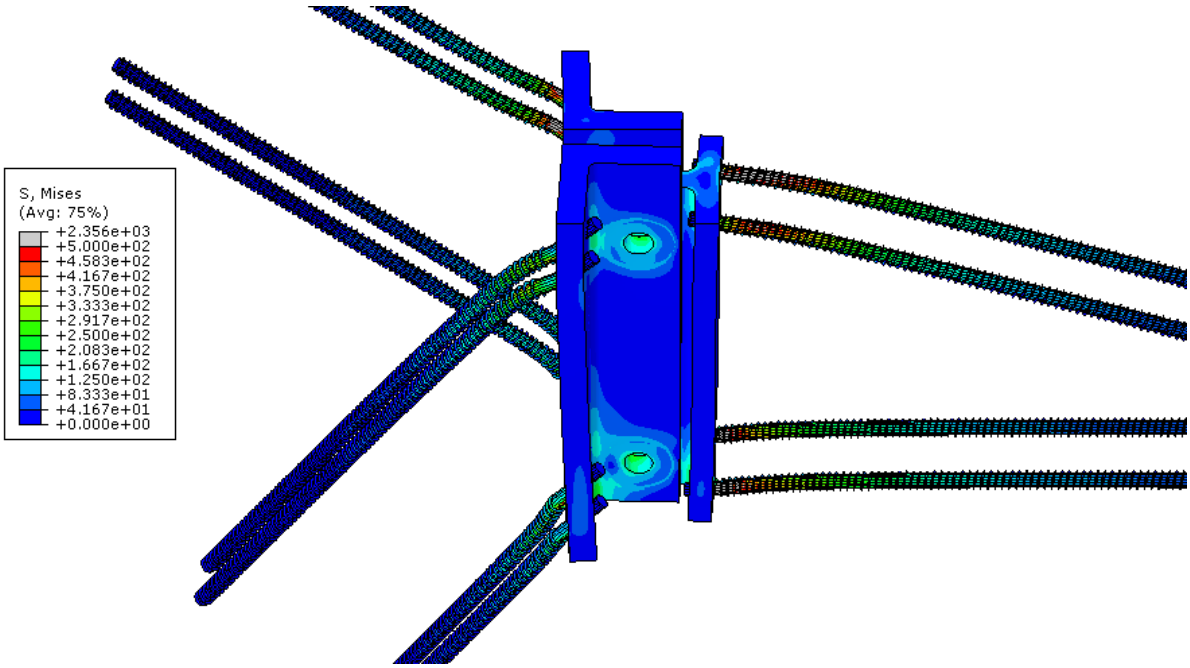

Figure 4.3: von Mises stresses and deformation from configuration 3. Deformation magnified by a factor of 30. Grey areas indicate stress levels greater than 500 MPa.
Acting moment: 42 kNm

5 Evaluation

This chapter evaluates the results presented in Chapter 4. It also evaluates the numerical models that have been used, both the techniques and some of the parameter choices made.

5.1 Numerical modelling

In this section, the numerical models will be evaluated with respect to choices made in Abaqus regarding interactions, constraint methods and modeling techniques. The stiffness results obtained during the optimization of the connection, described in section 3.2, will also be evaluated.

5.1.1 Optimization of connector and rod placement

Abaqus was used as the numerical tool to optimize the steel profiles and the rod orientation through numerical simulations. The improvements were essential in order to increase the rotational stiffness of the connection, as results in section 3.2 showed. This subsection evaluates the models and results obtained from using the cylindrical rod model.

Numerical models

To evaluate the LT- connector and the placement of the rods, a complete numerical model was made of the connection. One of the main advantages with a complete numerical model was to more correctly replicate the behavior of the connection. Timber elements were therefore defined with proper material properties and dimensions, and cohesive zones were utilized to simulate the withdrawal of the threaded rods. Including bending of the timber components and cohesive zones were essential in order to evaluate the different locations of the rods in the column.

Some simplified modelling techniques were however applied in the numerical models to reduce the computational time, as several configurations were to be compared. These simplifications were mainly done on the withdrawal of the threaded rods. As mentioned in sub-subsection 3.1.1.2, two withdrawal approaches were used when modelling in this thesis. Since the main focus in the earlier stages was to evaluate and optimize the steel connector and rod placement, withdrawal of the threaded rods was replicated using the cylindrical rod model. This model used a simplified modelling technique which excluded the threaded part of the rods, idealizing the rod-wood

interaction as a cylindrical interaction between steel and wood defined with cohesive surfaces. This approach reduced the number of elements and was more computationally efficient.

The steel profiles in the connector was connected to the rods using tie constraints properties in Abaqus, as the nuts were not included in the numerical models. Tie constraints in Abaqus leads to fully rigid interactions between the connecting surfaces, and hence the tie between the rods and the connector were simulated as fully rigid interactions. This is a simplification to what would be the case in reality, where nuts would be applied. However, as the nuts, when tightened, may withstand some local rotation, this is assumed to be a valid simplification.

Some simplifications and differences between the steel profiles in the connector occurred while modeling, especially during the thicknesses evaluation of the L-profiles. The profiles varied between having rounded and sharp edges. This difference is shown in Figure 5.1, where the 12 mm L-profile is modeled with sharp corners, while the 20 mm L-profile is modeled with rounded corners. It is assumed however, that this had minor impact on the rotational stiffness and that the comparison between profiles is valid despite the minor difference. Modelling with rounded corners however gives a favorable distribution of stresses in these areas.

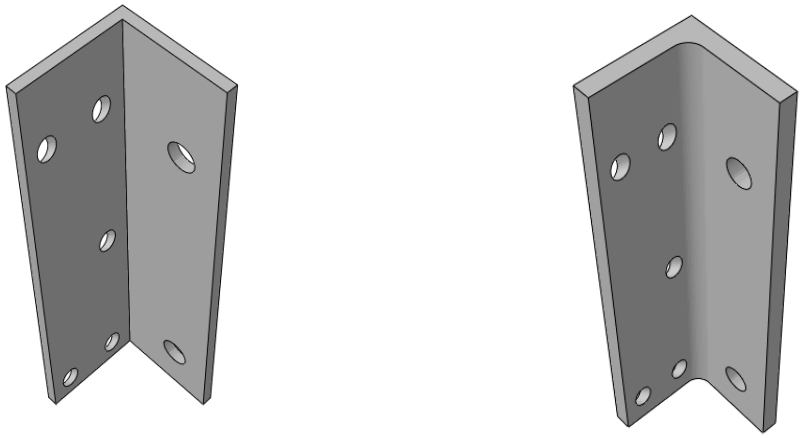

(a) Sharp corner (b) Rounded corner

Figure 5.1: Different corner modeling in the L-profile

Also, when parts were remodeled as improvements were made, it was not possible to partition the parts equally each time. This resulted in a variation in the number of distorted elements for the different configurations. Distorted elements have an influence on the accuracy of the results achieved in Abaqus [22]. However, since the number of distorted elements were kept to a minimum and the variations were low between the compared models, this was not assumed to have influenced the stiffness results and the comparison was assumed valid.

There were also some differences in the locations of the inclined holes when modeling L-profiles with various thicknesses. The spacing between the rods were the same for all configurations but the edge distances varied. Profiles with lower thickness 26 mm, 20 mm and 12 mm, had edge distance 100 mm and 40 mm to the top and bottom respectively. L-profiles with thickness greater than 26 mm had edge distances of 100 mm and 60 mm to top and bottom respectively, which became the final layout in Figure 3.19. This difference may have led to inaccuracies in the percental differences for profiles with a thickness greater than 26 mm in Table 3.5. This inaccuracy was however assumed to be minimal, as the spacing between the rods were the same for all configurations.

Cylindrical rod model

The rotational stiffness values obtained from the simulations using the cylindrical rod model, were assumed to be considerably higher than what could be expected in experimental testing. This was due to the inability to correctly replicate withdrawal of the threaded rods. The final proposal in 3.2.5, which used the cylindrical rod model, had a rotational stiffness of 12 991 kNm/rad. Configuration 5 with the threaded rod model, see Table 4.3, was the configuration closest to the one in 3.2.5. The rotational stiffness of configuration 5 was 4497 kNm/rad, which is about 65 % less stiff than the cylindrical rod-based proposal from 3.2.5. The two configurations differed in beam width, and the configuration using the threaded rod model did not include the middle rod, as described in subsection 3.3.2, but these differences are believed to have a minor impact on the rotational stiffness. A difference between the two rod modeling techniques was expected, but not in the range of what the results showed.

The cohesive withdrawal properties used in this thesis, simplified the elastic stiffness properties to $K_{tt} = K_{ss}$, with value 18.5 kNm/rad, which was based on calibrations to experimental results for rods with d = 20 mm, using the threaded rod model [30]. Modifying or recalibrating the stiffness properties for use in the cylindrical rod model is therefore essential to get this model to produce comparable results with the threaded rod model, and to what can be expected in experimental testing. However, the cylindrical rod model was useful for comparing various changes made to the connector, as it was computationally cheaper than the threaded rod model.

As results presented in subsection 3.2.3 showed, withdrawal of the rods had a limiting effect on the thickness for the L-profiles, resulting in 30 mm to be the optimal thickness. Since the cylindrical rod model was used consistently for all numerical models in section 3.2, the comparison between the parameters listed in that section, and the choices made based on them, are assumed to be valid.

Rotational stiffness

As Table 3.10 shows, from the initial connector with dimensions and design as explained in section 2.4, to the new proposed solution in 3.2.5, the total increase in rotational stiffness of the connection was ~ 60 %. A big part of this increased stiffness was due to changes performed on the L-profiles, which was found at the beginning to be the weakest component in the connection, and hence the limiting factor in order to obtain high rotational stiffness. Results listed in subsection 3.2.3 showed that improvements made to both L-profiles contributed the most to further stiffen the connection. Increasing the thickness from 12 mm to 30 mm increased the rotational stiffness with ~ 47 %, and when the extended height of the profiles is also considered, the total increase in rotational stiffness for the connection from just improving the L-profiles was ~ 50 %. This is approximately 80 % of the total increase in rotational stiffness achieved from improving the connector, which shows that improving the L-profiles was essential in order to increase the total rotational stiffness of the connection.

Relocating the rods in the column significantly improved the rotational stiffness of the connection when the L-profiles were given greater thicknesses. It was considered to have the second biggest effect on the overall increase in rotational stiffness, after improving the L-profiles, with ~ 8 %. There current placements of the rods could likely still be improved, and if further improvements give similar increases, they are definitely beneficial.

The T-profile had previously been improved by increasing the thickness [19], and less improvements were therefore performed for the profile in this thesis. The change that was done, the extended web, had a small effect on the rotational stiffness of the connection, as it only caused the connection to be 2.66 % stiffer. Still, it did prevent some bending of the L-profiles and reduced the von Mises stress distributions in certain areas, so it was considered a good solution.

5.1.2 Configurations using the threaded rod model

The ability to reproduce the withdrawal of the rods was essential when computing a complete numerical model of the connection, as the rods are the ties between the connector and the timber elements. The threaded rod model was therefore implemented in the numerical models, as this technique had proved to better replicate the withdrawal of the rods than to the cylindrical rod model [30].

Using the threaded rod model had both positive and negative aspects. Such an accurate model is a great tool in the developing stages, as it allows for both minor and major changes to be tested without having to do full scale experiments to verify every decision. Since it is very detailed it can obviously give a more detailed description of critical areas such as the interface plane between the wood and the outer diameter of the rod.

This level of detail also has negative aspects. First of all, the amount of fine meshed parts gives rise to a very large number of elements. The seven configurations using the threaded rod model had around 1.1 million elements. Such a high number results in a very long computational time. There are also a lot of surface interactions which increases the computational time even more. Because it is so detailed, it is also very time consuming to produce a full model. Abaqus is not a good software for parametric modelling. Many parameters, including spacings and rod-to-grain angles, required substantial changes for several parts, and many interactions had to be redefined when changing a minor detail. If possible, a simpler but still accurate model for representing axially loaded threaded rods should be developed.

Similar to the models used for optimizing the connector, the nuts tying the connector to the threaded rods were left out of the configurations using the threaded rod models as well. As previously explained, the rods were tied to the connector, which leads to fully rigid interactions. However, as the nuts may withstand some local rotation, this is assumed to be a valid simplification.

5.1.3 Friction surfaces

Abaqus provides several options for defining the friction interaction between the steel profiles. Many of the definitions used in this thesis were taken from findings from a previous study by Baartvedt & Pharo [19] and other available theory. This was also the case for the definition of master and slave surfaces and finite versus small sliding properties. It is difficult to predict how the definitions used in this thesis may affect the rotational stiffness, but previous results have showed that for the numerical simulations, insignificant differences between different definitions are observed. The choices were therefore assumed to be in good correlation to what can be expected in experimental results. However, proper selection of master and slave surface can be crucial for an interaction, and the choices made for the numerical models in this thesis may not correspond to findings from experimental testing.

The friction coefficient was set to $\mu = 0.45$, based on findings from Baartvedt & Pharo [19]. Neither in their study, nor in this thesis, has the friction coefficient been adequately explored. As mentioned in subsection 3.1.2, the control of the friction coefficient is very important, as it influences the slip factor between the mating surfaces, and hence may affect the rotational stiffness of the connection. In what way is not easy to predict.

5.2 Results

This section evaluates the results obtained from the configurations using the threaded rod model.

5.2.1 Rotational stiffness

From results in Chapter 4, it became clear that a rod-to-grain angle of 45° was not an optimal configuration. The overall rotational stiffness was lower compared to the three configurations with different column rod-to-grain angles. Partial stiffness values confirmed that the column fasteners were the weakest component for all configurations and this was especially clear when the rod-to-grain angle was 45°, as Table 4.5 shows. Partial stiffness values also revealed that the connector was the stiffest component and that the beam fasteners were in between. Improvements should therefore be made on the column fasteners, as the connection will not be stronger than its weakest point.

For the final two configurations, rod-to-grain angles of 70° and 75° in the column was selected based on results from Drageset & Hoff [18] who found those angles to give the highest stiffness values. Since having rods on one L-profile go in opposite directions only gave an increase in stiffness of almost 6 % for 45° rod-to-grain angle, it was chosen not to use such a solution, as it is less practical, as described in sub-subsection 3.2.3.3.

However, the rotational stiffness is significantly larger in configuration 1 than in configuration 6 and 7, with 20.6 % and 17.1 % higher stiffness respectively. Whether this difference is due to rods pointing in different directions or the fact that the rods have different rod-to-grain angles is uncertain, but it can seem as if having all the rods on one profile go in the same direction might not give sufficient stiffness with the LT-connector.

It was unexpected to find that a rod-to-grain angle of 5° in the beam was less stiff than 10°. This was opposite of what Drageset & Hoff found in their numerical analyses [18]. However, the model used in Drageset & Hoff was similar to the cylindrical rod model, in other words less detailed, and a comparison of the two angles was not done experimentally by Lied & Nordal [16]. It is uncertain what the reason might be for this difference in results, so this is something that could be investigated further.

As expected, a larger spacing between the rods in the beam gave an increased stiffness of almost 24.7 %, as it gives a larger moment arm. It should be mentioned that 410 mm spacing is likely not possible with the current flooring system used in the WoodSol project. 410 mm was used in this thesis because it was what Lied & Nordal used in their experimental tests [16] and was therefore better for comparison with their full-scale experiments. A maximum spacing of 390

mm has been considered likely based on discussions with other members of the WoodSol project.

5.2.2 Withdrawal stress

The full presentation of withdrawal stress distributions is provided in Appendix B. They are generally quite similar, however there are some differences worth noticing.

For configuration 2 and 3, where rod-to-grain angles were 45° and 10° in the column and beam respectively, the surface around the beam rod and the upward-going column rod showed similar stress distributions, while the stresses around the downward-going rod were smaller. This is reasonable as the distributions are in the tension zone, and therefore the downward-going rod will experience more bending than withdrawal. When the angle in the beam changed from 10° to 5° in configuration 4 and 5, the surface around the beam rod experienced higher stresses, while in the column, stresses stayed mainly the same. Withdrawal stresses around the column rods in configuration 1, where rod-to-grain angles were 55° and 70°, were smaller than for all the other configurations, despite having the highest acting moment.

Because it was desirable to observe the stresses around both an upwards- and downwards-going column rod, the same surfaces could not be used for all configurations. For configurations where rods on one L-profile all go in the same direction, one rod per L-profile obviously had to be used. In this case the two rods closest to the middle of the vertical centerline of the column were used. In configurations where rods on one L-profile go in opposite directions, one rod closest to the centerline and one rod closest to the edge had to be used. Appendix B has a more detailed description of what surfaces were used. Using different surfaces has an impact on the results, as the rods closest to the edge of the column will be less exposed to stresses, so a direct comparison might be inaccurate for some of the configurations.

An example of this issue is when the surface around the downward-going column rod in configuration 1 and 6, which both have a rod-to-grain angle of 70°, is compared. In configuration 1, the maximum stress level of the mean distribution is about 0.8 MPa, while for configuration 6 it is about 1.75 MPa, even though the acting moments are practically the same. The rod in configuration 1 is closest to the edge, whereas the rod in configuration 6 is closest to the middle.

On the other hand, the downward-going column rod in configuration 2 and 3 are also located differently, but the stress distributions around those rods showed very little difference. It would be expected that around the rod in configuration 2, stresses would be smaller, as it is closest to the edge of the column, and the rod in configuration 3 is closes to the middle, but this is not the case. The acting bending moment in configuration 3 is smaller, so this could be an explanation. A more detailed analysis of the withdrawal stress distributions with more comparable results

could be worth doing. The one carried out here has some inaccuracies, as described in this subsection, but it gave a brief overview of the withdrawal stress distributions, and how they were affected by the varying parameters.

5.2.3 Von Mises stresses and deformation

Appendix C gives a detailed description of von Mises stress distributions and deformed shapes from the different components in configuration 1-7 using the threaded rod model. Observing these figures confirms the findings regarding rotational stiffness discussed earlier in this chapter, and in chapter 4. The connector, which was found to be the stiffest component, has less deformation and von Mises stresses than the fasteners for all configurations.

The stress distributions in the connector does not change much for the seven configurations, and the differences that do occur is likely due to the change in acting bending moment. This correlates well to the partial stiffness values in Table 4.5, where the stiffness of the connector is fairly constant. Maximum stresses in both L-profiles and the T-profile are located around the holes on the side facing the timber element.

There are bigger differences in the fasteners. In the beam, the rods with rod-to-grain angle of 10° experience higher stresses and more deformation than rods with 5°. The column rods with rod-to-grain angle of 45° are more deformed than those with higher rod-to-grain angles. For most configurations, the 45° rods have lower stresses despite being more deformed. The maximum stresses for all rods are naturally around the connection point to the steel profiles.

Some local extreme values in the range 1000-2000 MPa are observed for all configurations. Whether these values are probable or a result of inaccuracies in the numerical analysis is not assessed, as the strength of the connection has not been the focus of this thesis. Either way, their existence should be noted and considered if this solution is further developed. If such high stresses do occur in experimental tests, the material will obviously yield which will affect the rotational stiffness.

6 Concluding remarks

This chapter summarizes the main discoveries from this thesis and gives some suggestions to work that can be done to improve the solution further.

6.1 Conclusion

As part of the WoodSol project, a moment resisting beam-to-column connection has been numerically evaluated with a friction connector and threaded rods as fasteners. The LT-connector developed by Baartvedt & Pharo [19] was further improved using the cylindrical rod model for simulating withdrawal of the rods. The improvements made gave great improvement to the overall stiffness, increasing it with nearly 60 %.

In order to correctly replicate the behavior of the connection in a numerical analysis, the method for simulating the withdrawal of the threaded rods proved to be essential. As results showed, the cylindrical rod model overestimated the rotational stiffness with nearly 65 %, based on results from the more accurate threaded rod model. This model has shown good correlation to previous experimental results using the circular profile connector.

Comparison between configuration 0 and 1 indicates that the LT-connector is 23.5 % stiffer than the circular profile connector from Lied & Nordal [16]. It is also a far more practical solution that requires less on-site work and is well suited for use in an industrialized structural system. Keeping the solution as practical as possible has been an important part of this thesis and the practicality has therefore been maintained throughout the entire process of improving the connection. Since the LT-connector has achieved higher rotational stiffness and is more practical, it should be considered a big improvement from the previous solutions from Lied & Nordal [16] and Drageset & Hoff [18].

However, the desired rotational stiffness of 10 000 kNm/rad has not yet been achieved with this connector. This appears to be due to a lack of stiffness in the fasteners, especially in the column. Both partial stiffness values, the von Mises stress distributions and the deformed shapes of the connection indicates that the connector is plenty stiff, and the rods are more critical. If this solution is to be developed further, the focus should therefore be to improve the rod configuration especially in the column, but also in the beam.

A rod-to-grain angle of 45° in the column proves to be a bad solution, as it gives a lower stiffness than higher angles. For configurations where all the rods connected to one L-profile go in the same direction, a rod-to-grain angle of 75° gave the highest rotational stiffness, with 7850 kNm/rad. However, the configuration with 55° and 70° rod-to-grain angles was by far the stiffest solution, with a rotational stiffness of 9188 kNm/rad. The problem with that configuration is the inability to slide the L-profile in place, but a solution allowing for such configurations might be necessary.

Having rods on one L-profile go in opposite directions had little effect when the rod-to-grain angle was 45°. However, there is a big difference between the two stiffest configurations mentioned above. This gives reason to believe that the effect of rods alternating directions on one profile could be bigger for higher rod-to-grain angles. A reason could be that in the tension zone, a downward-going rod might experience more bending than withdrawal, whereas it would be the opposite for the upward-going rod. This is in accordance with the discoveries from the withdrawal stress distributions. Combining these on one profile could lead to a better overall transfer of stresses, whereas having all the rods on one profile go in the same direction would lead to one profile more exposed to withdrawal than the other. This might be less clear with 45° rod-to-grain angle, since the overall stiffness of such a configuration is much lower.

The three stiffest configurations were configuration 1, 6 and 7, when the rod-to-grain angle for the column rods were larger than 45°. For all these cases, the rods experience less deformation than for an angle of 45°. Also, the von Mises stress distributions are not particularly large. The withdrawal stresses however were fairly large, so it can seem as if the main cause of the lack of stiffness in the column fasteners is due to withdrawal.

6.2 Suggestions to further work

This section gives some suggestions to further work that can be done to improve and further develop the solution using the LT-connector.

As mentioned in the conclusion, there are room for improvements of the partial stiffnesses of the fasteners in the beam and the column. There might be other rod configurations that can perform better than the ones explored in this thesis. Finding a way to allow rods that are connected to one profile to go in different directions should be attempted as it seems to give higher stiffness for larger rod-to-grain angles. The rod diameter has not been evaluated in this thesis, so investigating the effect of an increased rod diameter could perhaps be of interest.

A strength evaluation should be done to see how much force can be applied before the connection yields. In addition, calculating what forces and moments the connection must be able to transfer according to the Eurocode, could be valuable. This way it could be known how strong the connection has to be, and whether it meets those requirements or not. A strength evaluation could also give more information about the local extreme values seen in the von Mises stress distributions in this thesis.

No non-linear analyses or evaluation of ductility has been made. As mentioned in Chapter 1, timber structures must have ductile connections in order to avoid brittle failure. It is desirable that the connector yields before the fasteners, as it would be easier to replace. A ductility study would therefore be necessary once the connection has reached the desired rotational stiffness. Based on the findings in this thesis, the fasteners seem to be more exposed to high stresses than the connector and would probably yield first. Reducing the thickness of the connector could be one way to increase the ductility, but this would again lower the rotational stiffness of the connection.

Neither the friction coefficient nor the prestressed force was changed once decided. An interesting study would be to run tests with different friction coefficients, keeping the prestressed force constant, and see for what values the increase rate in rotational stiffness approaches zero. The same study can be done for the prestressed force by gradually increasing it while keeping the friction coefficient constant. These two studies could give a good indication to what prestressed force and friction coefficient that are optimal.

Full scale experimental testing is of large interest, as it would reveal how the connection preforms in real life. Results from experimental testing could verify the results obtained in this thesis or reveal errors. The threaded rod modeling technique proved to be accurate when compared to be experiments done with the circular profile [30]. If the same were to be the case for this new configuration, the reliability of the modeling technique would be

strengthened. Experimental testing would also provide useful results for the other suggested studies in this section.

Evaluating other parameters that were not included in this thesis such as fire resistance and dynamic behavior could also be done. Fire tests would reveal the fire capacity of the connections, while a dynamic loading experiments would provide info about fatigue and critical eigenfrequencies. The numerical models created in the process of this thesis can be a great tool for further development, as much more information can be extracted from them.

References

[1]. Woodsol project summary. http://www.woodsol.no/reservations. Accessed: 2018-04-03

[2]. Michael F. Ashby and David R. H. Jones. *Engineering materials 2*, Elsevier Ltd., 2013

[3]. Dette er tre-trenden byggebransjen ruster seg for. https://www.tu.no/storylabs/annonse-dette-er-tre-trenden-byggebransjen-ruster-seg-for/366527. Accessed: 2018-03-15

[4]. Global forest products facts and figures, 2016. http://www.fao.org/3/I7034EN/i7034en.pdf. Accessed: 2018-03-15

[5]. John Sunley and Barbara Bedding, *Timber in Construction*, BT Batsford Ltd., 1987

[6]. Francesco M. Massaro, *Moisture Dependency*, TKT4212 lecture notes, NTNU, 2017

[7]. Structural Timber Association, *Timber as a structural material – an introduction,* http://www.cti-timber.org/sites/default/files/STA_Timber_as_structural_material.pdf. Accessed: 2018-04-20

[8]. Byggforskserien, *Trevirke. Treslag og materialegenskaper*, 2015, https://byggforsk.no/dokument/578/trevirke_treslag_og_materialegenskaper. Accessed: 2018-04-20

[9]. European Committee for Standardization (CEN). *NS-EN 350:2016. Durability of wood and wood-based products. Testing and classification of the durability to biological agents of wood and wood-based materials*, Standard Norge, 2016

[10]. APA, *Glulam*, https://www.apawood.org/glulam. Accessed: 2018-04-24

[11]. Trefokus, *Limtre*, http://www.trefokus.no/proff/artikler/materialer/limtre. Accessed: 2018-04-24

[12]. Norges Byggforskningsinstitutt and Jan C. Krohn, *Trebaserte Byggekonstruksjoner*, Byggenæringens forlag AS, 2011

[13]. Byggforskserien, *Bjelker av tre. Dimensjonering,* https://byggforsk.no/dokument/304/bjelker_av_tre_dimensjonering. Accessed: 2018-04-24

[14]. Haris Stamatopoulos and Kjell A. Malo, *Withdrawal capacity of threaded rods embedded in timber elements*, NTNU, 2015

[15]. Haris Stamatopoulos and Kjell A. Malo, *Withdrawal stiffness of threaded rods embedded in timber elements*, NTNU, 2016

[16]. Kristine S. Lied and Kjersti I. Nordal, *A conceptual study of glulam connections using threaded rods and connecting circular steel profiles.* Master thesis, NTNU, 2016

[17]. Hallvard O. Veium, *Axially loaded threaded rods in glulam connections.* Master thesis, NTNU, 2015

[18]. Anders F. Drageset and Torbjørn H. Hoff, *Numerical analyses of moment resisting beam-to-column connections in timber structures.* Master thesis, NTNU 2017

[19]. Tobias Baartvedt and Henrik D. Pharo, *Numerical analysis of a steel connector, for use in moment resisting beam-to-column connections in timber structures.* Project study, NTNU, 2017

[20]. Kjell A. Malo and Haris Stamatopoulos, *Connections with threaded rods in moment resisting frames,* World timber conference on timber engineering in Vienna, Austria, 2016

[21]. Norske limtreprodusenters forening, *Limtreboka*, 2016

[22]. Haris Stamatopoulos; *Withdrawal properties of threaded rods embedded in glued-laminated timber elements*. PhD thesis, NTNU, 2016

[23]. Abaqus analysis user's guide, *38.1.2 Contact constraint enforcement methods in Abaqus/Standard.* http://abaqus.software.polimi.it/v6.14/books/usb/default.htm?startat=pt09ch38s01aus178.html#usb-cni-acontactconstraints-penalty. Accessed: 2018-02-13

[24]. Kolbein Bell. *An engineering approach to FINITE ELEMENT ANALYSIS of linear structural mechanics problems.* Fagbokforlaget, 2014.

[25]. Kjell M. Mathisen, *Numerical integration.* TKT4192 lecture notes, NTNU 2016

[26]. Lecture 11.3.2, *Connections with preloaded bolts,* University of Ljubljana. http://fgg-web.fgg.uni-lj.si/~/pmoze/esdep/master/wg11/l0320.htm. Accessed: 2018-02-22

[27]. Abaqus theory guide *5.1 contact modelling*. http://abaqus.software.polimi.it/v6.14/books/stm/default.htm. Accessed: 2018-02-13

[28]. Grigory .I. Barenblatt, *The Mathematical Theory of Equilibrium Cracks in Brittle Fracture*. Advances in Applied Mechanics vol. 7, pp 55-129, 1962

[29]. D.S. Dugdale, *Yielding of Steel Sheets Containing Slits*, Engineering Department, Univeristy College of Swansea, 1959

[30]. Haris Stamatopoulos, Aivars Vilguts and Kjell A. Malo, *Numerical modelling of axially-loaded threaded rods embedded in timber elements*. To be submitted

[31]. Figure inspired by Thorlabs. https://www.thorlabs.com/newgrouppage9.cfm?objectgroup_id=9015. Accessed: 2018-03-01

[32]. Figures taken from Banxin Fastener. http://www.salesfastener.com/plus/list.php?tid=6 Accessed: 2018-01-29

Appendices

A Details of configurations with threaded rod model

This appendix presents detailed geometry of the configurations tested that uses the threaded rod model. Convergence issues that arose when using the model, and how they were solved, are also included.

A.1 Geometry and details of configurations

This section dives detailed geometry and explanations for the seven configurations tested with the threaded rod model, as well as configuration 0.

Configuration 0

Configuration 0 is done with the configuration from Lied & Nordal [17]. This has already been done as part of an ongoing study [30].

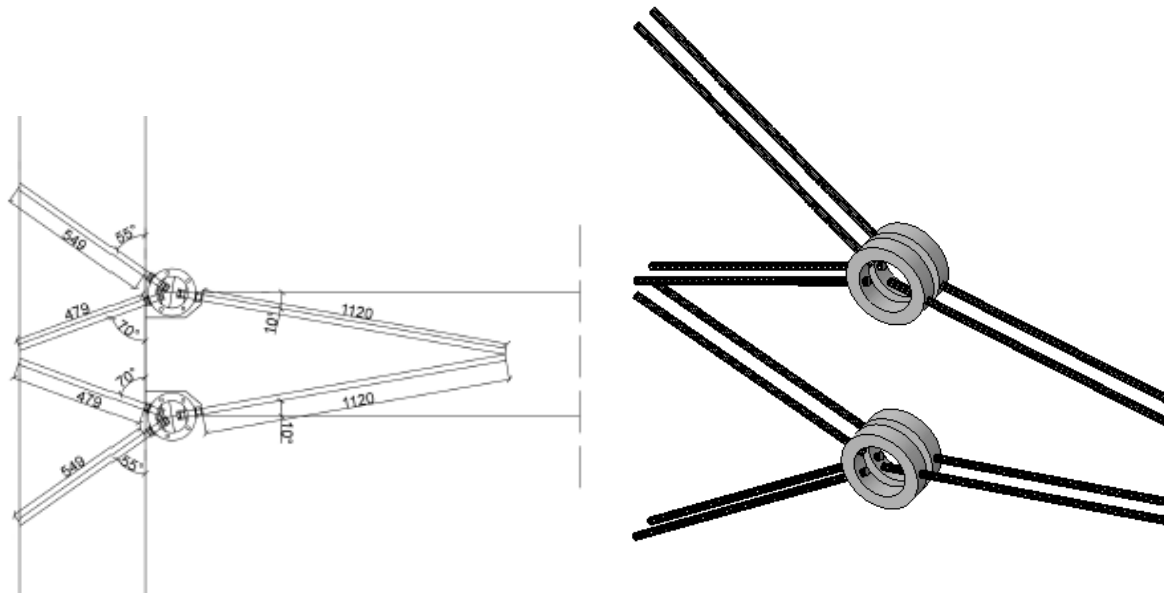

(a) Geometry (b) 3D details from numerical model

Figure A.1: Details of configuration 0

Configuration 1

Configuration 1 replaces the circular profile connector from configuration 0 with the new LT-connector. Most of the geometry is similar to configuration 0. This way the connectors alone can be compared to each other.

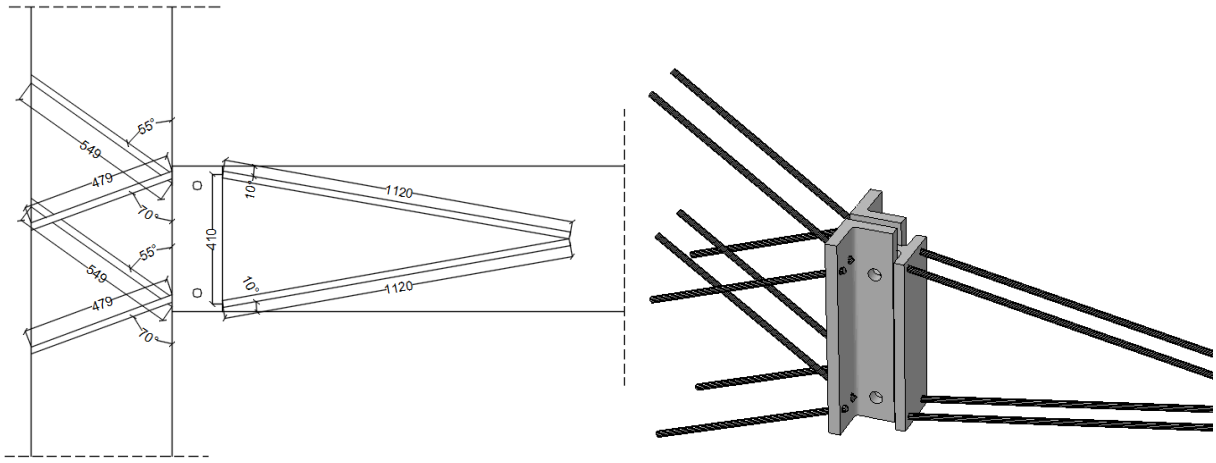

(a) Geometry (b) 3D details from numerical model

Figure A.2: Details of configuration 1

Configuration 2

Configuration 2 has a rod-to-grain angle of 45° in the column, which also leads to longer embedment lengths. This is the only difference from configuration 1, and therefore the effect of changing the rod-to-grain angle in the column will be clear.

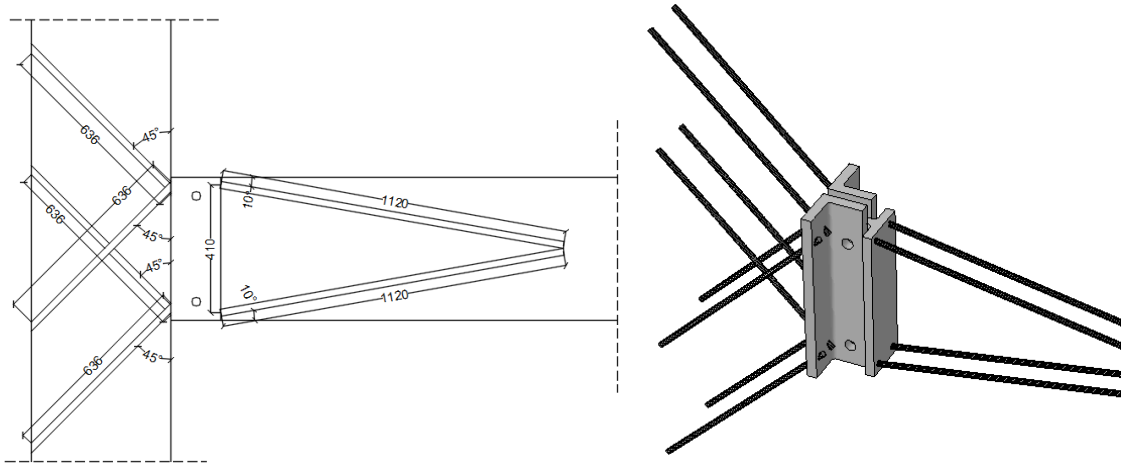

(a) Geometry (b) 3D details from numerical model

Figure A.3: Details of configuration 2

Configuration 3

Configuration 3 is very similar to configuration 2, the only difference is that the four rods connected to each L-profile goes in the same direction, instead of opposite directions. Comparing configuration 2 and 3 will reveal the impact of having a symmetrical rod configuration in the column.

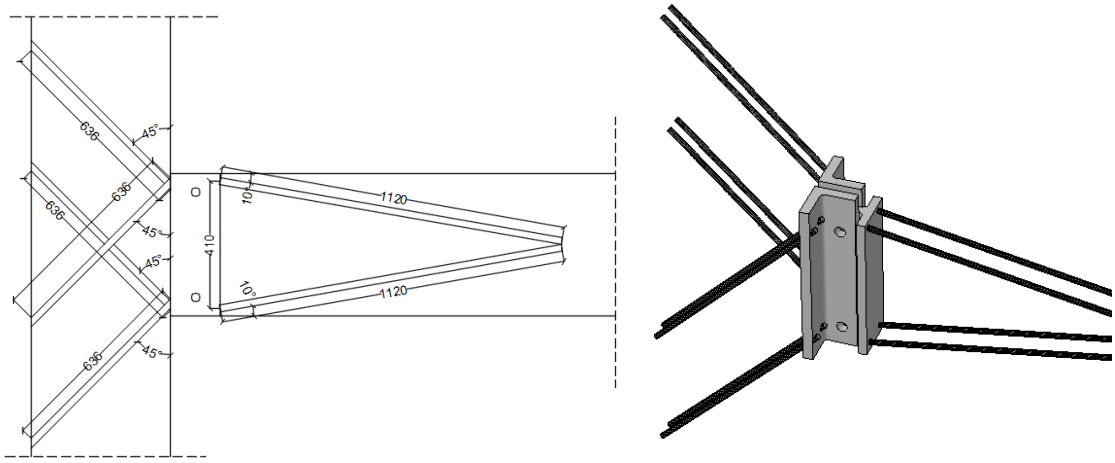

(a) Geometry (b) 3D details from numerical model

Figure A.4: Details of configuration 3

Configuration 4

Configuration 4 has a rod-to-grain angle in the beam of 5°. This is the only difference from configuration 3, where the angle was 10°.

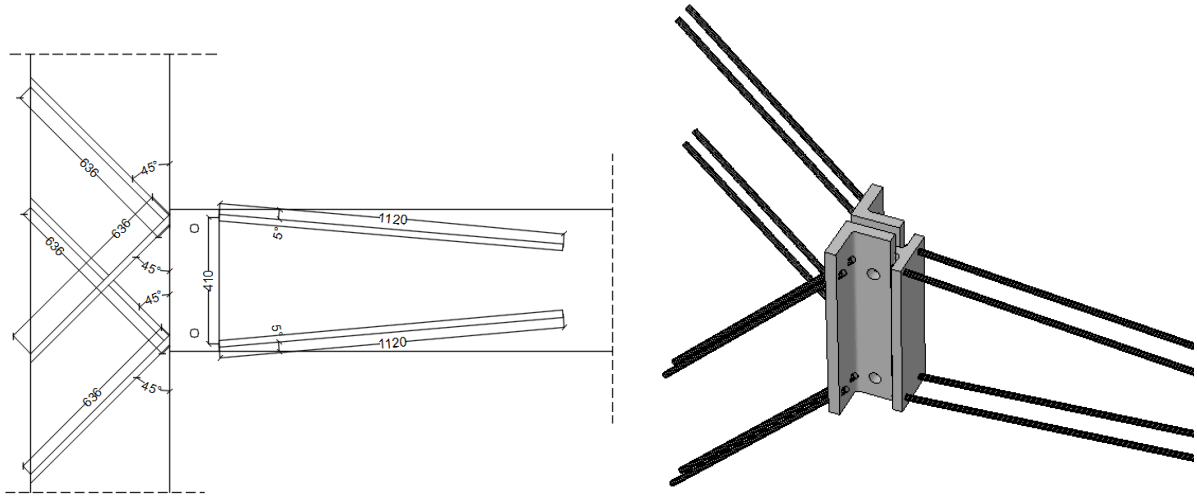

(a) Geometry (b) 3D details from numerical model

Figure A.5: Details of configuration 4

Configuration 5

In configuration 5, the spacing between the rods is reduced from 410 mm to 340 mm. This is the only change from configuration 4.

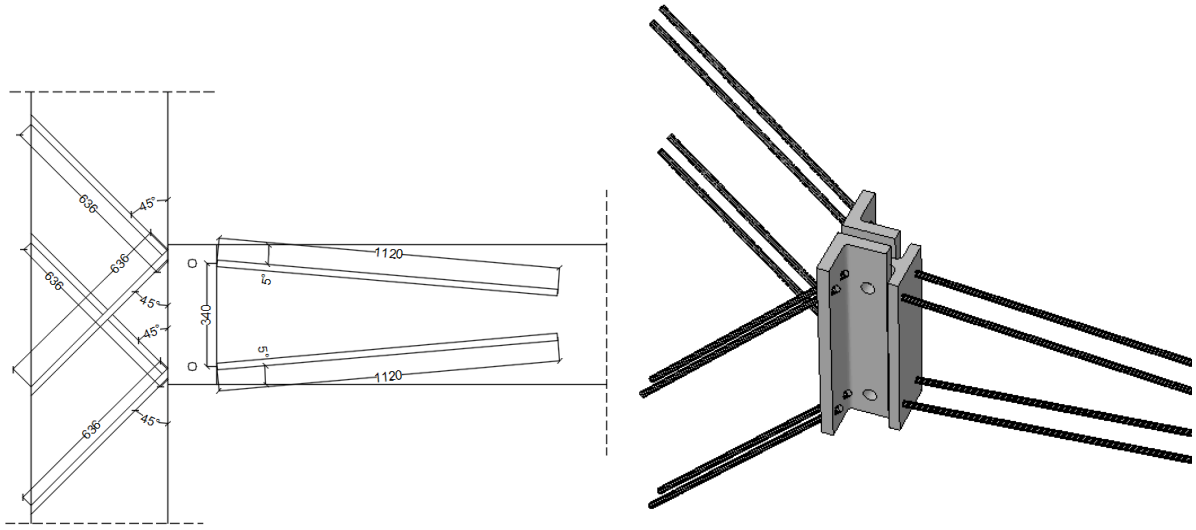

(a) Geometry (b) 3D details from numerical model

Figure A.6: Details of configuration 5

Configuration 6

The beam has rod-to-grain angle 10° and rod spacing of 410 mm. Rod-to-grain angle in column is 70°. Most comparable with configuration 3 where the only difference is the rod-to-grain angle in the column.

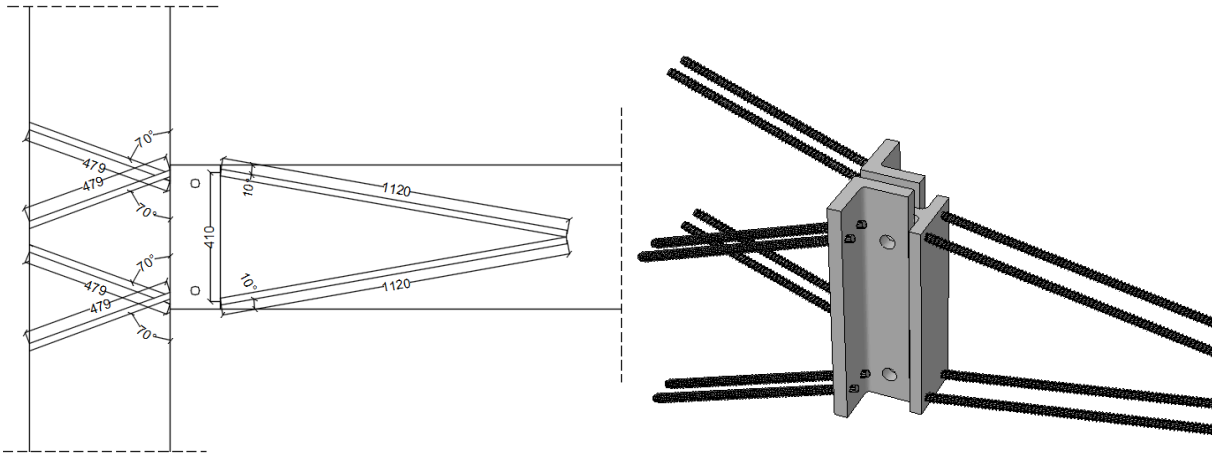

(a) Geometry (b) 3D details from numerical model

Figure A.7: Details of configuration 6

Configuration 7

In configuration 7, the only difference from configuration 6 is that the rod-to-grain angle in the column has been changed to 75°.

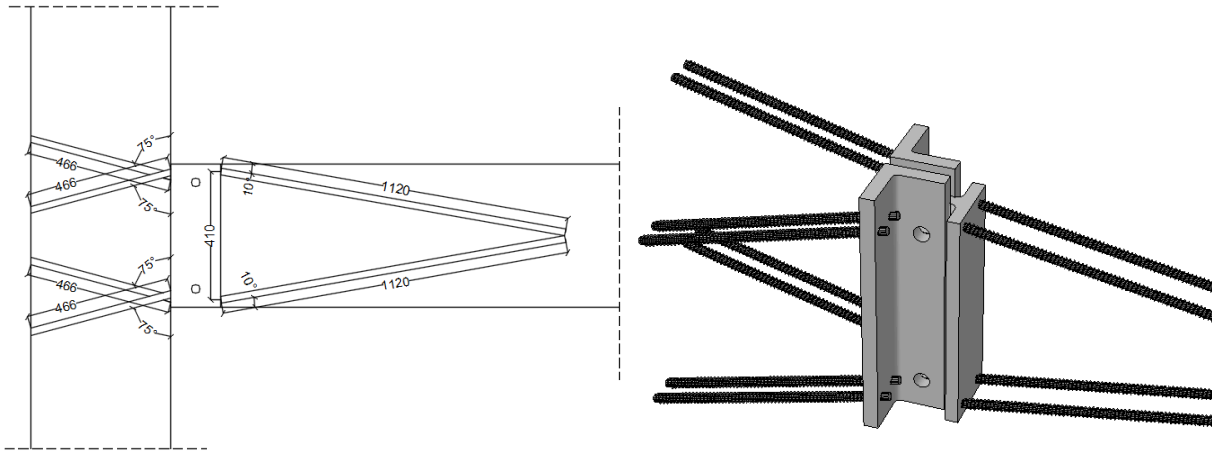

(a) Geometry (b) 3D details from numerical model

Figure A.8: Details of configuration 7

A.2 Convergence issues

Running analyses with the threaded rod model offered some convergence issues. In the first step of the calculation, where the forces representing the prestressed bolts were applied, Abaqus struggled to find convergence and gave the error message “displacement increment for contact is too big”. Much time went into troubleshooting this error. It was discovered that when the L- and T-profile were tied together using tie constraints, there were no problems with convergence. This was obviously not a good solution as it would give results that were too stiff.

Further investigation revealed that when analyses were run with the stiffener part described in 3.2.3.3, there was also no convergence issue. Using the stiffener would still give an inaccurate model, since it was decided that it was necessary to have two separate L-profiles for practical reasons, as discussed in 3.2.3.3.

However, in the interaction module in Abaqus, it is possible to create an interaction called *model change*. This interaction allows for a region to be deactivated in certain steps. This model change interaction was therefore given to the stiffener part in the step where the displacement is enforced on the beam. This is illustrated in Figure A.9 below.

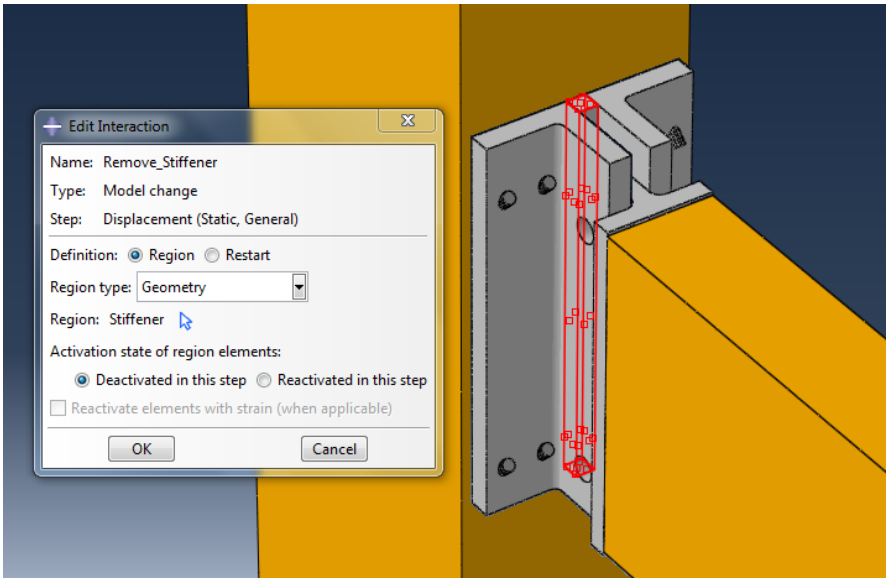

Figure A.9: Model change interraction

By using this interaction, the L-profiles are tied together while the force representing the bolts is applied, and once the deformation of the beam starts, the stiffener is effectively removed from the analysis. This method solved the convergence issues, while still allowing the model to be an accurate representation of the actual connection. It was used for all the configurations using the threaded rod model.

B Withdrawal stress distributions

The withdrawal stress distribution for configuration 1-7 in Table 4.1 are presented in detail in this appendix. As mentioned in Chapter 4, each rod-timber interface surface has 16 circumferential paths with individual stress distributions. These are all included in each plot along with the mean distribution. The x-axis indicates the embedment length, X_e, and the y-axis indicates the shear force, τ, at a given embedment length. Distributions around three rods were extracted per configuration, these rods circled in Figure B.1. In the column, surfaces around the downward-going rods are marked with green circles, and upward-going rods are marked with red circles. As seen in the figure, different rods had to be used when rods connected to one L-profile went in different directions.

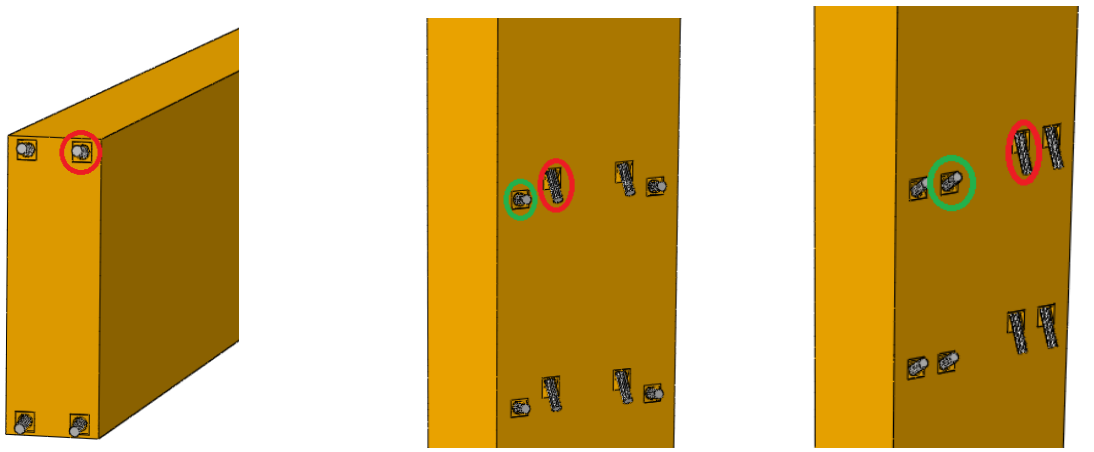

(a) Beam (b) Column, opposite rods per profile (c) Column, equal rods per profile

Figure B.1: Surfaces used for extracting shear distributions

Stresses in these distributions are taken from the 3rd increment. Acting bending moments for each configuration is given along with the results. A recap of the configurations analyzed is presented in Table B.1.

Tabell B.1: Summary of configurations

Configuration	**Rod-to-grain angle beam [deg]**	**Rod-to-grain angle column [deg]**	**Maximum spacing between rods in beam [mm]**
1	10	55, 70	410
2	10	45*	410
3	10	45	410
4	05	45	410
5	05	45	340
6	10	70	410
7	10	75	410

* Rods on one L-profile go in opposite direction

Configuration 1 – 33 kNm acting moment

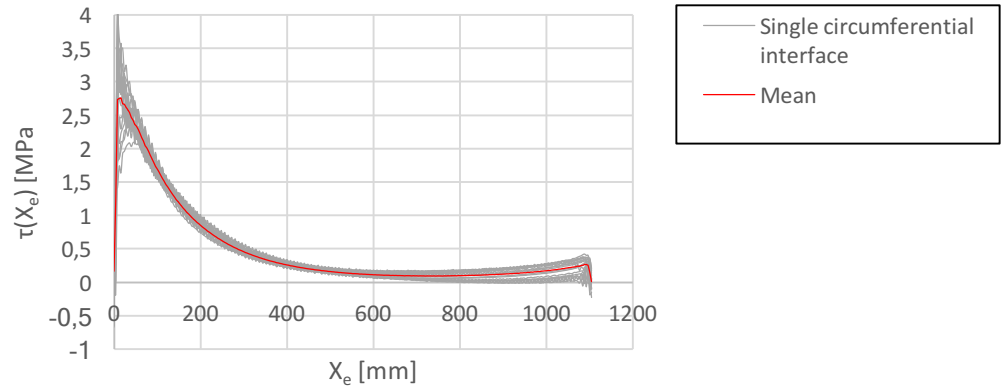

Figure B.2: Surface around 10° beam rod, configuration 1

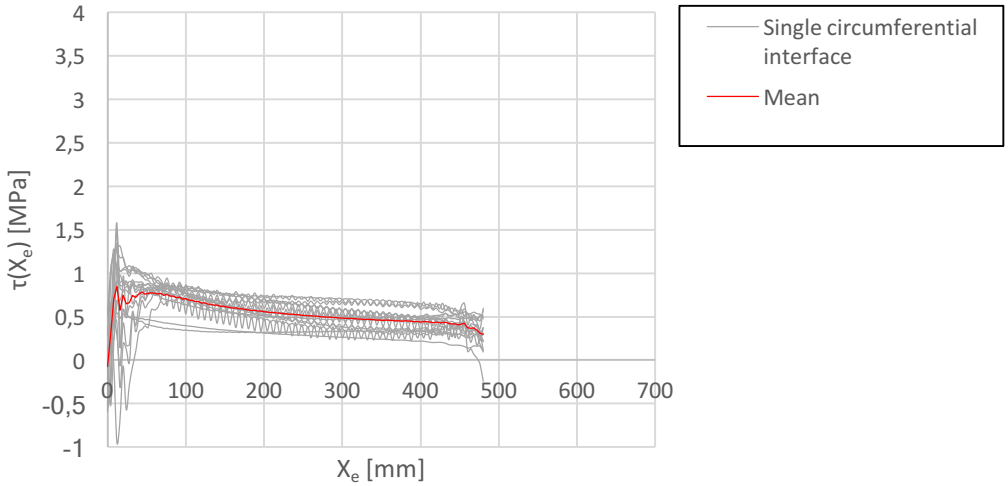

Figure B.3: Surface around 70° downward-going column rod, configuration 1

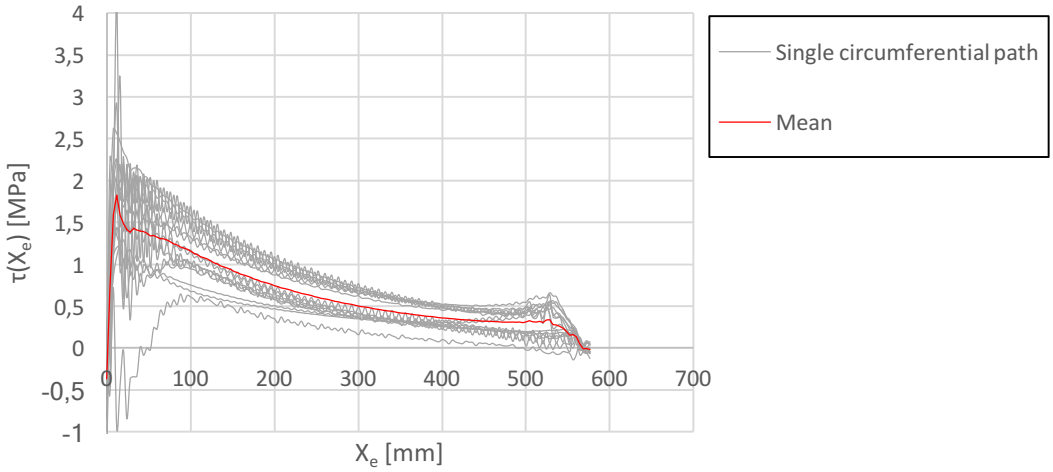

Figure B.4: Surface around 55° upward-going column rod, configuration 1

Configuration 2 – 29 kNm acting moment

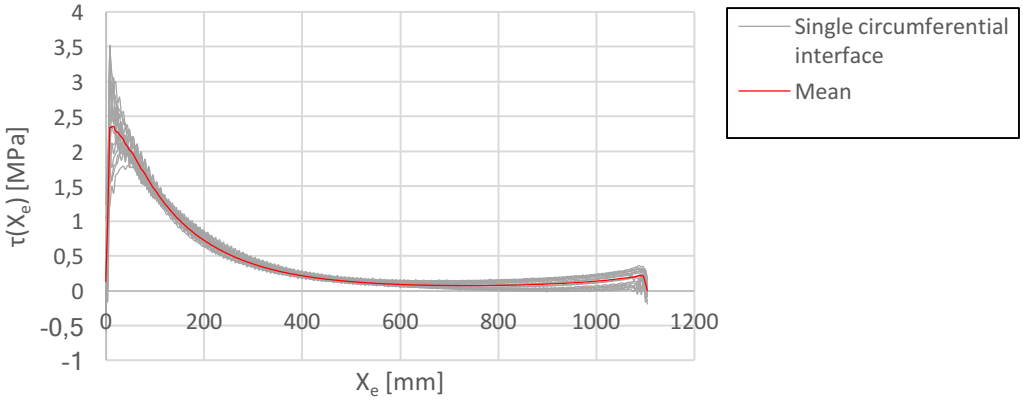

Figure B.5: Surface around 10° beam rod, configuration 2

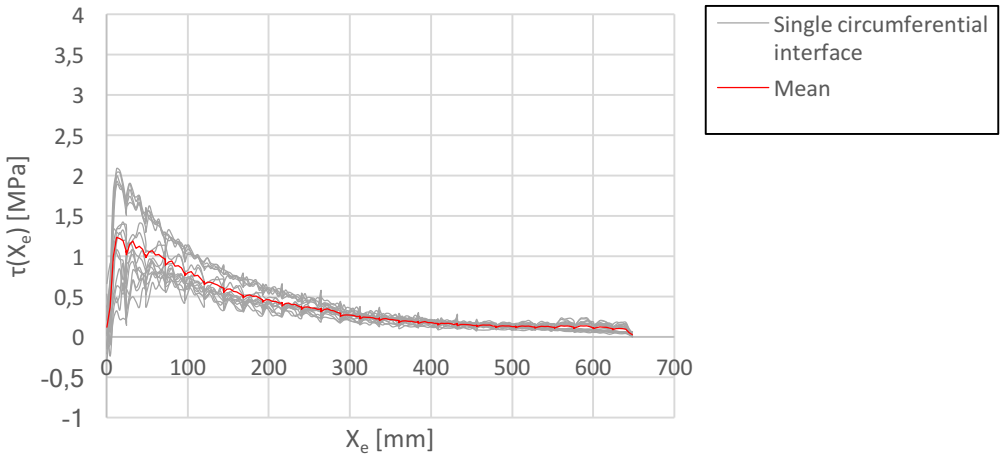

Figure B.6: Surface around 45° downward-going column rod, configuration 2

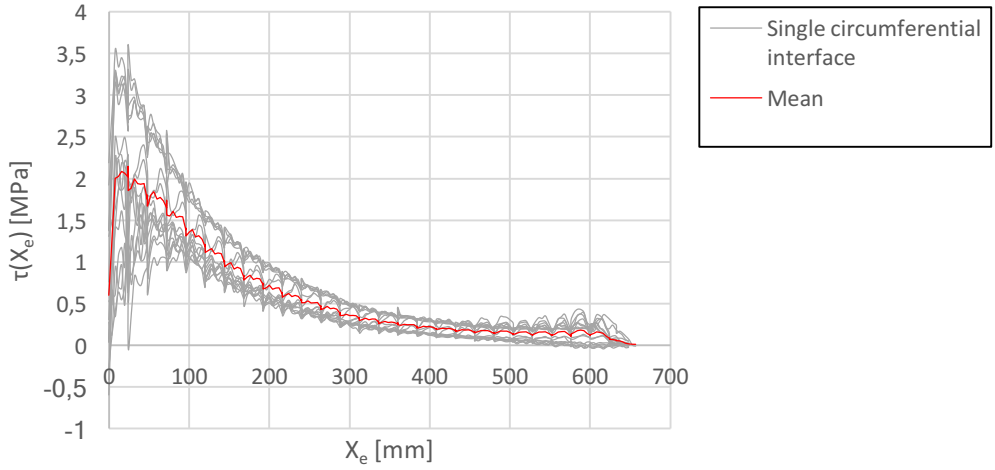

Figure B.7: Surface around 45° upward-going column rod, configuration 2

Configuration 3 – 25 kNm acting moment

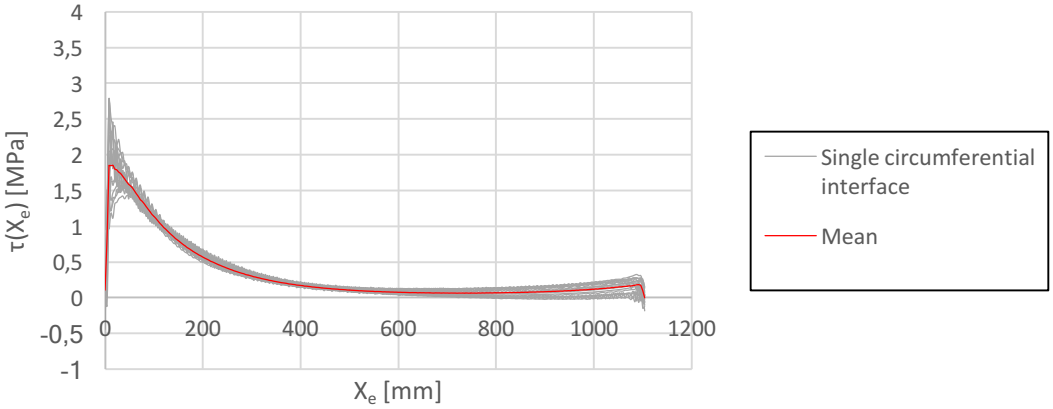

Figure B.8: Surface around 10° beam rod, configuration 3

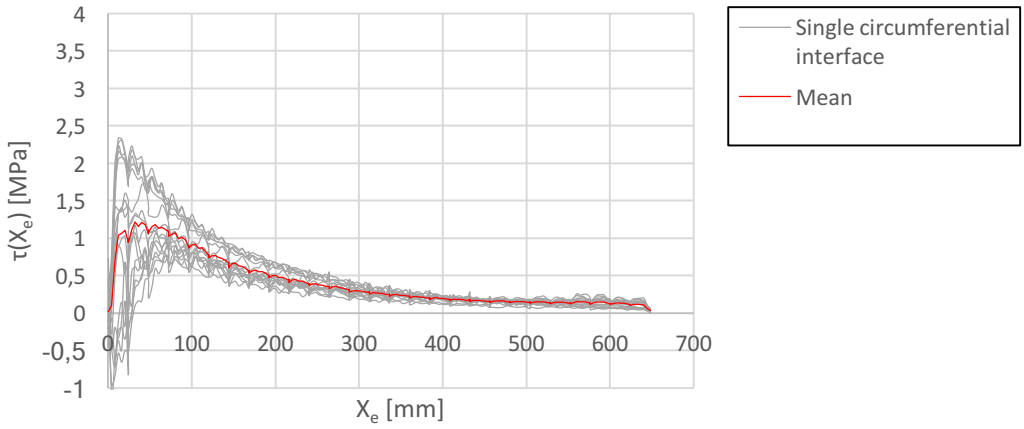

Figure B.9: Surface around 45° downward-going column rod, configuration 3

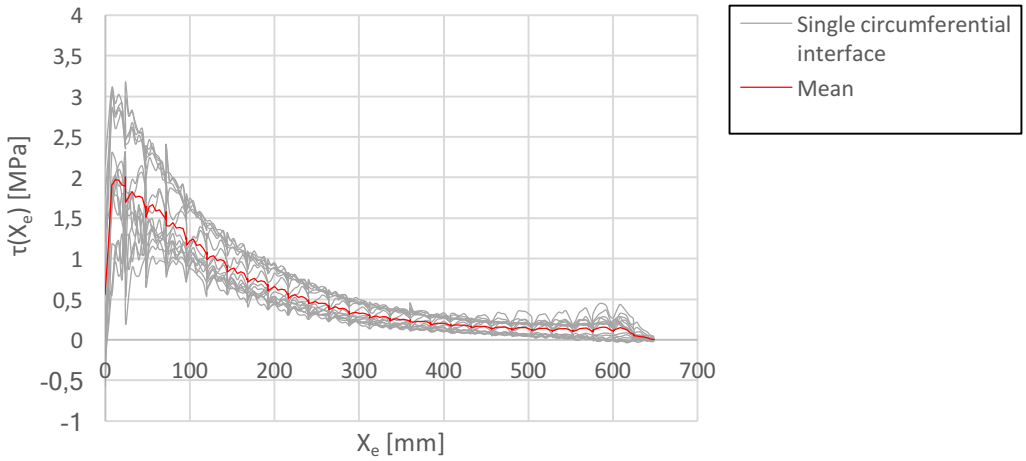

Figure B.10: Surface around 45° upward-going column rod, configuration 3

Configuration 4 – 23 kNm acting moment

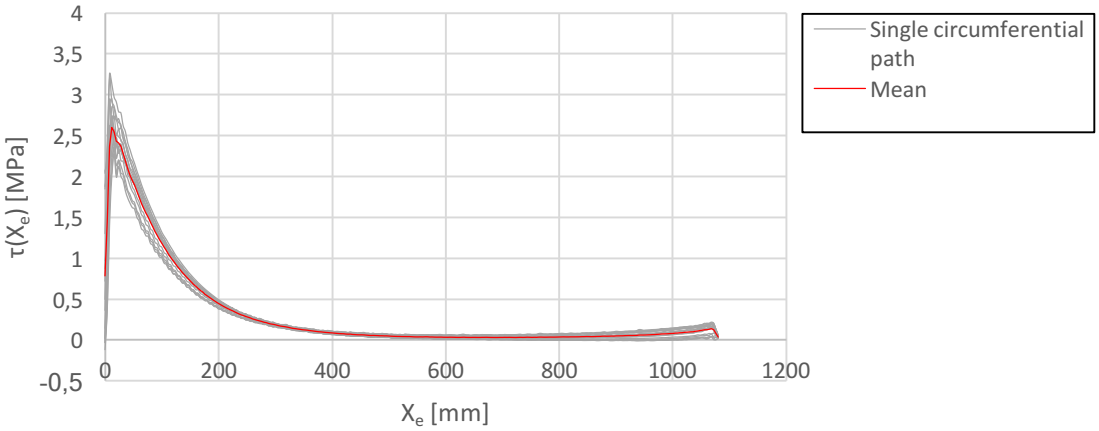

Figure B.11: Surface around 5° beam rod, configuration 4

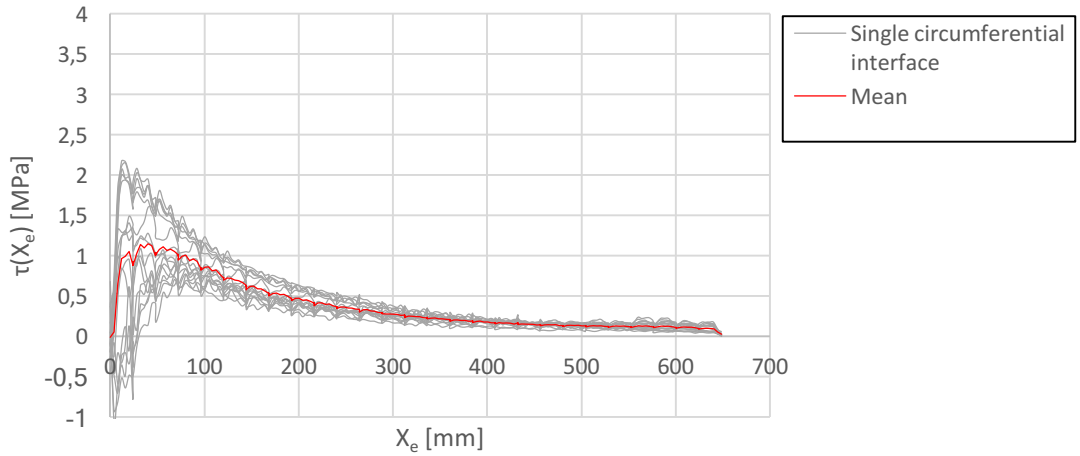

Figure B.12: Surface around 45° downward-going column rod, configuration 4

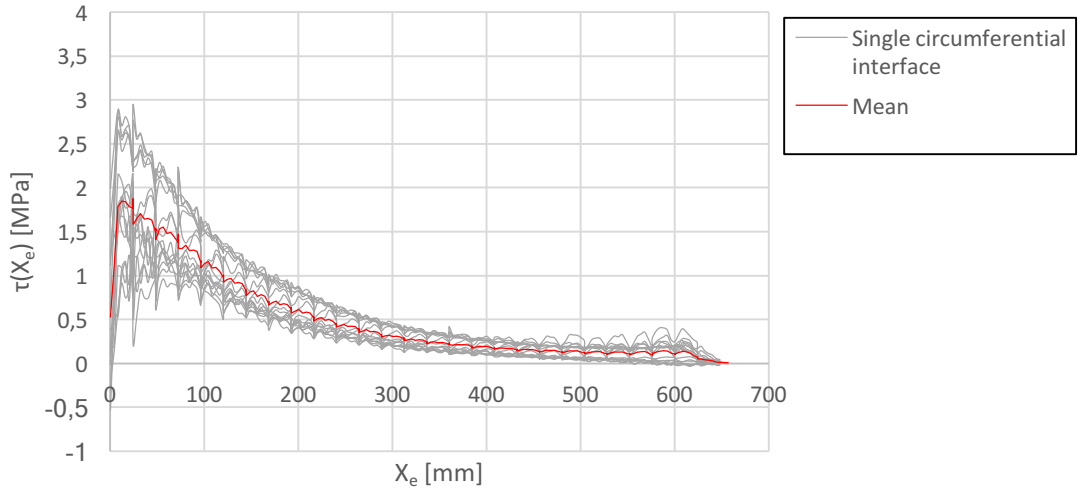

Figure B.13: Surface around 45° upward-going column rod, configuration 4

Configuration 5 – 21 kNm acting moment

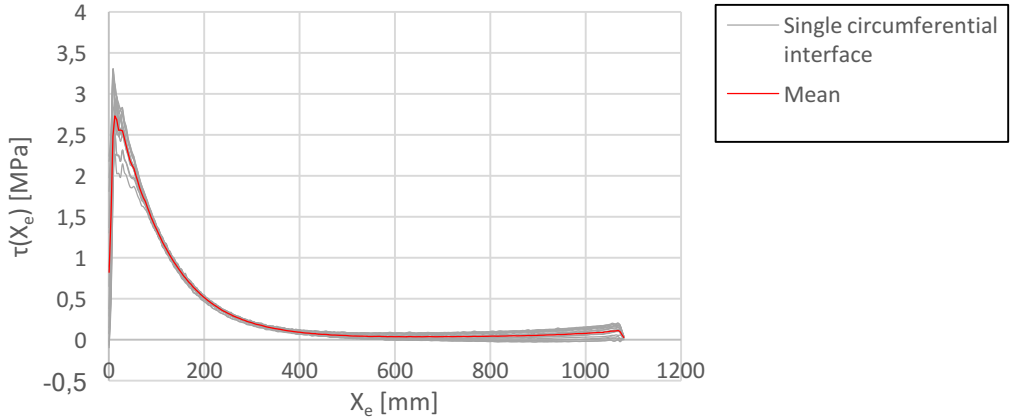

Figure B.14: Surface around 5° beam rod, configuration 5

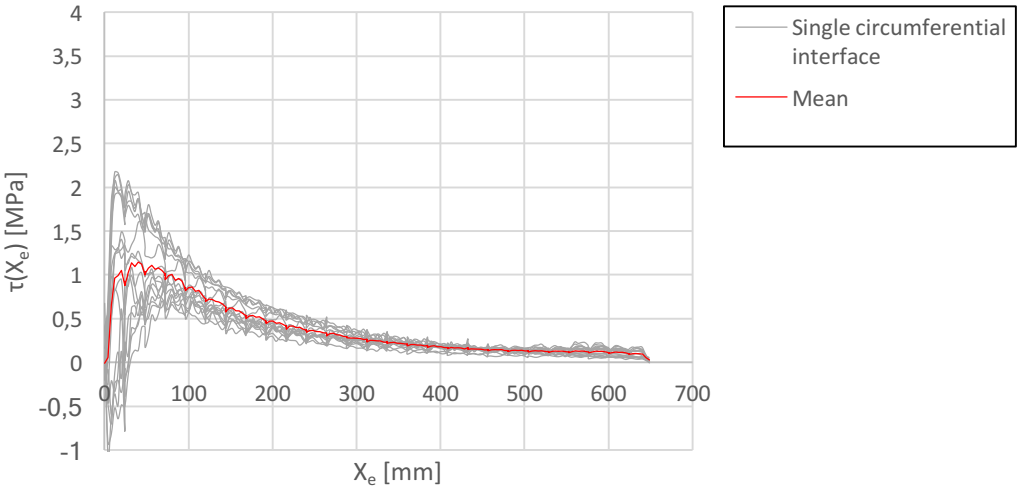

Figure B.15: Surface around 45° downward-going column rod, configuration 5

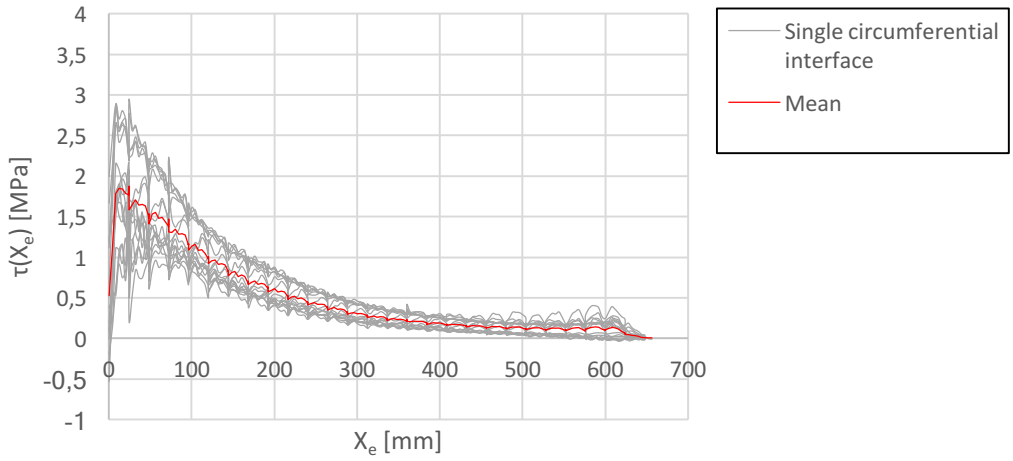

Figure B.16: Surface around 45° upward-going column rod, configuration 5

Configuration 6 – 32 kNm acting moment

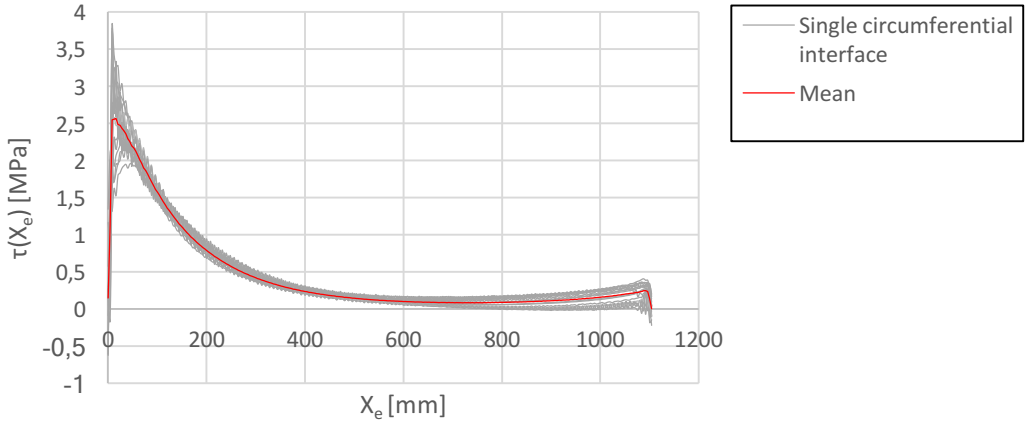

Figure B.17: Surface around 10° beam rod, configuration 6

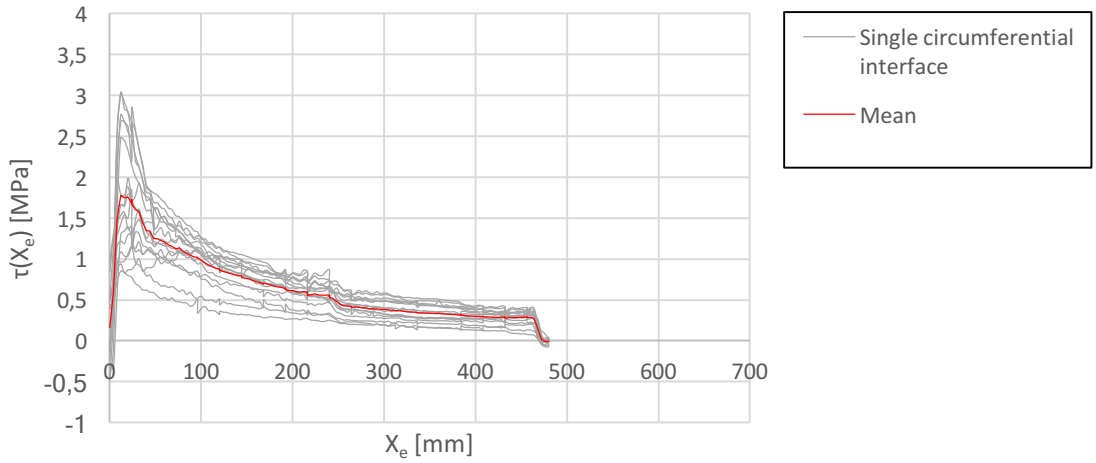

Figure B.18: Surface around 70° downward-going column rod, configuration 6

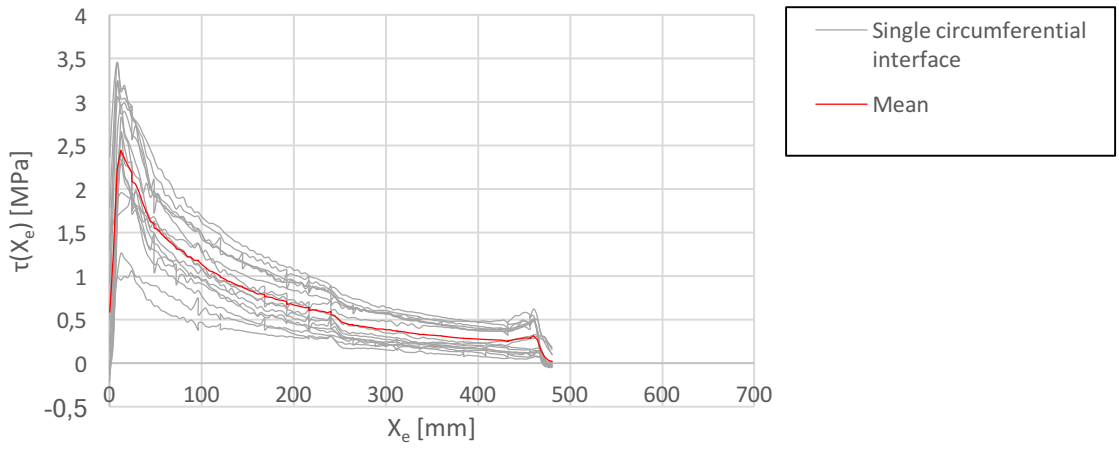

Figure B.19: Surface around 70° downward-going column rod, configuration 6

Configuration 7 – 30 kNm acting moment

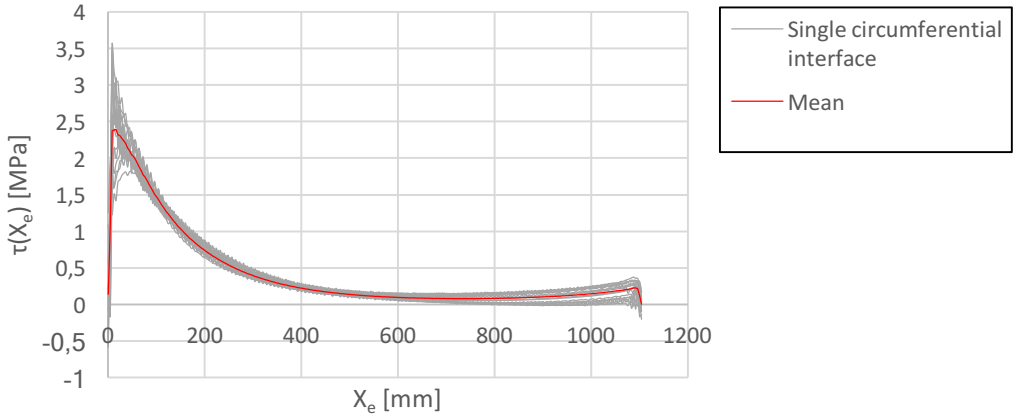

Figure B.20: Surface around 10° beam rod, configuration 7

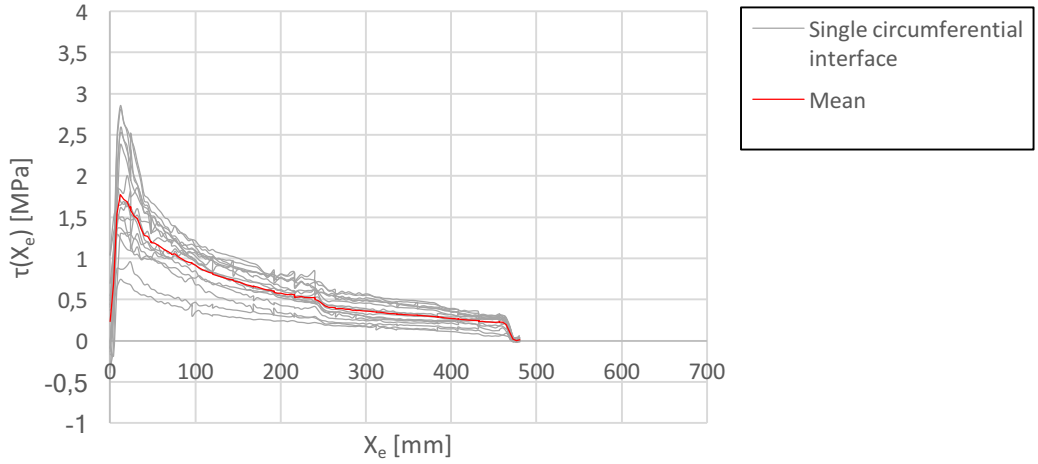

Figure B.21: Surface around 75° downward-going column rod, configuration 7

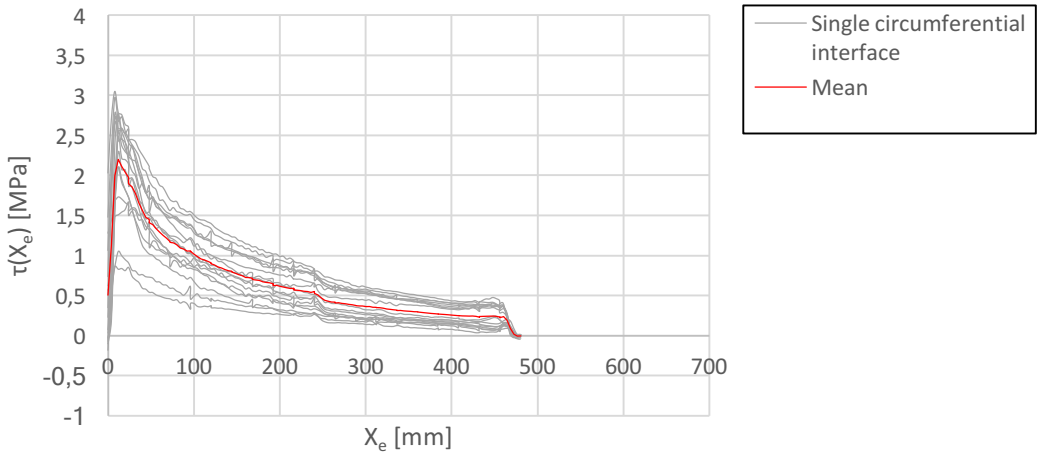

Figure B.22: Surface around 75° downward-going column rod, configuration 7

C Von Mises stress distributions and deformed shapes

Appendix C gives detailed images of the von Mises stresses in the different components of the connector. The timber elements are not included as stresses were very small compared to the fasteners and connector. Due to some local extreme values, all figures have a limit of 500 MPa to better see the distributions. Areas with larger stresses than 500 MPa are marked in grey. All distributions are obtained from the same displacement increment, and acting moment is presented for each configuration. The deformation scale factor is set to 30 so deformation patterns are easier to observe.

Configuration 1 – 33 kNm acting moment

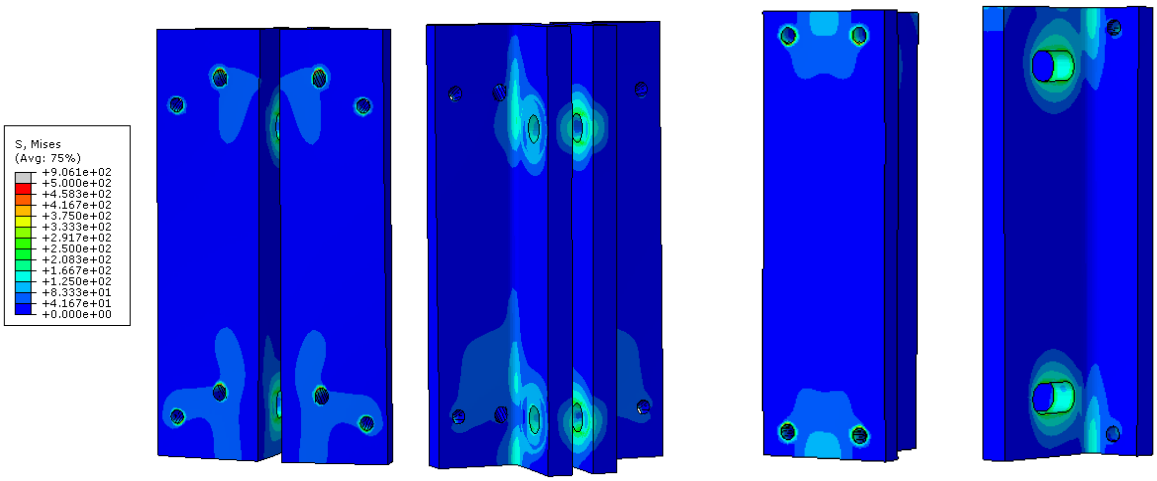

Figure C.1: von Mises stresses and deformation of connector, configuration 1

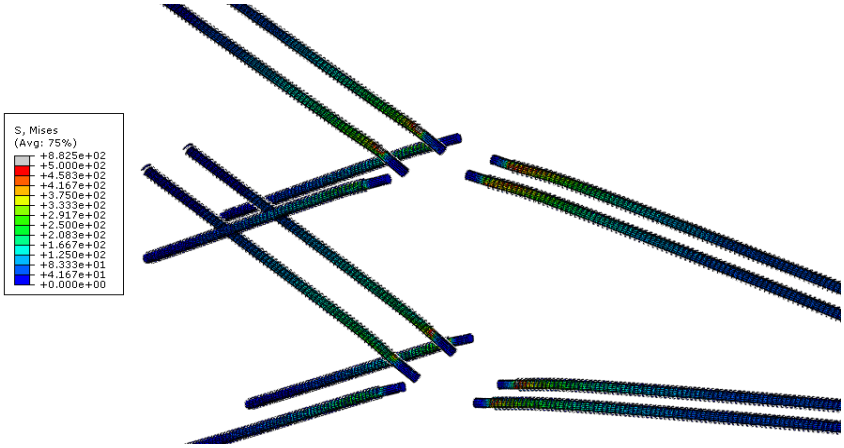

Figure C.2: von Mises stresses and deformation of fasteners, configuration 1

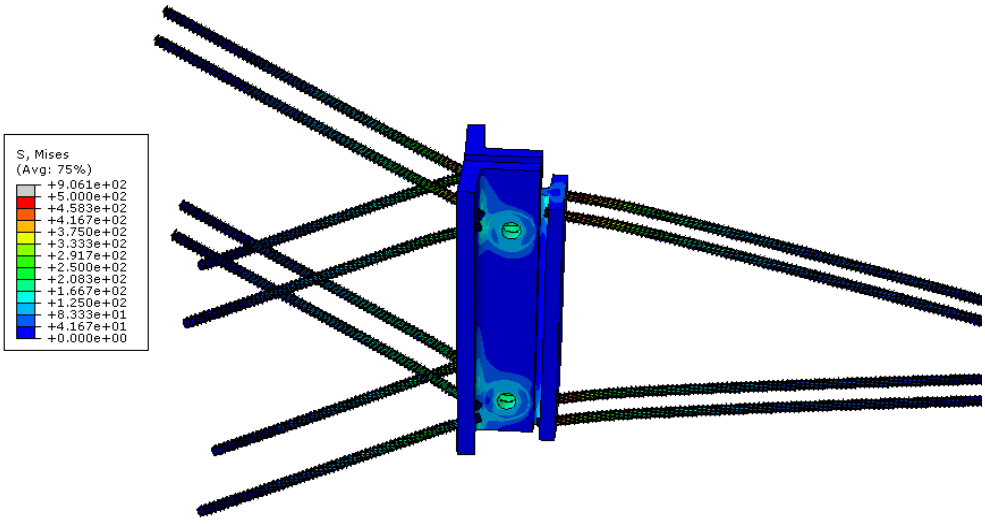

Figure C.3: von Mises stresses and deformation of connection (without timber elements), configuration 1

Configuration 2 – 29 kNm acting moment

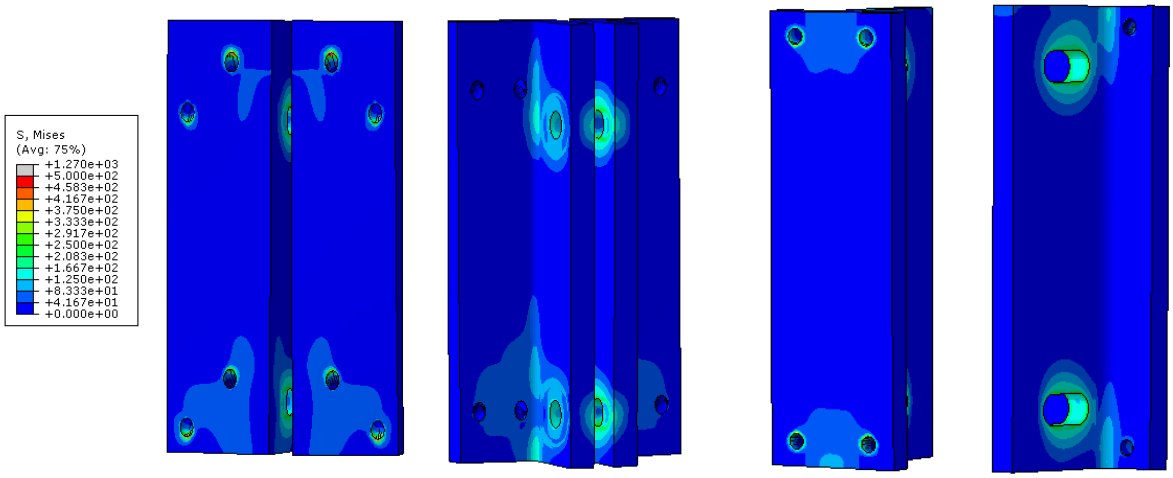

Figure C.4: von Mises stresses and deformation of connector, configuration 2

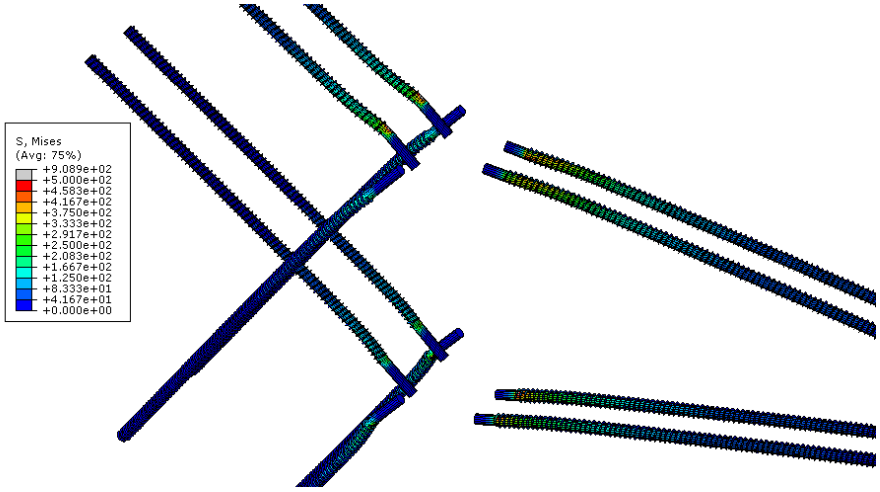

Figure C.5: von Mises stresses and deformation of fasteners, configuration 2

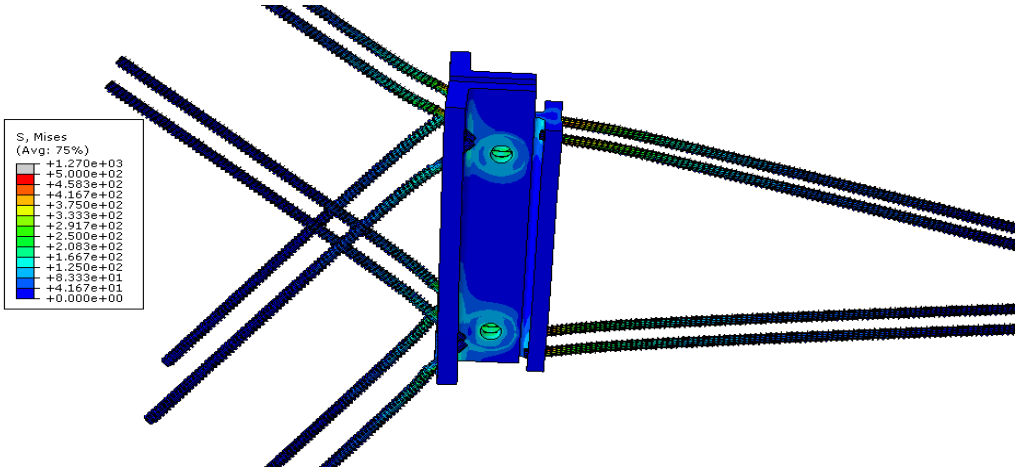

Figure C.6: von Mises stresses and deformation of connection (without timber elements), configuration 2

Configuration 3 – 25 kNm acting moment

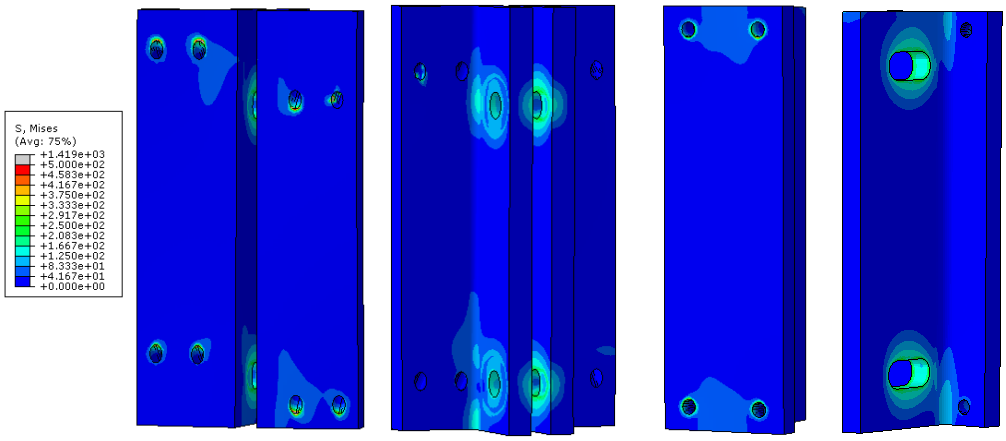

Figure C.7: von Mises stresses and deformation of connector, configuration 3

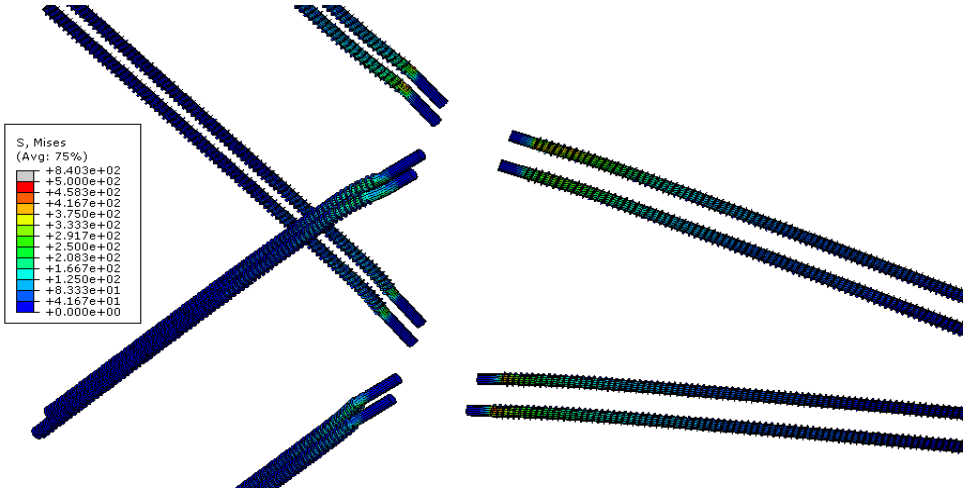

Figure C.8: von Mises stresses and deformation of fasteners, configuration 3

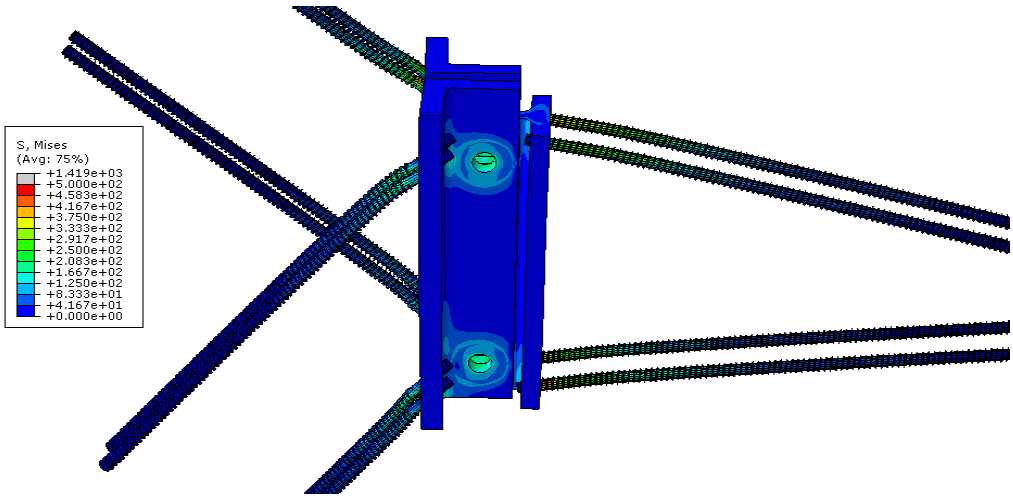

Figure C.9: von Mises stresses and deformation of connection (without timber elements), configuration 3

Configuration 4 – 23 kNm acting moment

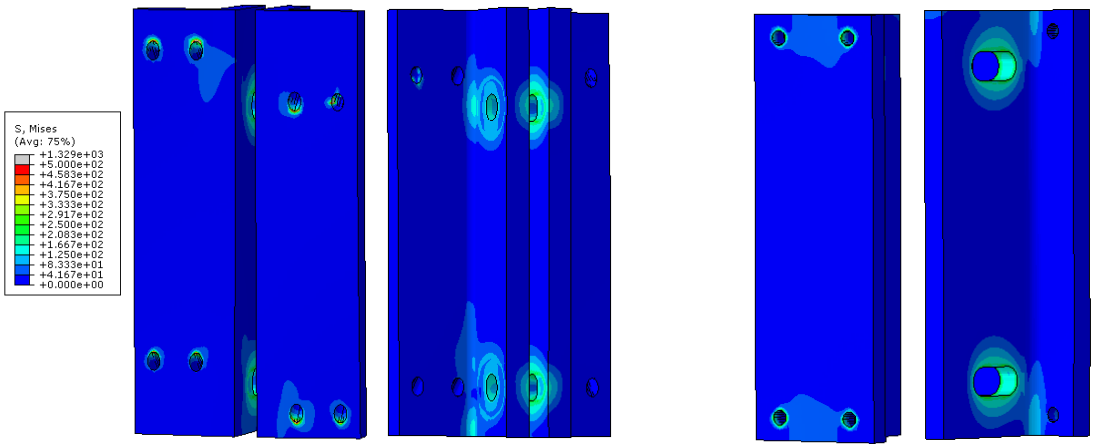

Figure C.10: von Mises stresses and deformation of connector, configuration 4

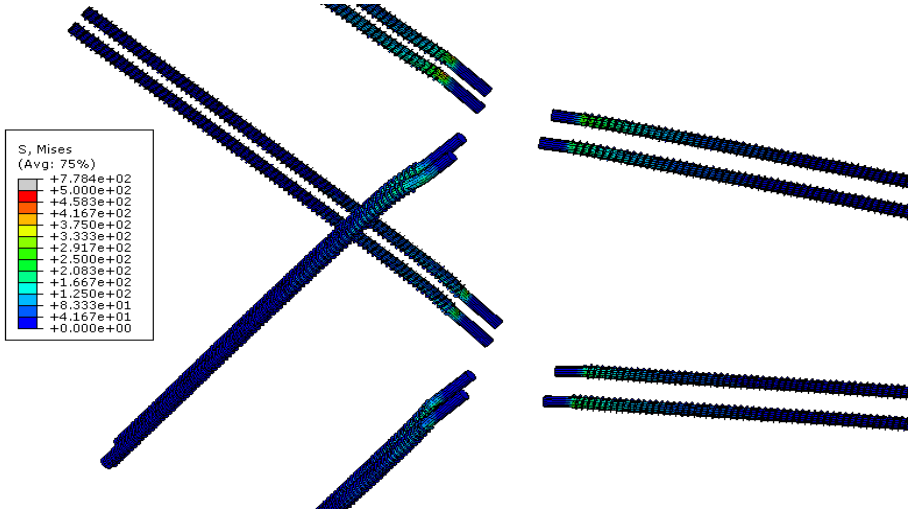

Figure C.11: von Mises stresses and deformation of fasteners, configuration 4

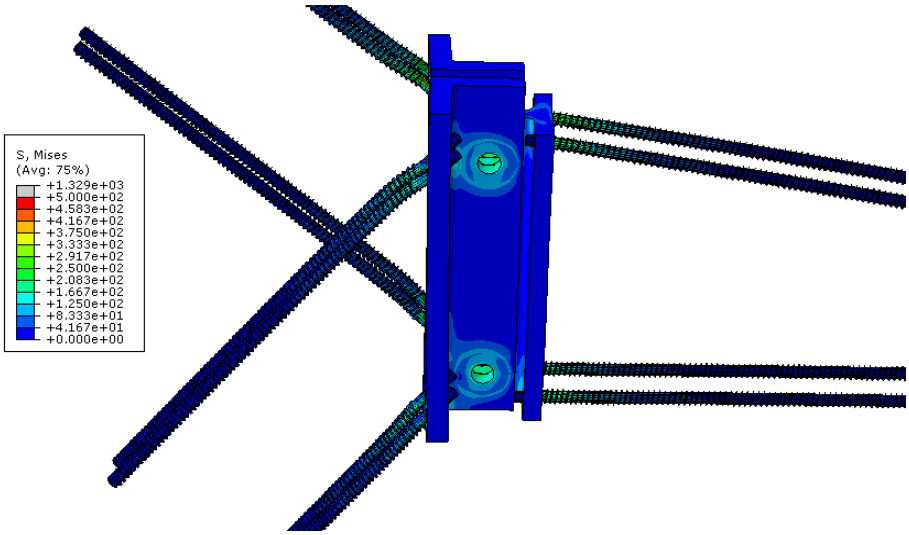

Figure C.12: von Mises stresses and deformation of connection (without timber elements), configuration 4

Configuration 5 – 21 kNm acting moment

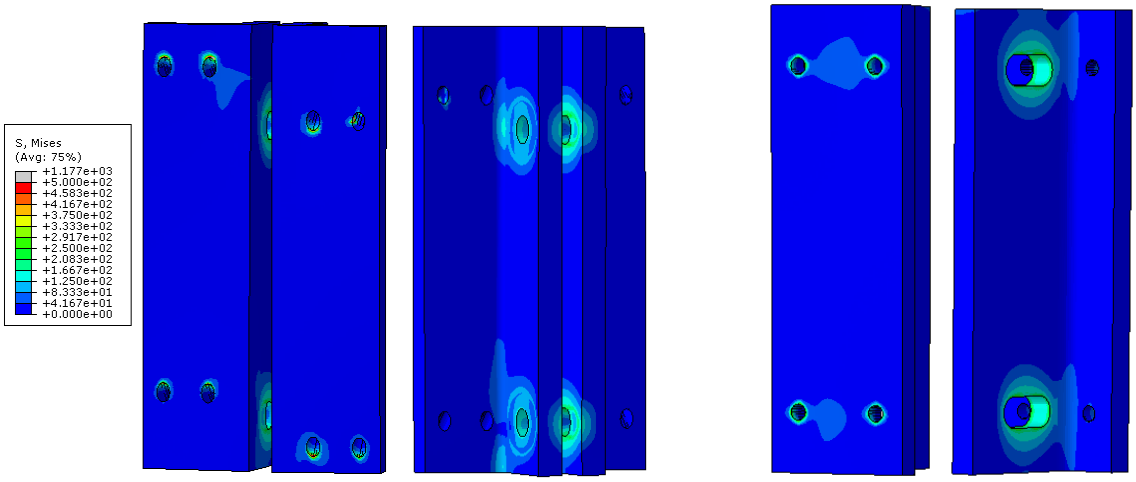

Figure C.13: von Mises stresses and deformation of connector, configuration 5

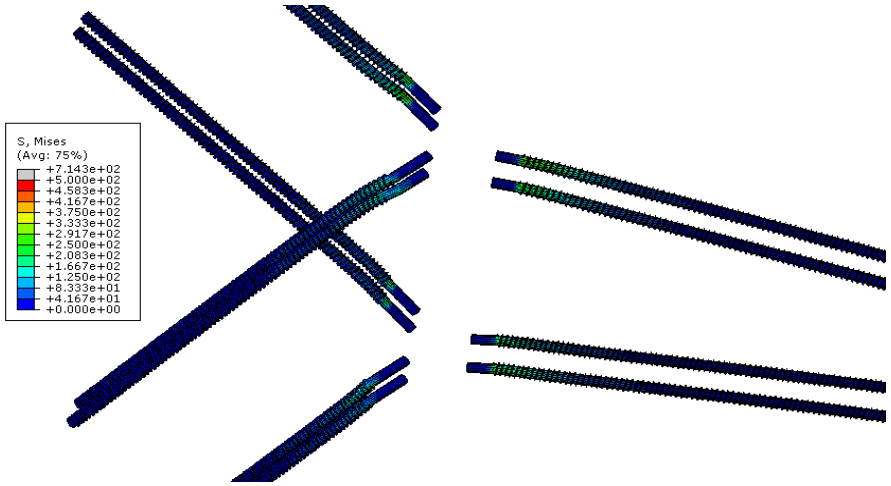

Figure C.14: von Mises stresses and deformation of fasteners, configuration 5

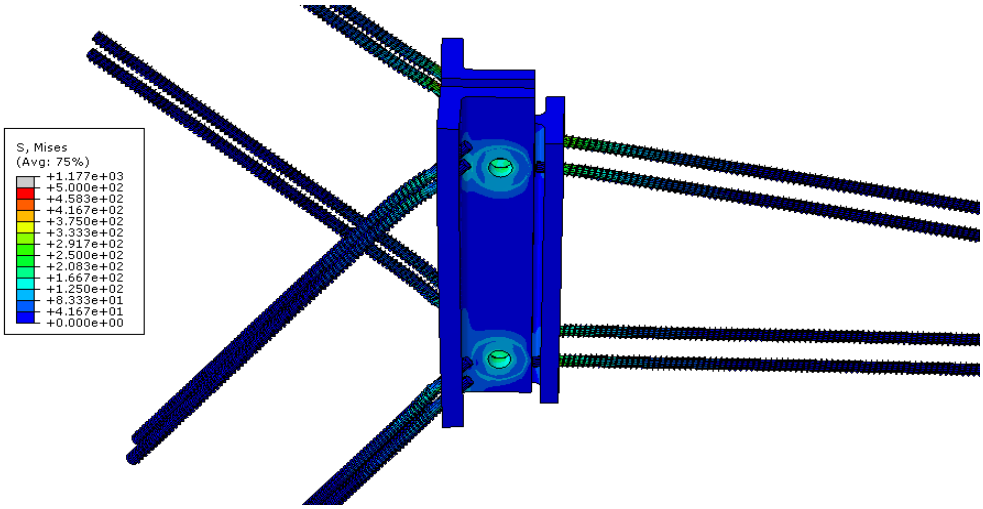

Figure C.15: von Mises stresses and deformation of connection (without timber elements), configuration 5

Configuration 6 – 32 kNm acting moment

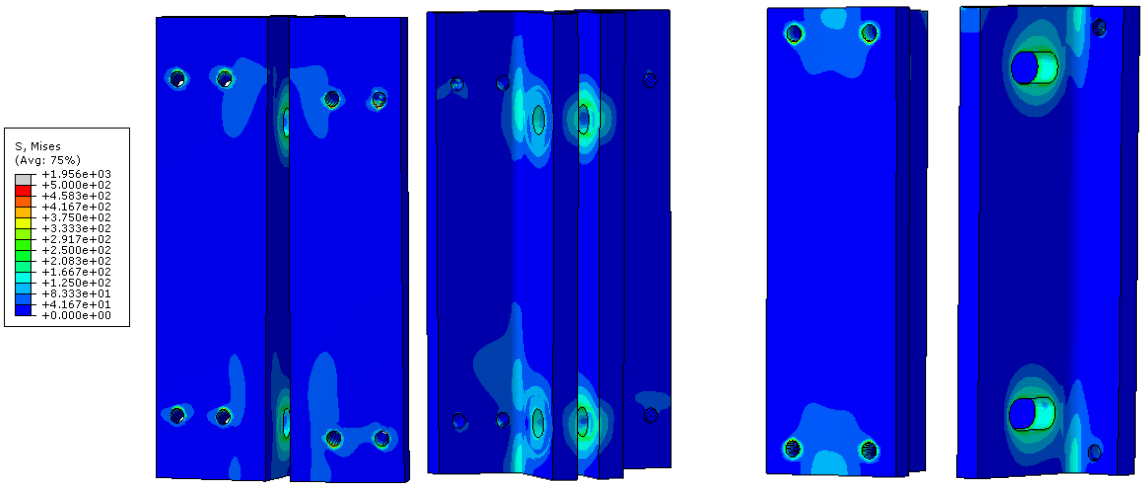

Figure C.16: von Mises stresses and deformation of connector, configuration 6

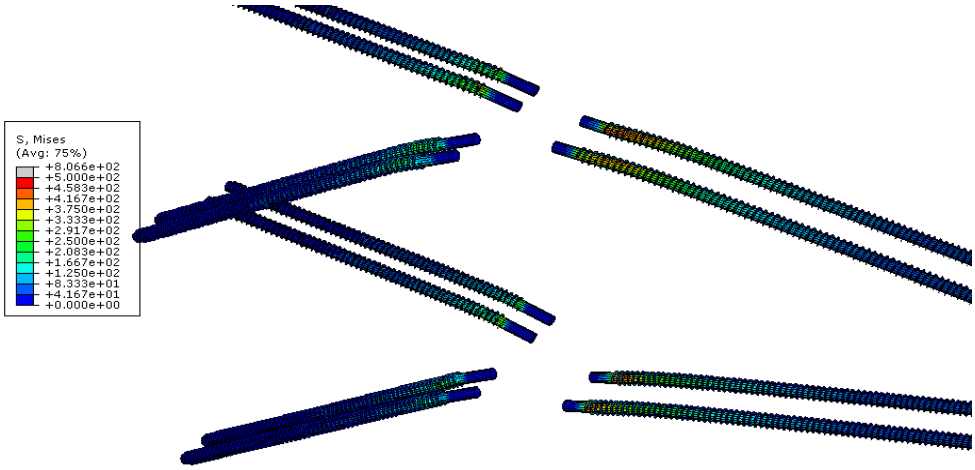

Figure C.17: von Mises stresses and deformation of fasteners, configuration 6

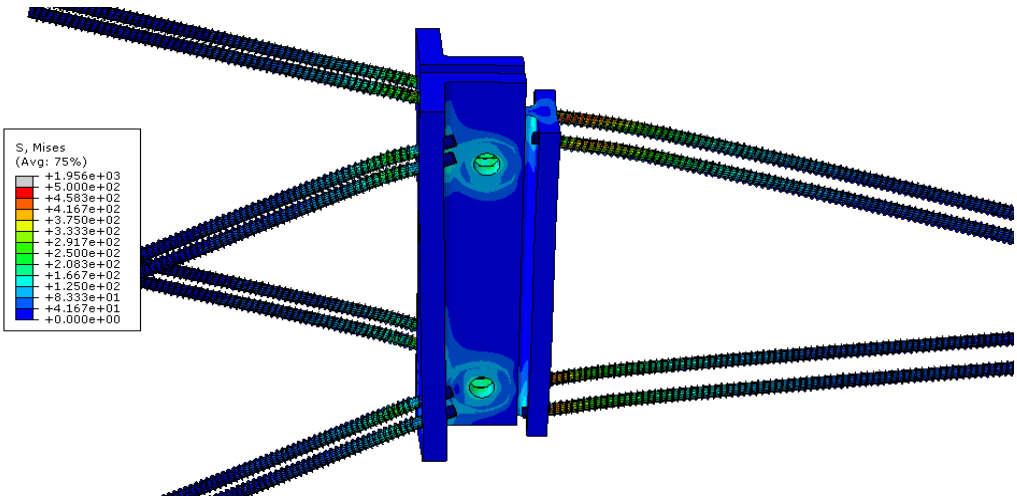

Figure C.18: von Mises stresses and deformation of connection (without timber elements), configuration 6

Configuration 7 – 30 kNm acting moment

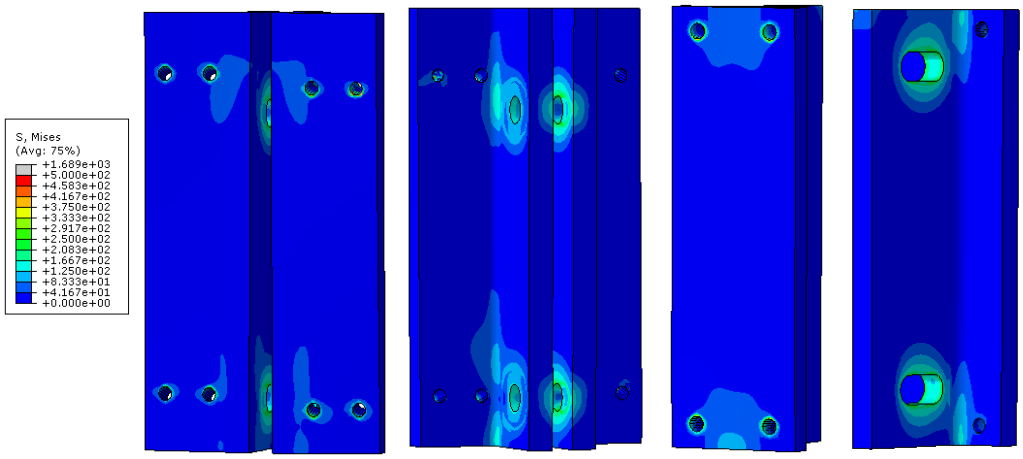

Figure C.19: von Mises stresses and deformation of connector, configuration 7

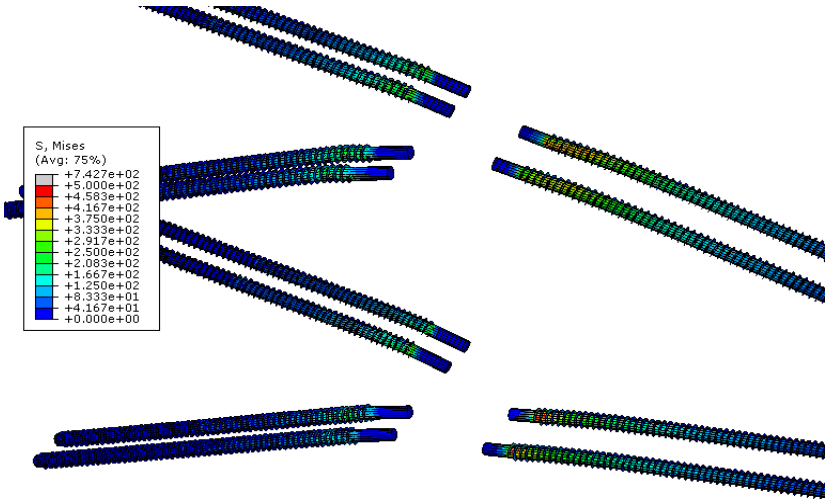

Figure C.20: von Mises stresses and deformation of fasteners, configuration 7

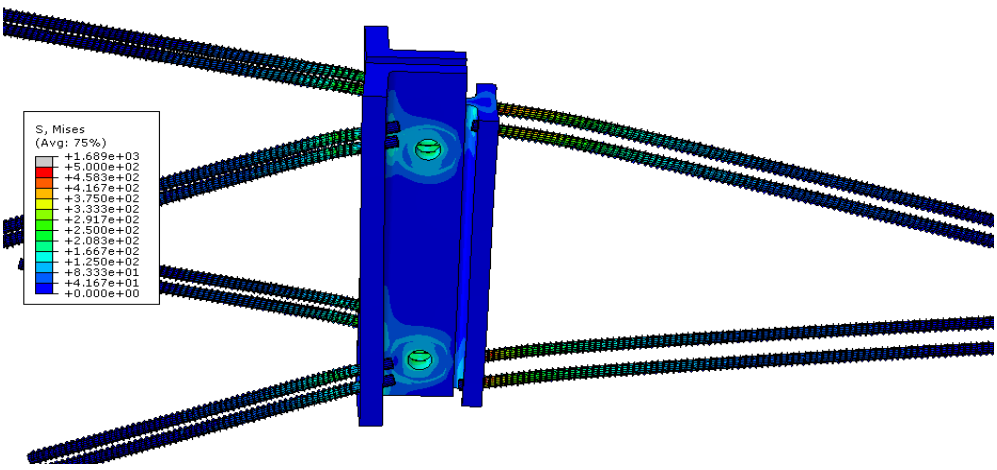

Figure C.21: von Mises stresses and deformation of connection (without timber elements), configuration 7

D Discarded ideas

This appendix describes two ideas that were developed, tested and discarded during the process of this thesis. An evaluation of why the ideas were discarded is also included.

D.1 40 mm continuous profile

As described in subsection 3.2.3, an attempt was made to reduce the large deformations in the top and bottom corners of the L-profiles. A new profile, believed to reduce this deformation, was tested. Instead of two separate L-profiles connected to the column, one solid plate would be connected. Two thinner plates would be welded on to the solid plate and connected to the T-profile, see Figure D.1.

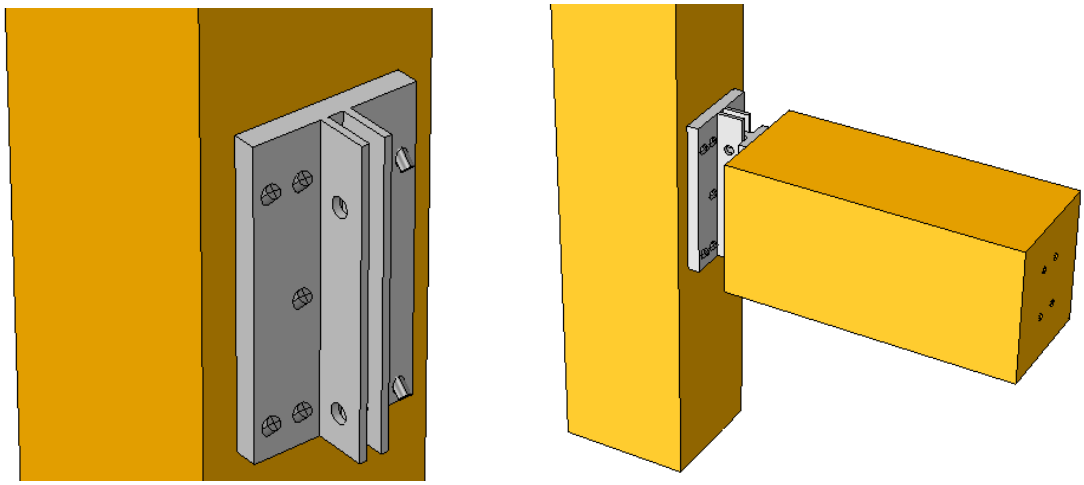

(a) Profile on column (b) Full connection

Figure D.1: Connection with continuous 40 mm profile

A continuous plate with a thickness of 40 mm was made. This was considered to be a reasonable upper limit to what would be possible to use in reality, and was tested before the thickness evaluation done in 3.2.3.1. The thin plates that would be welded on to the 40 mm plate were 13 mm thick, so that the combined thickness was the same as the T-profile, 26 mm. The profile was made in the same height as the long L-profiles, 520 mm. The T-profile remained the same as before, 26 mm thick and 460 mm tall. This analysis was run with the cylindrical rod model.

Results

The rotational stiffness of this configuration was 13680 kNm/rad. The distribution of von Mises stresses can be seen in Figure D.2. Due to some local extreme values, a limit of 500 MPa has been set to better view the distribution of stresses. The areas with stresses above 500 MPa are colored grey. A deformation scale factor of 10 has been so deformations are easier to observe.

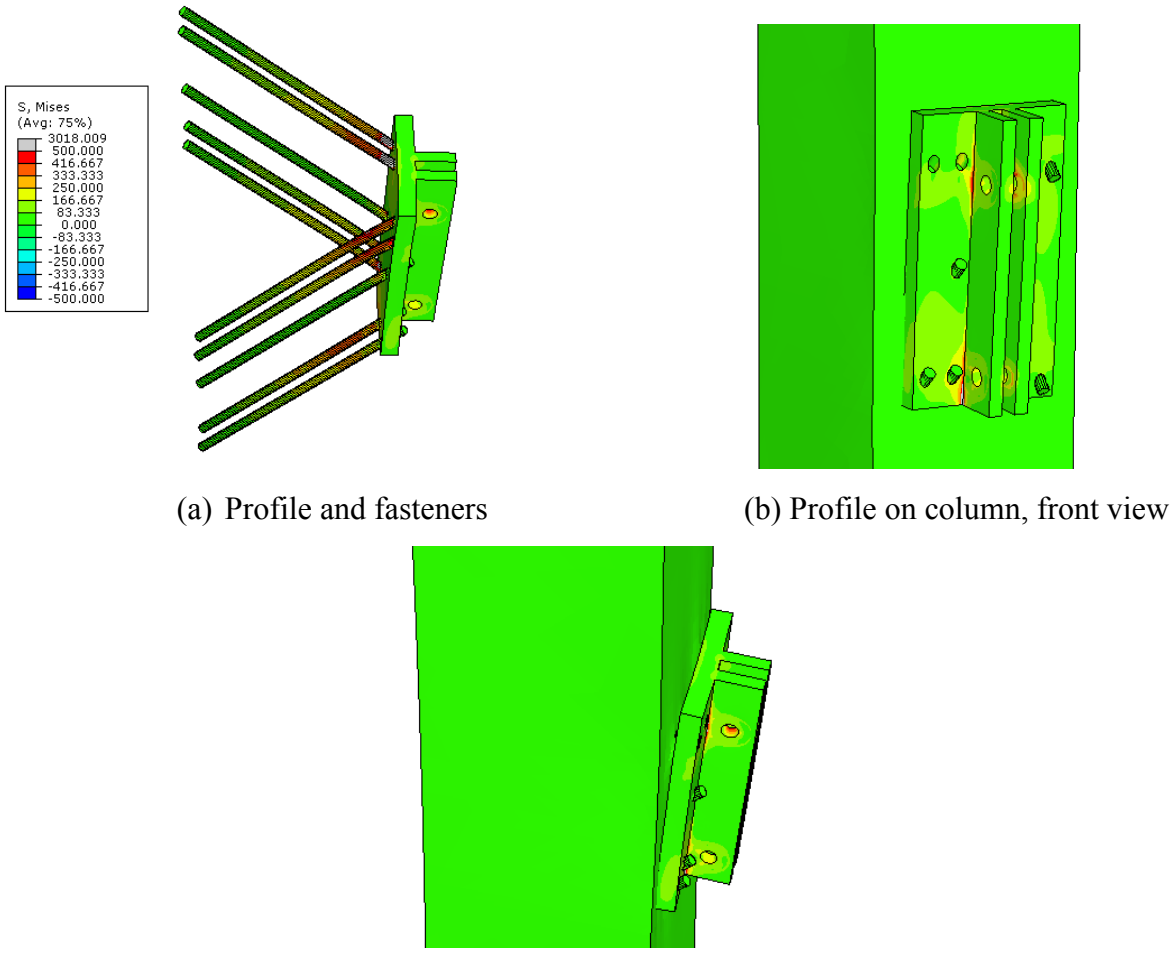

(a) Profile and fasteners

(b) Profile on column, front view

(c) Profile on column, side view

Figure D.2: von Mises stress distributions and deformation of 40 mm continuous profile

It is clear from the Figure D.2 (a) and (b) that the rods experience a lot more stresses than the plate. Figure D.2 (c) shows that there is very little deformation of the actual profile. It has rotated much more than it has deformed, which indicates that the withdrawal capacity of the rods was more critical than the bending capacity of the profile.

Evaluation

The rotational stiffness of 13680 kNm/rad is an increase of 15% compared to the previous solution with two separate L-profiles with thickness 26 mm. It was clear that withdrawal the rods were the critical component in this solution. This gives reason to believe that a thickness of 40 mm might be pointless since the connection will not experience the full effect of the thickness, due to rods deforming.
It became clear while studying this solution that it would be challenging to assemble. One solid profile like this would weigh approximately 50 kg. At the factory, machines could be used to place the profiles, but it is still very unmanageable. The biggest problem however is the fact that the rods are pointing in opposite directions on each side of the profile, as explained in sub-subsection 3.2.3.3. Therefore, no further analyses were run with a solid plate.

D.2 40 mm profile with flat bearing surfaces

During the process of testing the 40mm continuous profile, an idea of a profile that would not require any type of special washers or nuts, was thought of. In this case, as seen in Figure D.3, the profile would have angled cuts where the holes are, creating flat bearing surfaces for the nuts so that normal washers and nuts could be used.

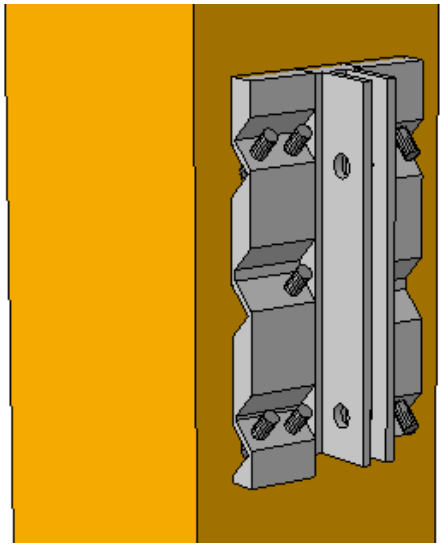

Figure D.3: 40 mm plate profile with flat bearing surfaces

To compare with the profile from D.1, this part was created as one continuous solid profile. As for the profile in D.1, this would be a poor solution as it would be challenging to connect one

continuous profile. However, this idea could just as easily have been used in a solution with two separate L-profiles.

The angled surfaces where the nuts would be connected had thickness 10 mm, and the maximum thickness of the plate facing the column was 42.4 mm. A height of 520 mm was used for this solution. The plates that would be connected to the T-profile were 13 mm thick. In the production phase, these plates would have to be welded on to the profile facing the column.

Results

The rotational stiffness of the connector with contact surfaces was 10724 kNm/rad which is 22% lower than the 40mm continuous profile. Figure D.4 shows the distribution of von Mises stresses in the plate. Due to some local extreme values, a limit of 500 MPa has been set to easier see the stress distribution. Areas with stresses larger than 500 MPa are marked in grey. The contact surfaces for the top and bottom nuts are the most stressed areas. This is reasonable as it is far from the neutral axis and the thickness is very small compared to the rest of the plate.

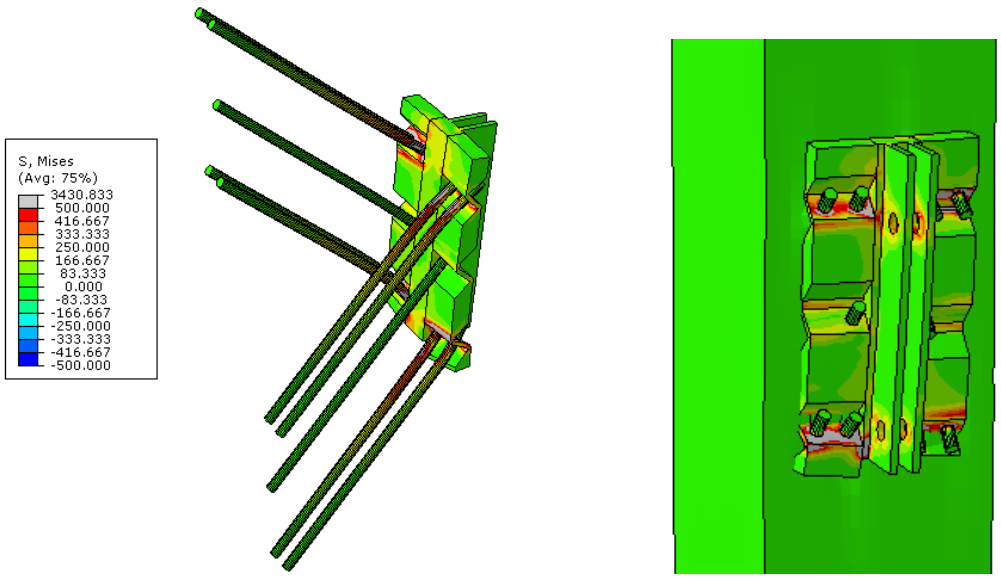

(a) Profile and fasteners (b) Profile on column

Figure D.4: von Mises stresses and deformation of 40 mm profile with flat bearing surfaces

Evaluation

This solution was discarded rather quickly after seeing the big loss in rotational stiffness. It is believed that the small thickness in the high stress areas at the top and bottom is part of the reason why this solution is so much softer than other thinner solutions.

E Documentation of numerical models

This section provides documentation of the numerical models used for optimizing the connection in section 3.2

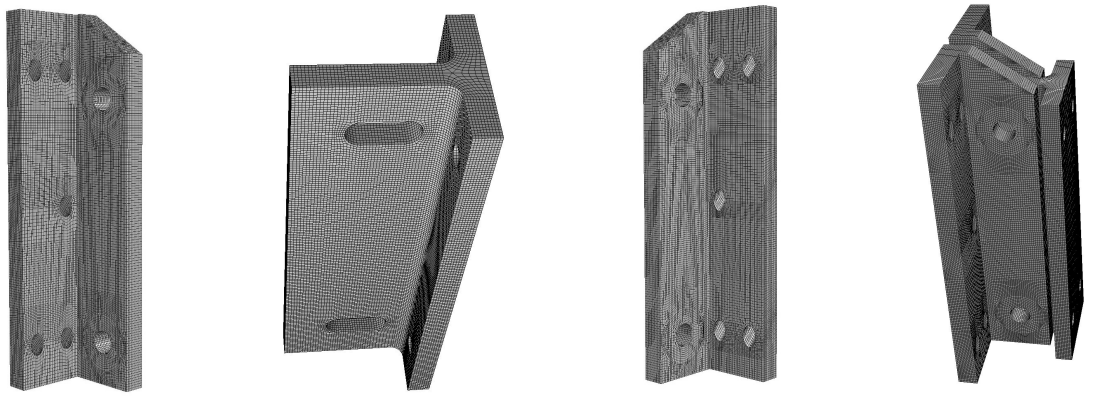

(a) Left L-profile (b) T-profile (c) Right L-profile (d) LT-connector

Figure E.1: Final proposal for steel profiles in LT-connector

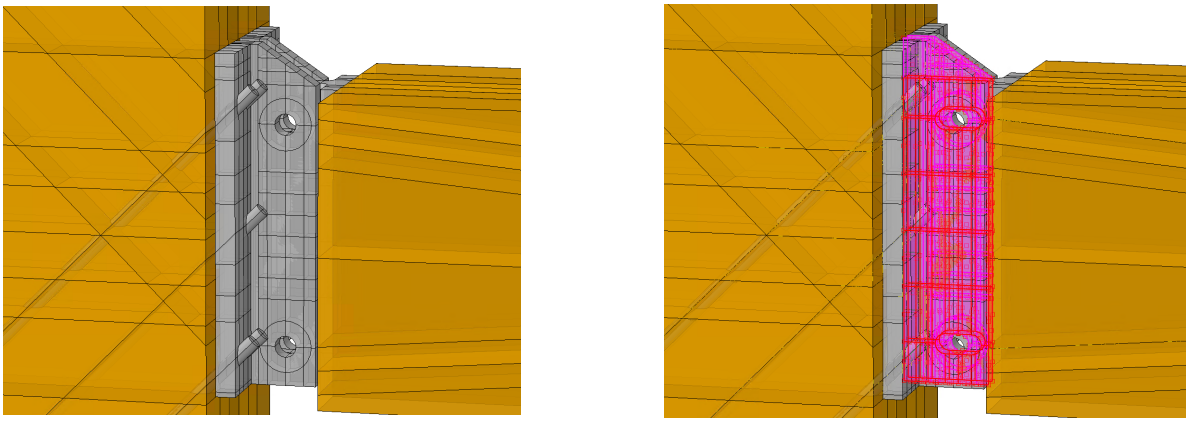

(a) LT-connector connected to timber elements (b) Friction surfaces between steel profiles displayed pink and red

Figure E.2: LT-connector connected to timber elements

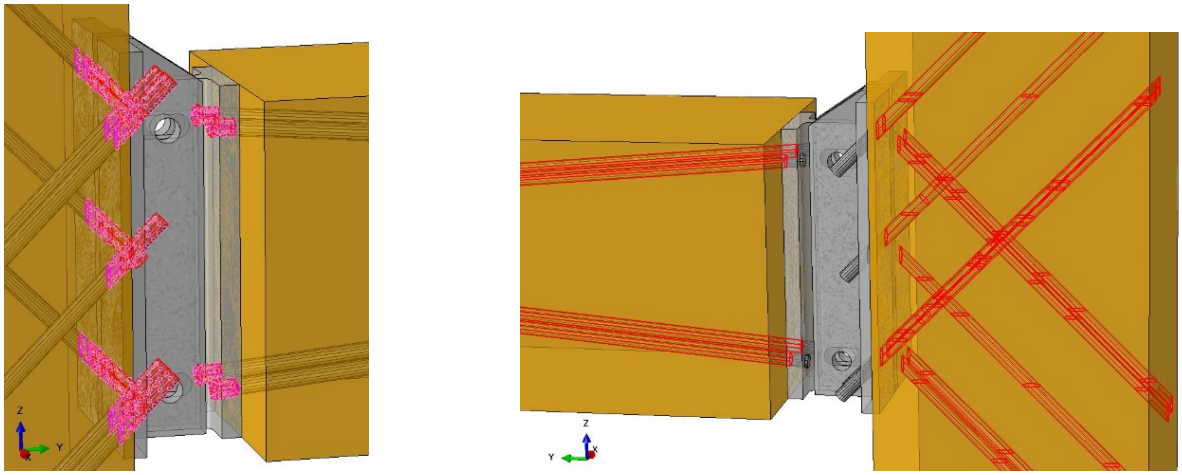

(a) Tied constraints between rods and LT-connector displayed in pink.

(b) Cohesive zones in circular rod models displayed in red.

Figure E.3: Tied constraints and cohesive zones

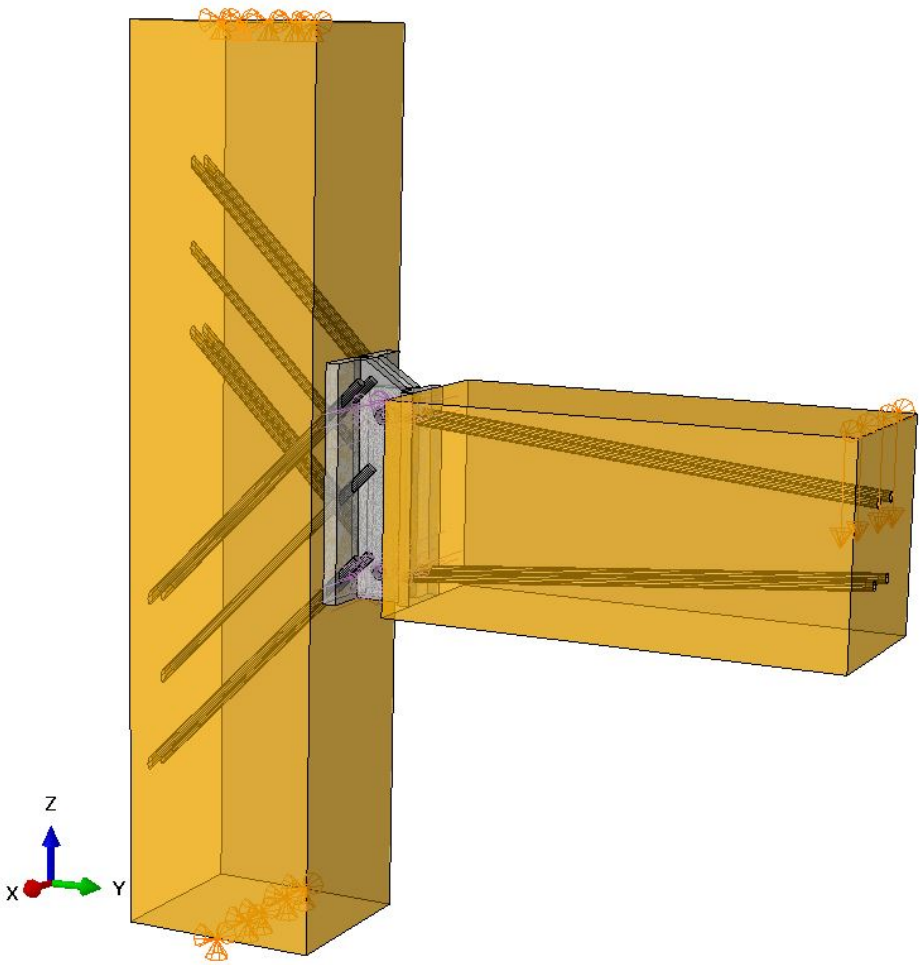

Figure E.4: Final proposal of connection with cylindrical rod model

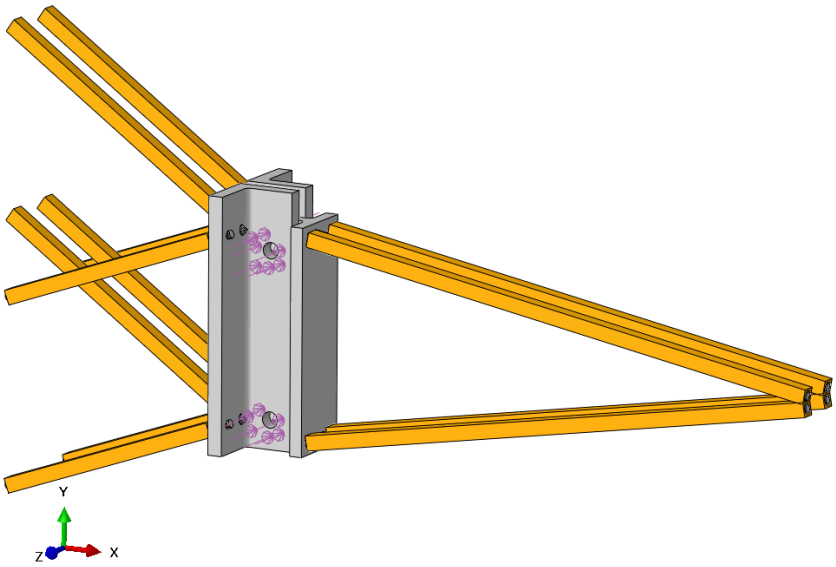

Figure E.5: Connector with the four parts used in the threaded rod model, configuration 1

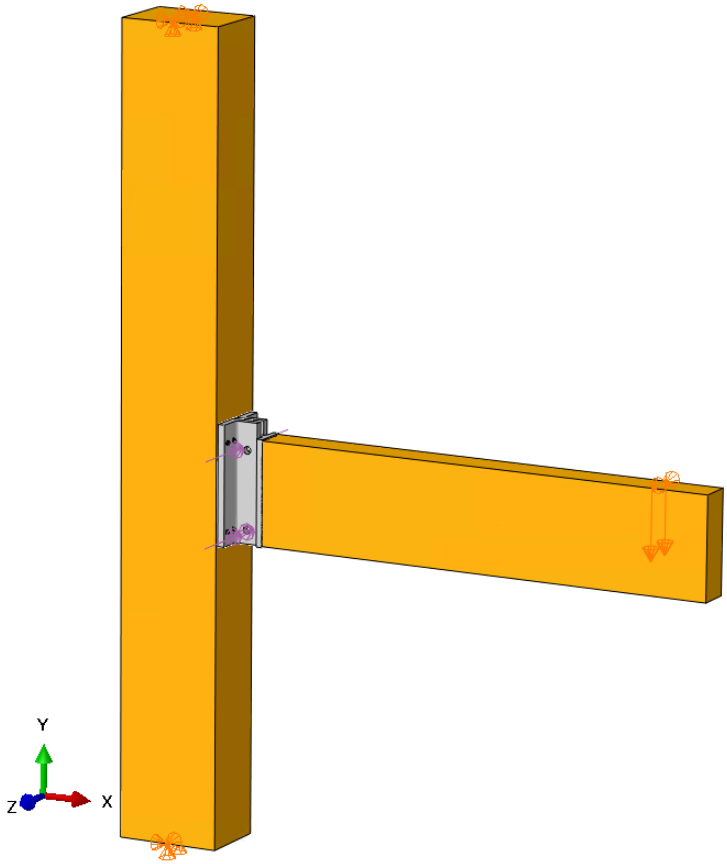

Figure E.6: Boundry conditions and loads on full configuration with threaded rod model